NOTICE

The quality of this microform is heavily dependent upon the quality of the original thesis submitted for microfilming. Every effort has been made to ensure the highest quality of reproduction possible.

If pages are missing, contact the university which granted the degree.

Some pages may have indistinct print especially if the original pages were typed with a poor typewriter ribbon or if the university sent us an inferior photocopy.

Reproduction in full or in part of this microform is governed by the Canadian Copyright Act, R.S.C. 1970, c. C-30, and subsequent amendments.

AVIS

La qualité de cette microforme dépend grandement de la qualité de la thèse soumise au microfilmage. Nous avons tout fait pour assurer une qualité supérieure de reproduction.

S'il manque des pages, veuillez communiquer avec l'université qui a conféré le grade.

La qualité d'impression de certaines pages peut laisser à désirer, surtout si les pages originales ont été dactylographiées à l'aide d'un ruban usé ou si l'université nous a fait parvenir une photocopie de qualité inférieure.

La reproduction, même partielle, de cette microforme est soumise à la Loi canadienne sur le droit d'auteur, SRC 1970, c. C-30, et ses amendements subséquents.

Canada

EVALUATION AND CONTROL OF NOISE TRANSMISSION THROUGH A CAVITY BACKED FLEXIBLE PLATE

Mahesharaja Balike

A Thesis
in
The Department
of
Mechanical Engineering

Presented in Partial Fulfillment of the Requirements
for
the Degree of Master of Applied Science
at
Concordia University
Montreal, Quebec, Canada

August 1993

ISBN 0-315-87302-7

Canada

Abstract

Evaluation and Control of Noise Transmission though a Cavity Backed Flexible Plate

Mahesharaja Balike

The sound transmission loss through a cavity backed flexible plate is analyzed using the modal coupling analysis technique. The modal coupling analysis of the cavity-panel system is carried out by combining the deflection modes of a clamped plate, derived from the plate characteristic functions, and the cavity modes. The noise transmission characteristics obtained using plate characteristic functions are compared to those obtained using the beam characteristic functions in Rayliegh-Ritz method. The noise transmission characteristics of a plate-cavity system are measured in terms of transmitted sound pressure and intensity levels under uniform pressure distribution over the panel. The analytical results are compared to those established from the measurements to gain certain confidence in the model. Although the comparison provided a qualitative verification, a total quantitative validation could not be done due to inability to realize clamped boundary condition. A parametric study is carried out to highlight the influence of various structural and cavity fluid parameters on the noise reduction. The study showed that the structural damping, cavity damping, cavity size, panel thickness, panel density, and the fluid density affect the noise reduction properties of the panel-cavity system. The results reveal that for deterministic and uniformly distributed external sound pressure, an improvement in noise reduction can be realized through appropriate selection of structural and fluid parameters. In an attempt to improve the control of low frequency noise caused by structural deflection modes, an active noise control concept comprising point control forces is formulated and investigated. An analytical model of the panel-cavity system, comprising multiple actively controlled point forces acting directly on the panel, is

developed. The influence of control forces generated using proportional control laws and arbitrary phase difference on the noise reduction properties is investigated for different feedback response variables and control gains. The noise reduction characteristics are compared to those derived from the analysis of the passive panel cavity system, and it is concluded that the control forces generated proportional to the panel velocity response offer most significant potential in reducing the sound transmission.

Acknowledgement

The author wishes to express deep sense of gratitude and appreciation to his supervisors, Dr. S. Rakheja and Dr. R. B. Bhat for their continued support, encouragement, and guidance during the course of this work.

Thanks are also due to Dr. Guy, Dr. C. Rajalingam, Dan Juras, Dale Rathwell, and G. Mundkur for their help at various stages of this work.

The financial support by the Mechanical Engineering Department at Concordia University, is further acknowledged.

Special thanks are due to my parents for their moral support.

Contents

List of Figures ix

List of Tables xiii

Nomenclature xiv

1 Introduction and Problem Definition 1

1.1 General 1

1.2 Transmission of Sound in Enclosures - A Literature Review . . . 2

1.2.1 Passive Control of Sound Transmission 4

1.2.2 Active Control of Sound Transmission 5

1.3 Scope of the Thesis Research 8

2 Analysis of Sound Transmission Loss through a Cavity Backed Flexible Plate 11

2.1 Introduction 11

2.2 Modal Coupling Analysis 12

2.2.1 Interior Acoustic Pressure 13

2.2.2 Motion of the Flexible Plate 18

2.2.3 Plate Characteristic Functions 20

2.2.4 Cavity Pressure and Noise Reduction 26

2.3 Numerical Results and Discussion 28

2.3.1 Natural Frequencies of the Plate and Cavity 29

2.3.2 Comparison of Noise Reduction Obtained using PCF and BCF 33

2.3.3 Effect of Various Structural and Geometrical Parameters . . . 35

2.4 Summary 43

3 An Experimental study of the Plate-Cavity System **44**

3.1 Introduction 44

3.2 Measurement of Sound Transmission Loss 45

3.3 Experimental Apparatus and Measurement Procedures 47

3.4 Results and Discussion 49

3.4.1 Natural Frequency of the Plate 49

3.4.2 Measurement and Analysis of Noise Transmission Loss 51

3.5 Summary 67

4 Active Control of Noise Transmission through a Cavity Backed Plate 68

4.1 Introduction 68

4.2 Mathematical Model 70

4.3 Results and Discussion 73

4.4 Summary 86

5 Conclusion and Future Work 87

5.1 Conclusions 87

5.2 Recommendation for Future Work 88

Appendices 96

A Evaluation of L_{ijmn} and p^f_{mn} 95

A.1 Evaluation of L_{ijmn} 95

A.2 Evaluation of p^e_{mn} 96

B Beam and Plate Characteristic Functions 98

C Calibration of the Intensity Probe 100

List of Figures

2.1 Geometry of the cavity backed flexible plate 14

2.2 Comparison of NR obtained by PCF and BCF ($\zeta_{mn} = \gamma_{ijk} = 0.02$) . . 34

2.3 Comparison of NR obtained by PCF and BCF ($\zeta_{mn} = \gamma_{ijk} = 0.05$) . . 34

2.4 Comparison of NR obtained by PCF and BCF ($\zeta_{mn} = \gamma_{ijk} = 0.1$) . . 35

2.5 NR against frequency for different damping ratios 37

2.6 NR against frequency at different positions 37

2.7 NR against frequency at different depths 38

2.8 NR against frequency for cavities of different depth 39

2.9 NR against frequency for different cavity sizes 39

2.10 NR against frequency for different plate thickness 40

2.11 NR against frequency for different plate densities 41

2.12 NR against frequency for different cavity fluid densities 42

2.13 NR against frequency for different plate boundary conditions 42

3.1 Geometry of the test enclosure 48

3.2 Schematic of the experimental apparatus 48

3.3 Measured frequency response function of the flexible plate 50

3.4 Contour map of the external sound pressure measured near the plate surface 52

3.5 Contour map of the external sound pressure at the location, when plate-cavity system is removed 52

3.6 Contour map of sound intensity I_z near the plate surface . 53

3.7 Contour map of the external sound intensity at the location, when plate-cavity system is removed 53

3.8 Sound pressure spectrum measured at the plate surface (x/a y/b 0.5) with and without the test enclosure 54

3.9 Sound intensity spectrum measured at the plate surface (x/a y/b 0.5) with and without the test enclosure 55

3.10 Contour map of the sound pressure measured outside the backwall 57

3.11 Contour map of the sound intensity at the measured outside the backwall 57

3.12 Cavity sound pressure spectrum measured at x/a y/b 0.5, z/d 0.25 59

3.13 Cavity sound pressure spectrum measured at x/a y/b 0.5, z/d 0.5 59

3.14 Cavity sound pressure spectrum measured at x/a y/b 0.5, z/d 0.75 60

3.15 Cavity sound intensity spectrum measured at $x/a = y/b = 0.5$, $z/d = 0.25$ 60

3.16 Cavity sound intensity spectrum measured at $x/a = y/b = 0.5$, $z/d = 0.5$ 61

3.17 Cavity sound intensity spectrum measured at $x/a = y/b = 0.5$, $z/d = 0.75$ 61

3.18 Measured NR at $x/a = y/b = 0.5$, $z/d = 0.5$ 62

3.19 Measured NR at $x/a = y/b = 0.5$, $z/d = 0.75$ 63

3.20 Comparison of experimental and analytical NR at $x/a = y/b = z/d = 0.25$ under white noise excitation 63

3.21 Comparison of experimental and analytical NR at $x/a = y/b = z/d = 0.25$ under sinusoidal excitation 65

3.22 Comparison of measured NR for cavities of different depth 65

3.23 Comparison of NR measured at different location along z-axis under white noise excitation 66

3.24 Comparison of NR measured at different location along z-axis under sinusoidal excitation 66

4.1 Effect of position feedback control on NR-clamped plate 75

4.2 Effect of position feedback control on NR-simply supported plate . . 75

4.3 Effect of velocity feedback control on NR-clamped plate 76

4.4 Effect of velocity feedback control on NR-simply supported plate . . . 76

4.5 Effect of acceleration feedback control on NR clamped plate . . 77

4.6 Effect of acceleration feedback control on NR simply supported plate 77

4.7 Effect of position feedback control force at different phase angles on NR 79

4.8 Effect of velocity feedback control force at different phase angles on NR 79

4.9 Effect of control force with position and velocity feedback on NR . . . 81

4.10 Effect of control force with position, velocity and acceleration feedback on NR 81

4.11 Effect of position feedback control force on NR, located at x/a y/b 0.25 82

4.12 Effect of velocity feedback control force on NR, located at x/a y/b 0.25 83

4.13 Effect of acceleration feedback control force on NR, located at x/a $y/b = 0.25$ 84

4.14 Effect of two control forces on NR- position feedback 85

4.15 Effect of two control forces on NR- velocity feedback 85

4.16 Effect of two control forces on NR position and velocity feedback . 86

C.1 Sound intensity levels measured in the coupler along two direction . 102

C.2 Sound pressure levels measured in the coupler along two direction 103

List of Tables

2.1 Material properties of the cavity-plate system 29

2.2 Natural frequencies of the simply supported plate 30

2.3 Natural frequencies of the clamped plate 31

2.4 Natural frequencies of the rigid cavity 32

B.1 CC Beam characteristic function parameters 98

B.2 CCCC Plate characteristic function parameters 99

C.1 Comparison of measured P-I index with the minimum requirement . . 104

Nomenclature

a, b, d	Cavity dimensions in x, y, and z directions respectively (m)
c	Speed of sound (m/s)
C	Equivalent viscous damping of the plate (Ns/m^3)
C_1, C_2, C_3, C_4	Constants of integration in x direction
$C_1^*, C_2^*, C_3^*, C_4^*$	Constants of integration in x direction
C_{ijk}	Cavity modal pressure coefficients
D	Flexural rigidity of the plate (Nm)
e_i, e_j, e_k	Normalizing factors for the cavity eigenfunctions
E	Modulus of elasticity of plate (N/m^2)
f_{pq}	Control force at the point (x_p, y_q)
F_d, F_v, F_a	Control forces (N)
F_{ijk}	Cavity forcing functions
G	Modulus of rigidity, $[E/2(1+\nu)]$
h	Thickness of plate (m)
$H_{ijk}(\omega)$	Frequency response function of the cavity
$H_{mn}(\omega)$	Frequency response function of the plate
i, j, k	Cavity modal indices
I	Sound intensity
$J_{mn}(\omega)$	Frequency response function of the plate cavity system
L_{ijmn}	Acoustic stiffness coupling coefficient
L_I	Sound intensity level
L_P	Sound pressure level
m, n, r, s	Plate modal indices
$M(x), M(y)$	Plate bending moments in x and y directions
$p(t)$	Instantaneous sound pressure
$p^c(x, y, z, t)$	Cavity acoustic pressure (N/m^2)
$p^e(x, y, t)$	External acoustic pressure (N/m^2)
$p_{mn}^c(\omega)$	Generalized cavity force

$p'_{mn}(\omega)$	Generalized external force
p_1, p_2, q_1, q_2	Roots of reduced equation
$q_{mn}(\omega)$	Generalized coordinates for plate deflection
t	Time (s)
$u(t)$	Instantaneous particle velocity
$V(x), V(y)$	Plate shear forces in x and y directions
w	Transverse plate deflection (m)
X_{ijk}	Orthonormal cavity eigenfunctions
$X(x)$	Plate characteristic functions in x direction
$Y(y)$	Plate characteristic functions in y direction
α	Plate aspect ratio
β	Non-dimensional frequency $(\frac{\omega}{\omega_{11}})$
γ_{ijk}	Cavity modal damping coefficients
δ	Dirac delta function
δ_{PI}	Local sound pressure-intensity index
Δ	Laplacian operator $(\partial^2/\partial x^2 + \partial^2/\partial y^2)$
∇	Laplacian operator in 3-dimension$(\partial^2/\partial x^2 + \partial^2/\partial y^2 + \partial^2/\partial z^2)$
ζ_{mn}	Panel modal damping coefficients
ν	Poisson's ratio
ϕ	Deflection shape of plate in x direction
ϕ_a, ϕ_d, ϕ_v	Phase angles between the control forces and the feedback state variables
ρ_a	Cavity fluid density (kg/m^3)
ρ_p	Plate density (kg/m^3)
ψ	Deflection shape in y direction
$\psi_{mn}(x, y)$	Orthonormal eigenfunctions of the plate
ω	Excitation frequency
ω_{ijk}	Natural frequencies of the cavity (rad/s)
ω_{mn}	Natural frequencies of the plate (rad/s)
Ω	Non-dimensional frequency parameter, $\left[\omega a^2\sqrt{\frac{\rho_p h}{D}}\right]$

Chapter 1

Introduction and Problem Definition

1.1 General

The noise levels inside many aircrafts, ground vehicles and industrial workplaces are known to exceed the acceptable comfort limits, established by NIOSH (National Institute of Occupational Safety and Health). In majority of the enclosures, the interior sound is caused by various external sources. While the interior noise of buildings may be caused by air flow in the ducts, external wind and traffic, the noise inside an aircraft fuselage and ground vehicles is primarily attributed to engine or structural vibration and the boundary layer turbulence. The interior noise generated by structural vibration that is caused by the external vibration and pressure fluctuations, predominates at low frequencies, corresponding to the first few structure and cavity resonances. In view of the the adverse influence of prolonged exposure to excessive noise levels on the health, safety and performance rate of passengers/operators, it is extremely desirable to reduce the interior noise levels.

The attenuation of transmitted noise levels may be realized by reducing the noise either at the source or along the path or at the receiver location. The implementation

of one or more of these methods, however, is dependent upon the application, sources, and target noise levels. In case of aircrafts or ground vehicles the primary 'source' is often the external disturbance which may not be amenable for control. In the aircraft interior, viewed as the 'receiver', noise may be reduced by treating the interior walls with acoustical absorbant materials. Such materials, however, may not be effective in the entire frequency range of interest. The acoustic absorption materials frequently used in aircraft fuselages are known to be less effective at low frequencies. The noise attenuation through the reduction of noise transmission along the path, such as the vibrating walls of the enclosure (fuselage), may thus be explored.

In this study, sound transmission characteristics of a clamped plate forming a wall of a rectangular cavity are evaluated using the method of modal coupling analysis in conjunction with the plate characteristic functions. The sound transmission loss of a cavity panel system are measured in the laboratory and compared to those derived from the analytical model. Actively controlled point forces, generated using state feedback, are applied to achieve noise reduction within the cavity. In the next section, a review of relevant literature is presented and the scope of the dissertation research is formulated.

1.2 Transmission of Sound in Enclosures - A Literature Review

The acoustical analysis of the complex structure of the fuselage or vehicle body is quite complicated for a detailed mathematical treatment. A simplified enclosure model comprising a rectangular box with five rigid walls and one acoustically flexible wall has been extensively used to analyze the noise transmission characteristics.

The problem of sound transmission through a panel into a rectangular cavity was first analysed by Lyon [1] in the early 60s, assuming negligible influence of cavity

on the panel vibration, while the panel natural frequency was considered lower than the first natural frequency of the cavity. Dowell and Voss [2] investigated the effect of the cavity on the modal response of the panel and evaluated the system natural frequencies, while the cavity was considered to serve as a stiffness to the fundamental panel mode.

Following Lyon's study, numerous efforts have been made to analyze the noise transmission through a panel into a cavity. Pretlove [3,4] suggested an alternative method to evaluate the system natural frequencies, which was further extended to analyze the forced vibration of a cavity backed plate. Kihlman [5] derived the solution to the wave equation with inhomogeneous boundary conditions, and discussed the behaviour of a panel-cavity system at frequencies above the panel critical frequency. An alternative solution to this problem was proposed by Bhattacharya and Crocker [6], and their analysis explained the phenomenon of wave coincidence. In the later years, Guy and Bhattacharya [7] compared the theoretical and experimental values of noise reduction and described the phenomenon of negative noise reduction in the cavity. In the early 80s Narayanan and Shanbhag [8,9] investigated the noise reduction properties of sandwich panels.

The response characteristics of the coupled panel-cavity system have been determined using two methods: (i) by assuming the coupled system as a single system [10]; and (ii) modal coupling analysis [11]. The analysis of a complex coupled system such as an aircraft fuselage using the first method, however, would be quite cumbersome. The modal coupling analysis involves analysis of in vacuo modal response of the panel and the blocked modal response of the cavity, and is considerably simpler than the first method. The acoustic wave equation is used to describe the interior sound field, while the wave equation for an isotropic panel is used to describe the panel vibration response. The interaction of the interior sound field with the panel is represented by the velocity continuity at the panel internal surface.

While majority of the above studies deal with analysis of simply supported

plates, McDonald et al. [12] compared the noise reduction through the cavity backed plate for different plate boundary conditions, using the beam characteristic functions in Rayleigh-Ritz method. The effects of both, deterministic and random external pressure excitations, on noise reduction was investigated. Since the beam characteristic functions do not represent the plate modes exactly and the transmitted sound is strongly related to the flexible panel response, a need to accurately analyze the plate response has been identified.

A set of plate characteristic functions were developed by Bhat et al [13,14] to accurately determine the plate modes with different boundary conditions. The use of plate characteristic functions to express plate modes will result in more accurate estimation of noise reduction. Bhat and Mundkur [15] used plate characteristic functions to investigate the sound transmission loss through a panel mounted on a rigid infinite baffle. The plate characteristic functions were determined through the exact solution of the reduced equation, using an iterative method. The plate partial differential equation was reduced to an ordinary differential equation by substituting an assumed approximate solution that satisfies the boundary conditions along one direction of the panel. The reduction method, commonly known as Kantorovich method, is applied sequentially on either direction of the plate and iterations are performed until convergence is achieved for the natural frequency coefficients. The results of the study have demonstrated that the plate characteristic functions provide a more accurate estimation of natural frequencies and plate response than the beam characteristic functions in the Rayleigh-Ritz method. Further, the computational time required by the method using plate characteristic functions is considerably less than that needed for the method based on beam characteristic functions in Rayleigh-Ritz method.

1.2.1 Passive Control of Sound Transmission

Upon determination of sound transmission loss characteristics of a structure, noise transmission loss can be improved through either passive or active means. The

passive control of sound transmission involves determination of structural parameters that improve the sound transmission loss, damping treatment of structures, application of acoustic absorbant materials, etc. The active control of sound transmission is attained either through implementation of a feedback controlled secondary sound source or through active vibration control. The active noise control methods offer considerable potential to attenuate noise due to their ability to change the secondary sources or control forces with variations in external disturbances and the system response.

The low frequency interior noise can be controiled through control of vibration of the structure forming the enclosure. The modal coupling and the forced vibration analyses of the panel-cavity system yield the vibration and acoustical response characteristics of the system. The vibration behaviour and thus the noise transmission loss characteristics of a structure are strongly related to its parameters. A number of studies have been carried out to explore the noise attenuation potentials of different materials and material properties [8,12]. Results of these studies have clearly demonstrated that a viscoelastic material sandwiched between two elastic plates offers an extremely efficient means to dissipate vibrational energy [16]. One-dimensional sound transmission through sandwich panels was investigated by Dym et al. [17], and the sandwich panels to reduce noise transmission in a panel-cavity system have been investigated in many studies [8,9,18] Passive control of sound transmission, however, poses certain inherent limitations due to fixed parameters. The desired transmission losses may be achieved only for a small variation around a given external disturbance. Since the external disturbances are random in nature, the passive control technique does not provide significant improvement in the sound transmission loss

1.2.2 Active Control of Sound Transmission

The mechanism of active control of noise transmission has been studied intensively in the recent years. The desire to reduce the internal noise levels in aircrafts

and moving vehicles, together with developments in modern control engineering, signal processing and high speed microprocessors, have prompted an increasing number of these studies. The desirable performance characteristics can be achieved through feedback control, by introducing a secondary disturbance, based on the system's response as measured by the feedback sensors.

Active control systems can supply energy, when needed, as well as dissipate energy, while the passive system can only dissipate or temporarily store energy. The active control can thus provide superior noise attenuation performance. Active control of sound transmission can be achieved in two ways: (i) through introduction of a secondary source of controlled tonal quality and loudness; and (ii) through introduction of actively controlled forces.

In the first method, the active noise suppression is achieved by introducing a secondary source of carefully controlled tonal quality and loudness, that interferes destructively with the primary field causing the noise. For deterministic excitations, the nature of control signal for the secondary source is readily specified using frequency-domain analysis, provided a measure of fluctuations in the primary sound source strength is available. The control signal is filtered and amplified to generate the desired secondary source strength. The problem thus reduces to that of design of this control filter and control gain to minimize the cost function. Nelson et al. [19] have analysed the effectiveness of such an active control system, using frequency domain analysis, when an enclosed field is excited harmonically. The secondary source, however, was unable to respond to changes in the primary source, specifically when the strength of the primary source varied randomly. A time domain analysis technique has been applied to determine a causally constrained optimal controller for stationary random primary excitations [20].

The second method of active noise control, known as active structural acoustic control, was introduced as a natural extension of the active vibration control. Numerous investigations, both analytical and experimental, have been carried out

on active vibration control of elastic structures [21,22,23]. These active vibration control techniques use state feedback controllers to generate an active control force that introduces desirable damping characteristics to the structure. The controllers are primarily designed to suppress the transient response, and to reject a continuous disturbance force acting on the structure. For vibration control, the feedback state vector is frequently based on the modal coordinates of the structure. The concepts in active force generators, developed for vibration control, have been also explored to achieve active noise control and to realize smart structures.

Several investigations have been performed on the active control of sound radiation from elastic structures using force inputs. Analytical and experimental studies conducted by Fuller [24,25] concluded that control forces applied directly to a plate can significantly reduce the radiated sound pressure. A radiated power cost function was formulated and minimized to derive the optimal control gains that resulted in reduction in the far field sound pressure. A Linear Quadratic Regulator (LQR) controller design used for the vibration control, was developed by Meirovitch [26] to control the sound radiation.

Research on active control of sound transmission in a coupled fluid structure system was originally initiated by a desire to effectively control transmission of low frequency propeller generated noise into an aircraft through its fuselage. Active control of noise in ducts has generally met with considerable success [27], although application to three dimensional sound fields have proven to be somewhat more difficult. Considerable progress, however, is evident in the active control of three dimensional coupled fluid-structure systems. Fuller et al. [28,29,30] have investigated the active control of noise transmission into a cylindrical structure. Warner and Bernhard [31] proposed a digital control of sound transmission in three-dimensional enclosures. Many investigations have been carried out to control the noise transmission through a panel into an rectangular enclosure using point control forces. Pan et al. [32, 33, 34] studied, both analytically and experimentally, the acoustic mechanism associated

with the vibrational control and the noise transmission into a rectangular enclosure through a simply supported plate. The study concluded that minimum sound energy is obtained by suppressing the panel vibration, when the response is dominated by the panel modes. A control force that can adjust the panel velocity distribution, can be effectively used, when the system response is dominated by the cavity controlled modes. The study also concluded that in the later case, there may be an increased locally reactive sound intensity flow and increased panel vibration levels.

The effectiveness of an active noise control system, employing an actively controlled force, is strongly related to the number of force generators and their locations. The effect of location of a control force generator on the noise and vibration transmission characteristics of structures has been investigated by Meirovitch et al. [35] and Bullmore et al. [36]. Meirovitch [35] showed that the number of active force generators required is equal to the number of modes to be controlled. The study conducted by Bullmore et al. [36] showed that the control forces must be located so that they can most effectively couple with the dominant cavity modes excited by the primary source.

1.3 Scope of the Thesis Research

Acoustical absorbant materials provide only limited attenuation of low frequency noise transmitted into enclosures. Other passive means of noise control provide attenuation only in the limited frequency bands and for small variations in the external noise sources. The active methods of noise control offer considerable performance potentials by varying the structural properties in response to changing response and excitation variables. The control of low frequency noise transmitted into enclosures, however, necessitates an accurate estimation of the noise and vibration characteristics of the coupled panel-cavity system. Since the plate characteristic functions represent the vibration modes of the plates more accurately, an accurate

analysis of the coupled plate-cavity system may be carried out using these functions. The objectives of this thesis research are thus formulated as follows:

- Analyze the noise transmission characteristics of a cavity backed flexible panel using the plate characteristic functions.
- Investigate the influence of various structural and fluid parameters on the noise transmission loss.
- Validate the analytical model through measurement of transmission loss of a panel-cavity system in the laboratory.
- Formulate an active noise control scheme and develop an analytical model of the panel-cavity system subject to actively controlled point forces.
- Investigate the noise attenuation performance characteristics of the proposed active noise control system.

An analytical model of a cavity backed flexible plate is formulated to determine its sound transmission characteristics, and presented in chapter 2. The external pressure excitation is assumed to be spatially uniform all over the plate. Modal coupling analysis technique, comprising in-vacuo modal response of the plate and blocked modal response of the cavity, is applied to determine the sound transmission loss characteristics. The modal response characteristics of the panel and the cavity are then combined together to yield the response of the coupled plate cavity system. The application of plate characteristic functions to study the noise transmission is described and the results are compared to those obtained using the beam characteristic functions. The influence of different structural and fluid parameters on the noise transmission is discussed.

A laboratory model of the panel-cavity system was fabricated and experiments were performed to validate the corresponding analytical model. The noise transmission characteristic of the panel-cavity system were measured using two techniques: (i)

sound pressure method; and (ii) sound intensity method. The detailed experimental procedure, data analysis, and the experimental results are presented in chapter 3. The experimental results are compared to the analytical results, and the limitations of the analytical and experimental models are discussed.

Active control of sound transmission through a flexible panel into a rectangular cavity, based upon point control forces applied to the panel, is analytically studied in chapter 4. The response characteristics of the coupled panel-cavity system with multiple point control forces applied to the panel are analyzed using the modal coupling analysis technique. The active control forces are generated using the state feedback and a proportional control law with certain phase angle. The noise transmission characteristics of the panel-cavity system with active control forces generated using position, velocity and acceleration feedback are evaluated for uniform sound pressure distribution.

Finally, the conclusions derived from the study together with the highlights and the recommended future directions are presented in chapter 5.

Chapter 2

Analysis of Sound Transmission Loss through a Cavity Backed Flexible Plate

2.1 Introduction

The acoustical analysis of the complex structure of the fuselage or vehicle body is quite complicated for a detailed mathematical treatment. A simplified enclosure model comprising a rectangular box with five rigid walls and one acoustically flexible wall has been extensively used to analyze the noise transmission characteristics of a coupled structure-cavity system.

The response characteristics of the coupled panel-cavity system can be determined by two methods: (i) by assuming the panel-cavity system as an equivalent single system; and (ii) modal coupling analysis. The modal coupling analysis involves analysis of in-vacuo modal response of the panel and the blocked modal response of the cavity, and is considerably simpler than the first method. The acoustic wave equation is used to describe the interior sound field, while the wave equation for an isotropic panel is used to describe the panel vibration response. The interaction of

the interior sound field with the panel is represented by the velocity continuity at the panel internal surface.

The response characteristics of the coupled panel-cavity system with clamped boundary conditions have been evaluated using beam characteristic functions in Rayleigh-Ritz method to represent the plate modes [12]. Beam characteristic functions, however, do not represent the plate modes exactly, and errors may be encountered in the evaluation of the noise transmission analysis [15]. Plate characteristic functions represent plate modes more accurately and may yield more accurate estimation of noise transmission characteristics.

In this chapter, modal coupling analysis is technique used to evaluate the noise transmission loss through the coupled plate-cavity system is presented. Plate characteristic functions are used to represent the plate modes in the evaluation of noise reduction. The noise reduction obtained using plate characteristic functions is compared with that obtained using beam characteristic functions. The influence of various structural and fluid parameters on noise reduction is discussed.

2.2 Modal Coupling Analysis

The response characteristics of a coupled flexible plate-cavity system can be effectively evaluated using the modal coupling analysis technique. The technique involves in-vacuo modal response analysis of the flexible plate and blocked modal response analysis of the cavity. The acoustic wave equation is used to describe the interior sound field, while the panel vibration response is described by the wave equation for an isotropic flexible plate [11,12]. The modal coupling analysis is described in this section.

2.2.1 Interior Acoustic Pressure

Consider a hard walled rectangular cavity of volume $v = abd$, as shown in the Figure 2.1. The wall located at $z = 0$ represents the flexible plate while the remaining walls are considered to be acoustically rigid. The flexible plate is subjected to an external sound pressure $p^e(x, y, t)$ resulting in the internal cavity pressure, $p^c(x, y, z, t)$. The external pressure is a function of x, y coordinates and the time, whereas the cavity pressure is a function of x, y, z coordinates and the time.

The sound pressure p^c, inside the cavity is governed by the linear acoustic wave equation, given by:

$$\nabla^2 p^c - \frac{1}{c^2}\frac{\partial^2 p^c}{\partial t^2} = 0 \tag{2.1}$$

where, $\nabla^2 = \frac{\partial^2}{\partial x^2} + \frac{\partial^2}{\partial y^2} + \frac{\partial^2}{\partial z^2}$, c is the speed of sound in the fluid within the enclosure. The boundary conditions to be satisfied are:

$$\frac{\partial p^c}{\partial n} = \begin{cases} -\rho_a \ddot{w}(x, y, t) & \text{on flexible wall} \\ 0 & \text{on rigid walls} \end{cases} \tag{2.2}$$

where $\frac{\partial p^c}{\partial n}$ represents the derivative of the cavity pressure in the direction normal to the wall surfaces of the cavity, w is the displacement of the flexible plate, and ρ_a is mass density of air. The sound pressure in Equation (2.1) can be written in terms of orthonormal cavity eigenfunctions as:

$$p^c(x, y, z, t) = \sum_{i=0}^{\infty}\sum_{j=0}^{\infty} \phi_{ij}(z, t)\sqrt{d}X_{i,j0}(x, y) \tag{2.3}$$

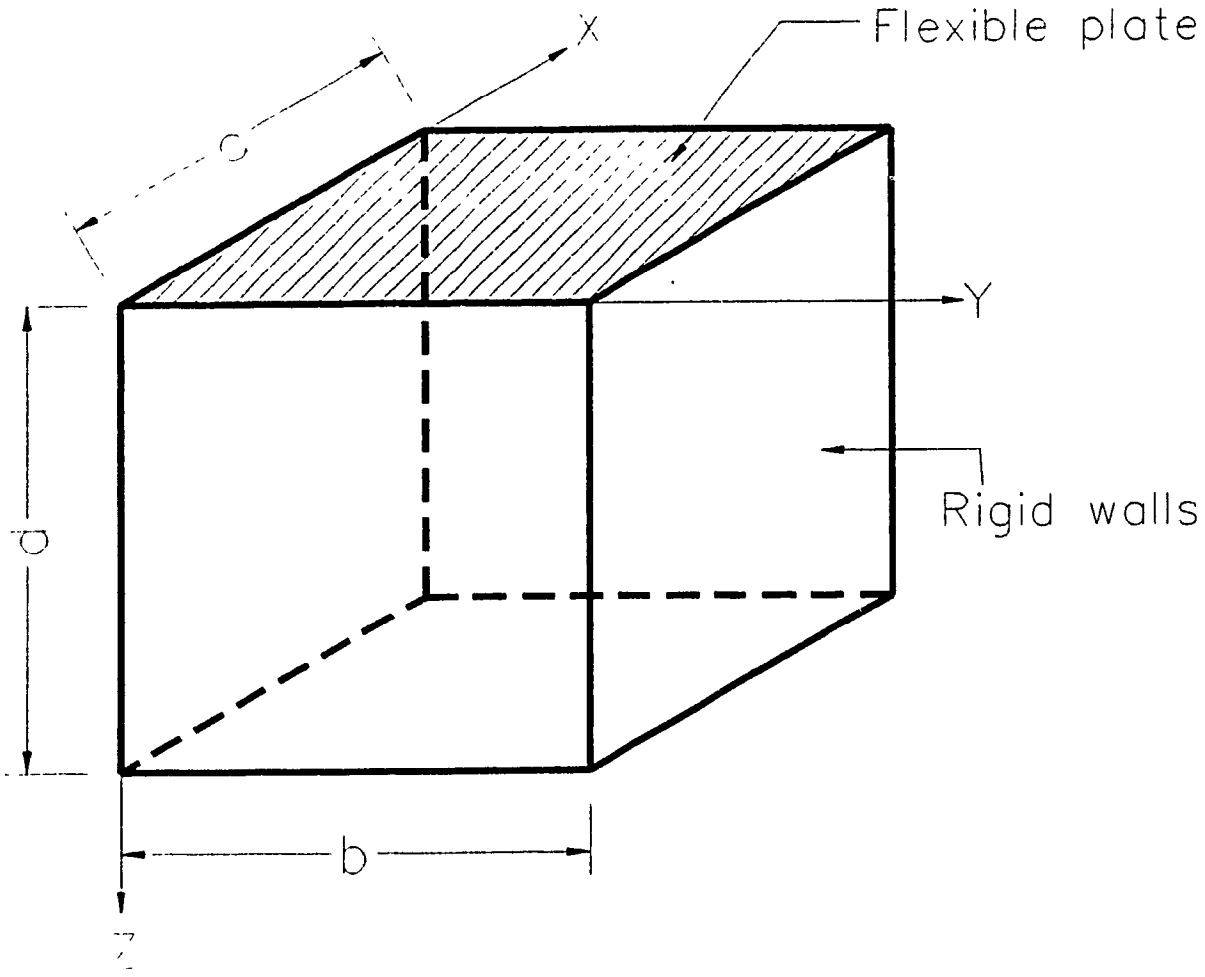

Figure 2.1: Geometry of the cavity backed flexible plate

where $\phi_{ij}(z,t)$ are the cavity pressure coefficients, and X_{ijk} are the orthonormal cavity eigenfunctions given by:

$$X_{ijk} = \sqrt{\frac{e_i e_j e_k}{abd}} \cos\left(\frac{i\pi x}{a}\right) \cos\left(\frac{j\pi y}{b}\right) \cos\left(\frac{k\pi z}{d}\right)$$

$$e_l = \begin{cases} 1 & \text{if } l = 0 \\ 2 & \text{if } l \neq 0 \end{cases} \qquad l = i,\ j,\ k$$

Using the boundary conditions and the cavity eigenfunctions the flexible panel motion can be expressed as:

$$-\rho_a \ddot{w} = \sum_{i=0}^{\infty} \sum_{j=0}^{\infty} G_{ij}(t) \sqrt{d} X_{ij0}(x,y) \tag{2.4}$$

Using orthogonality of normal modes X_{ijk},

$$G_{ij}(t) = \int_0^a \int_0^b -\rho_a \ddot{w} \sqrt{d} X_{ij0}(x,y) dx dy \tag{2.5}$$

The solution of Equation (2.1) can be easily obtained by transforming the homogeneous differential equation with non-homogeneous boundary conditions into a non homogeneous differential equation with homogeneous boundary condition [8,12]. This can be achieved by assuming $\phi_{ij}(z,t)$ as:

$$\phi_{ij}(z,t) = \alpha_{ij}(z,t) + Z_{ij}(z,t) \tag{2.6}$$

where α_{ij} is solution of the associated homogeneous problem and Z_{ij} is chosen to satisfy the non-homogeneous part of the boundary condition. Using Equations (2.6) and (2.3) in Equation (2.1), the non-homogeneous differential equation is obtained as:

$$\frac{d^2}{dz^2}\alpha_{ij} - \frac{1}{c^2}\ddot{\alpha}_{ij} - A_{ij}\alpha_{ij} = -\frac{d^2}{dz^2}Z_{ij} + \frac{1}{c^2}\ddot{Z}_{ij} + A_{ij}Z_{ij} \tag{2.7}$$

where $A_{ij} = \pi^2[(\frac{i}{a})^2 + (\frac{j}{b})^2]$. Since Z_{ij} has been selected as the solution satisfying the non-homogeneous part of the boundary condition, the following must be satisfied:

$$\left[\frac{\partial Z_{ij}}{\partial z}\right]_{z=0} = G_{ij}(t) \tag{2.8}$$

A continuous function that satisfies the Equation (2.8) can be assumed to represent the solution for Z_{ij}. Such a function is a polynomial of the form:

$$Z_{ij}(z,t) = f(z)G_{ij}(t) \tag{2.9}$$

where,

$$f(z) = \left[z - \frac{z^2}{2d}\right] \tag{2.10}$$

The associated homogeneous boundary value problem yields a solution of the form:

$$\alpha_{ij}(z,t) = \sum_{k=0}^{\infty} C_{ijk}(t)\cos\left(\frac{k\pi z}{d}\right) \tag{2.11}$$

where the quantities C_{ijk} represent the cavity modal pressure coefficients. Equations (2.10) and (2.11) together with Equation (2.2) yield the solution of sound pressure inside the cavity as:

$$p'(x,y,z,t) = \sum_{i=0}^{\infty}\sum_{j=0}^{\infty}\sum_{k=0}^{\infty} C_{ijk}(t)X_{ijk}(x,y,z) + \sum_{i=0}^{\infty}\sum_{j=0}^{\infty} f(z)G_{ij}(t)\sqrt{d}X_{ij0}(x,y) \tag{2.12}$$

The expressions for the cavity modal pressure coefficients can be obtained by substituting for α_{ij} and Z_{ij} from the Equations (2.9) and (2.11), respectively, in the non-homogeneous differential Equation (2.7) as [12]:

$$\ddot{C}_{ijk} + \omega_{ijk}^2 C_{ijk} = F_{ijk}(t) \tag{2.13}$$

where the quantities F_{ijk} represent the forcing functions and are given by:

$$F_{ijk}(t) = \sqrt{ab} \int_0^d \left[f(z)\ddot{C}_{ij} + \omega_{ij0}^2 f(z) C_{ij} - \frac{1}{c^2} \frac{d^2 f(z)}{dz^2} C_{ij} \right] X_{00} \cdot dz \tag{2.14}$$

and ω_{ijk} are the cavity modal frequencies, defined as:

$$\omega_{ijk} = c\pi^2 \left[\left(\frac{i}{a}\right)^2 + \left(\frac{j}{b}\right)^2 + \left(\frac{k}{d}\right)^2 \right]^{\frac{1}{2}} \tag{2.15}$$

The solutions of Equation (2.13) yields the undamped cavity modal pressure coefficients, C_{ijk}. The cavity, however, possess the damping due to absorption capability of the walls, and viscosity of air. In order to represent the actual system damping in the cavity, Equation (2.13) is rewritten as:

$$\ddot{C}_{ijk} + 2\gamma_{ijk}\omega_{ijk}\dot{C}_{ijk} + \omega_{ijk}^2 C_{ijk} = F_{ijk}(t) \tag{2.16}$$

where the coefficients γ_{ijk} represent the modal damping constants of the cavity. The solution of Equation (2.16) yields the damped modal pressure coefficients of the cavity. The cavity pressure can then be evaluated from Equation (2.12) for the pressure coefficients. The pressure coefficients C_{ijk} can be obtained by solving Equation (2.16) in time domain with specified initial conditions. However, the linear characteristic

of the governing equations considered are more conveniently solved in the frequency domain. The Fourier transform of Equation (2.16) yields:

$$\bar{C}_{ijk}(\omega) = H_{ijk}\bar{G}_{ij}(\omega) \tag{2.17}$$

where H_{ijk} is known as the frequency response function of the cavity and is given by,

$$H_{ijk}(\omega) = \begin{cases} \frac{d(\omega_{ij0}^2 - \omega^2)}{2k\pi^2(\omega_{ijk}^2 - \omega^2 + 2i\gamma_{ijk}\omega_{ijk}\omega)} & \text{if } k \neq 0 \\ \\ \frac{d(-\omega_{ij0}^2 + \omega^2) - \frac{3\epsilon^2}{d^2}}{\omega_{ijk}^2 - \omega^2 + 2i\gamma_{ijk}\omega_{ijk}\omega} & \text{if } k = 0 \end{cases} \tag{2.18}$$

Similarly, Fourier transform of the Equation (2.12) and substitution of $\bar{C}_{ijk}$ from Equation (2.17), the cavity pressure can be written in frequency domain as:

$$\bar{p}'(x, y, z, \omega) = \sum_{i=0}^{\infty}\sum_{j=0}^{\infty}\sum_{k=0}^{\infty} H_{ijk}\bar{G}_{ij}(\omega)X_{ijk}(x, y, z) + \sum_{i=0}^{\infty}\sum_{j=0}^{\infty} f(z)\bar{G}_{ij}(\omega)\sqrt{d}X_{ij0}(x, y) \tag{2.19}$$

where ( ) represents the Fourier transform of the corresponding function in time and can be noted that Equation (2.19) describes the cavity pressure as a function of the panel motions w through the term $\bar{G}_{ij}$. It is thus necessary to analyse the panel motion in order to determine the cavity pressure.

2.2.2 Motion of the Flexible Plate

The governing differential equation of motion for a flexible plate, assuming small deflections, can be written in the frequency domain as:

$$D\Delta^2\bar{w} + \iota\omega C\bar{w} - \rho_p h\omega^2 w = p^r(x,y,\omega) - p^c(x,y,0,\omega) \tag{2.20}$$

where

$$\Delta^2 = \partial^4/\partial x^4 + 2\partial^4/\partial x^2\partial y^2 + \partial^4/\partial y^4$$

and D is the flexural rigidity, C is the equivalent damping coefficient of the plate, h is the thickness of the flexible plate, and ρ_p is the mass density. $p^r(x,y,\omega)$ and $\bar{p}^c(x,y,0,\omega)$ represent the Fourier transform of incident pressure and transmitted (or internal) cavity pressure, respectively.

The plate deflection $\bar{w}$ can be assumed in the form:

$$w = \sum_{m=1}^{\infty}\sum_{n=1}^{\infty} q_{mn}(\omega)\psi_{mn}(x,y) \tag{2.21}$$

where $\bar{q}_{mn}$ are the generalized coordinates and $\psi_{mn} = X_m(x)\bullet Y_n(y)$ are the orthonormal plate modes, which depend on the plate boundary conditions. $X_m(x)$ and $Y_n(y)$ are the mode shapes, satisfying the boundary conditions, in x and y directions respectively. For a panel, simply supported on all sides, the mode shapes can be assumed of the form:

$$\psi_{mn}(x,y) = \frac{2}{\sqrt{ab}}\sin\left(\frac{m\pi x}{a}\right)\sin\left(\frac{n\pi y}{b}\right) \tag{2.22}$$

For the clamped boundary condition, considered in this analysis, the plate modes are expressed as the product of plate characteristic functions in x and y directions, presented in the following subsection. Substituting Equation (2.21) into (2.20) and utilizing the orthogonality properties of the mode shapes yields:

$$q_{mn} = H_{mn}(\omega)\left[p^r_{mn} - p^c_{mn}(q_{mn})\right] \tag{2.23}$$

where p'_{mn} and p^c_{mn} are generalized external and cavity forces, respectively, and $H_{mn}(\omega)$ is the frequency response function of the plate given by:

$$H_{mn}(\omega) = (\omega_{mn}^2 - \omega^2 + 2i\zeta_{mn}\omega_{mn}\omega)^{-1} \tag{2.24}$$

where ω_{mn} are the plate natural frequencies and ζ_{mn} are the modal damping coefficients of the plate. The natural frequencies of a clamped are obtained using the plate characteristic functions, while the natural frequencies of a simply supported plate may be obtained by solving Equations (2.20) to (2.22). Using the orthogonality between mode shapes, the generalized external and cavity forces are expressed as:

$$p'_{mn}(\omega) = \frac{1}{\rho_p h}\int_0^a \int_0^b \bar{p}^e(x,y,\omega)\psi_{mn}(x,y)dxdy \tag{2.25}$$

$$p^c_{mn}(\omega) = \frac{1}{\rho_p h}\int_0^a \int_0^b \bar{p}^c(x,y,0,\omega)\psi_{mn}(x,y)dxdy \tag{2.26}$$

2.2.3 Plate Characteristic Functions

The plate characteristic functions are obtained by reducing the plate partial differential equation to an ordinary differential equation and then solving it exactly. The reduction process is carried out using the Kantorovich method, where approximate deflection shapes are assumed in one direction, while the Galerkin's averaging process employed to achieve an ordinary differential equation in the other direction. When this procedure is carried out in a sequential manner along either direction, the solution converges to a set of characteristic functions along with converging eigenvalues. The corresponding values of natural frequencies, ω_{mn} are also obtained in the process. The derivation procedure procedure is summarized below [13].

Vibration of a plate is associated with the minimum of the integral, which represents the total energy:

$$I = \int\int_A \left\{ (\Delta w)^2 - 2(1-\nu)\left[\frac{\partial^2 w}{\partial \xi^2}\frac{\partial^2 w}{\partial \eta^2} - \left(\frac{\partial^2 w}{\partial \xi \partial \eta} \right)^2 \right] + \frac{\rho_p h}{D}\left(\frac{dw}{dt} \right)^2 \right\} d\xi d\eta$$
$$-2\int_\Gamma V(s) w ds + 2\int_\Gamma M(s)\frac{\partial w}{\partial n} ds \quad (2.27)$$

where $\Delta = \frac{\partial^2}{\partial \xi^2} + \frac{\partial^2}{\partial \eta^2}$ is the Laplacian operator, D is the plate flexural rigidity, E is the modulus of elasticity, m is the mass per unit area of the plate, ν is the Poisson's ratio, w is the plate deflection, and ξ and η are the Cartesian coordinates. $M(s)$ is the bending moment and $V(s)$ is the shear force along the boundaries. The double integral is over the area of the plate whereas the line integral is along the boundaries of the plate, where s is along the boundary and n is a direction normal to the boundary. The necessary condition for the minimum of the integral I is obtained by considering a small variation in the deflection w as $w + g\varepsilon$. The first derivative of the resulting integral with respect to g is then equated to zero, leading to [38]

$$\int\int_A \left(\Delta^2 w + \frac{\rho_p h}{D}\frac{\partial^2 w}{\partial t^2} \right) \epsilon d\xi d\eta + \int_\Gamma M(s)\frac{\partial \epsilon}{\partial n} ds - \int_\Gamma V(s)\epsilon ds \quad 0 \qquad (2.28)$$

For a rectangular plate is where and the boundaries are parallel to the coordinate axes, the moment and shear force distribution along the boundaries ($\xi \quad 0, a$) are given by:

$$M(\xi) = \left\{ \frac{\partial^2 w}{\partial \xi^2} + \nu\frac{\partial^2 w}{\partial \eta^2} \right\}_{at\ \xi=0,a}$$

$$V(\xi) = \left\{ \frac{\partial^3 w}{\partial \xi^3} + (2-\nu)\frac{\partial^3 w}{\partial \xi \partial \eta^2} \right\}_{at\ \xi \quad 0,a} \qquad (2.29)$$

The moments and shear forces along the boundaries ($\eta = 0, b$) can be described by similar expressions. For free harmonic vibration, the solution may be assumed in the separable form:

$$w(x,y) = X(x)Y(y)e^{i\omega t} \tag{2.30}$$

where $x = \xi/a$ and $y = \eta/b$.

An iterative procedure is implemented to reduce the partial differential equation of the plate to an ordinary differential equation. The procedure is initiated by assuming initialiy the deflection shape along one direction, such as y. The assumed deflection function may be any function of y satisfying at least the geometrical boundary conditions along y. In the present analysis, beam characteristic functions are employed. Substituting $Y(y)$ into Equation (2.28), resulting differential equation in x direction is given by:

$$\begin{aligned}\frac{ab}{a^4}\int_0^1\int_0^1 \left[X''''Y + 2\alpha^2 X''\ddot{Y} + \alpha^4 X\ddot{\ddot{Y}} - \frac{\omega^2\rho_p h XY}{D}\right] Y\delta X dx dy \\ + \frac{ab}{a^4}\int_0^1 [\alpha^4 X\ddot{Y} + \nu\alpha^2 X''Y]\dot{Y}\delta X dx \\ - \frac{ab}{a^4}\int_0^1 [\alpha^4 X\ddot{\dot{Y}} + (2-\nu)\alpha^2 X''\dot{Y}]Y\delta X dx = 0\end{aligned} \tag{2.31}$$

where $\varepsilon = \delta w = Y\delta X + X\delta Y$. Since Y is assumed a priori, $\delta Y = 0$. Hence, $\varepsilon = \delta w = Y\delta X$ and $\frac{\partial \varepsilon}{\partial y} = \delta\dot{w} = \dot{Y}\delta X$. Further, $(\,)' = \frac{\partial}{\partial x}$ and $\dot{(\,)} = \frac{\partial}{\partial y}$. $\alpha = a/b$ is the plate aspect ratio where a and b are the side lengths of the plate along ξ and η directions, respectively. After performing the integration, the ordinary differential equation in the x direction is obtained as:

$$\begin{aligned}X'''' + 2\alpha^2[B - (1-\nu)(G_0 + G_1)]X'' \\ + \alpha^4\left[C - \frac{\Omega^2}{\alpha^4} + H_0 + H_1 - J_0 - J_1\right]X = 0\end{aligned} \tag{2.32}$$

with $A = \int_0^1 Y^2 dy$, $B = \frac{1}{A}\int_0^1 Y\ddot{Y}dy$, $C = \frac{1}{A}\int_0^1 Y\ddot{Y}\,dy$, $G_0 = \frac{1}{A}(Y\dot{Y})_{y=0}$, $G_1 = \frac{1}{A}(Y\dot{Y})_{y=1}$, $H_0 = \frac{1}{A}(\dot{Y}\ddot{Y})_{y=0}$, $H_1 = \frac{1}{A}(\dot{Y}\ddot{Y})_{y=1}$, $J_0 = \frac{1}{A}(Y\ddot{Y})_{y=0}$, $J_1 = \frac{1}{A}(Y\ddot{Y})_{y=1}$, and $\Omega^2 = \frac{\omega^2\rho_p h a^4}{D}$

Equation (2.32) can be expressed in the form:

$$X'''' + 2\beta X'' + \gamma X = 0 \tag{2.33}$$

where

$$\beta = \alpha^2[B - (1-\nu)(G_0 + G_1)]$$

$$\gamma = \alpha^4\left[C - \frac{\Omega^2}{\alpha^4} + H_0 + H_1 - J_0 - J_1\right]$$

Similarly by assuming a priori $X(x)$ and substituting this in the partial differential equation with $\delta w = X\delta Y$, $\delta w' = X'\delta Y$, it is possible to obtain an ordinary differential equation in the form:

$$\ddot{\ddot{Y}} + 2\beta^*\ddot{Y} + \gamma^* Y = 0 \tag{2.34}$$

where

$$\beta^* = \frac{1}{\alpha^2}[B^* - (1-\nu)(G_0^* + G_1^*)]$$

$$\gamma^* = \frac{1}{\alpha^4}[C^* + H_0^* + H_1^* - J_0^* - J_1^* - \Omega^2]$$

The quantities B^*, C^*, G_0^*, G_1^*, H_0^*, H_1^*, J_0^* and J_1^* must be evaluated appropriately along y, using equations similar to Equation (2.32). Assuming $X = X_0 e^{\lambda x}$, the solution of Equation (2.33) results in the auxiliary equation:

$$\lambda^4 + 2\beta\lambda^2 + \gamma = 0 \tag{2.35}$$

The roots are given by:

$$\lambda_{1,2}^2 = -\beta \pm \left(\beta^2 - \gamma\right)^{1/2} \tag{2.36}$$

Further, the solution of Equation (2.33) can be written as:

$$X(x) = C_1 \sin p_1 x + C_2 \cos p_1 x + C_3 \sinh p_2 x + C_4 \cosh p_2 x \tag{2.37}$$

where p_1 and p_2 are defined as:

$$p_{1,2} = \pm\left[\pm\beta + \left(\beta^2 - \gamma\right)^{1/2}\right]^{1/2} \tag{2.38}$$

Similarly in the y direction, the solution of Equation (2.34) can be expressed as:

$$Y(y) = C_1^* \sin q_1 y + C_2^* \cos q_1 y + C_3^* \sinh q_2 y + C_4^* \cosh q_2 y \tag{2.39}$$

where q_1 and q_2 are given as:

$$q_{1,2} = \pm\left[\pm\beta^* + \left(\beta^{*2} - \gamma^*\right)^{1/2}\right]^{1/2} \tag{2.40}$$

The boundary conditions at a plate edge for different cases are:

Clamped:

$$X(x) = X'(x) = 0 \tag{2.41}$$

Simply supported:

$$\begin{aligned} X(x) &= 0 \\ X''(x) + \nu\alpha^2 B X(x) &= 0 \end{aligned} \tag{2.42}$$

Free:

$$X''(x) + \nu\alpha^2 B X(x) = 0$$
$$X'''(x) + (2-\nu)\alpha^2 B X'(x) = 0 \tag{2.43}$$

The different boundary conditions at the plate edges in y direction are:

Clamped:

$$Y(y) = \dot{Y}(y) = 0 \tag{2.44}$$

Simply-supported:

$$Y(y) = 0$$
$$\alpha^2 \ddot{Y}(y) + \nu B^* Y(y) = 0 \tag{2.45}$$

Free:

$$\alpha^2 \ddot{Y}(y) + \nu B^* Y(y) = 0$$
$$\alpha^2 \dddot{Y}(y) + (2-\nu) B^* \dot{Y}(y) = 0 \tag{2.46}$$

It is not possible to satisfy the conditions at a free edge. Hence, in Equations (2.42) and (2.43), the work done by the moment and shear force at the edge, say $x = 0$, integrated along y direction is equated to zero. Similarly in Equations (2.45) and (2.46), the work done by moment and shear forces at the edge, say $y = 0$, integrated along x direction is equated to zero. Substituting corresponding conditions in the Equations (2.37) and (2.39), two frequency equations are obtained consisting of infinite number of roots for the non-dimensional frequency parameters Ω_{ij}. By assuming the beam function, say $Y(y)$, the first root in x direction is obtained, and by using the function $X(x)$ corresponding to this root, the first root of the frequency equation in y direction is found. The resulting functions in both x and y directions are plate characteristic functions. Successive iterations along alternate directions is

carried out until convergence for first root, to obtain the first natural frequency, $\Omega_{(1,1)}$. Using similar procedure for first root in y direction and second root in x direction will give natural frequency $\Omega_{(2,1)}$. Continuing in this manner for all the roots will yield frequencies $\Omega_{(1,1)}$, $\Omega_{(2,1)}$,..., $\Omega_{(i,1)}$. When the same process is used with second root in y direction and first, second, ... roots in x direction will result in $\Omega_{(i,2)}$ (i = 1, 2, ...). Likewise, taking subsequent roots in y direction and first, second, ... roots in x direction will give all the roots $\Omega_{i,j}$ (i = 1, 2, ..., and j = 1, 2, ...).

2.2.4 Cavity Pressure and Noise Reduction

The cavity pressure can be evaluated upon combining the plate motion with the fluid motion at $z = 0$. Substituting the Fourier transform of Equation (2.5) in Equation (2.19), the cavity pressure can be obtained in terms of the plate motion in the frequency domain. The resulting equation, along with the expression for the plate motion from Equation (2.21), can be used in Equation (2.26) to obtain the generalized cavity force as:

$$p^c_{mn} = \frac{\rho_a \omega^2}{\rho_p h} \sum_{i=0}^{\infty} \sum_{j=0}^{\infty} \sum_{k=0}^{\infty} H_{ijk} \sum_{m=1}^{\infty} \sum_{n=1}^{\infty} \bar{q}_{rs} L_{ijmn} L_{ijrs} \tag{2.47}$$

where, $L_{ijmn} L_{ijrs}$ are the acoustic stiffness coupling coefficients which couple the plate vibration modes with the acoustic modes of the cavity, and are given by:

$$L_{ijmn} = \int_0^a \int_0^b \sqrt{d} X_{ij0}(x, y) \psi_{mn}(x, y) dx dy \tag{2.48}$$

where $X_{ij0}(x, y)$ and $\psi_{mn}(x, y)$ are the orthogonal eigenfunctions of the cavity and the plate, respectively. Upon substituting for the generalized cavity force, $\bar{p}^c_{mn}$, from Equation (2.47) in (2.23) the generalized coordinates, q_{mn} of the coupled plate-cavity system can be expressed as:

$$\bar{q}_{mn} = H_{mn}\left(p^c_{mn} - \frac{\rho_a\omega^2}{\rho_p h}\sum_{i=0}^{\infty}\sum_{j=0}^{\infty}\sum_{k=0}^{\infty} H_{ijk}\sum_{m=1}^{\infty}\sum_{n=1}^{\infty} q_{rs} L_{ijmn} L_{ijrs}\right) \tag{2.49}$$

The plate motion and the acoustic field inside the cavity can be determined by solving the above coupled system of equations for $\bar{q}_{mn}$. The products $L_{ijmn}L_{ijrs}$ represent the acoustic stiffness coupling between the plate modes mn and rs through the fluid motion in the cavity at $z = 0$. For a very shallow cavity, it has been established that the cross acoustic terms ($r \neq m,\ s \neq n$) are negligible when compared to the direct terms ($r = m,\ s = n$) [3,4,11]. Using this deduction, Equation (2.49) may be represented by the following un-coupled set of equations:

$$\bar{q}_{mn} = \left[\frac{p^c_{mn}}{[H_{mn}]^{-1} + \frac{\rho_a\omega^2}{\rho_p h}\sum_{i=0}^{\infty}\sum_{j=0}^{\infty}\sum_{k=0}^{\infty} H_{ijk} L^2_{ijmn}}\right] \tag{2.50}$$

Equation (2.50) can be represented in the simplified form as:

$$\bar{q}_{mn} = J_{mn} p^c_{mn} \tag{2.51}$$

where J_{mn} is the frequency response function of the coupled plate cavity system and is given by:

$$J_{mn} = \left[\omega^2_{mn} - \omega^2 + 2i\zeta_{mn}\omega_{mn}\omega + \frac{\rho_a\omega^2}{\rho_p h}\sum_{i=0}^{\infty}\sum_{j=0}^{\infty}\sum_{k=0}^{\infty} H_{ijk} L^2_{ijmn}\right]^{-1} \tag{2.52}$$

Upon combining Equations (2.19), (2.23) and (2.50), the cavity pressure can be expressed as:

$$p^t(x,y,z,\omega) = \rho_a\omega^2\sum_{i=0}^{\infty}\sum_{j=0}^{\infty}\left[\Delta(z)+\sum_{k=0}^{\infty}\sqrt{abd}H_{ijk}(\omega)X_{00k}(z)\right]$$

$$\sum_{m=1}^{\infty}\sum_{n=1}^{\infty}\ddot{q}_{mn}L_{ijmn}\sqrt{d}X_{ij0}(x,y) \tag{2.53}$$

The sound transmission through the plate to a point inside the cavity can be determined in terms of external and internal cavity sound pressures, expressed in dB as:

$$NR = 20\log\left[\frac{\bar{p}^e(x,y,\omega)}{\bar{p}^c(x,y,z,\omega)}\right] \tag{2.54}$$

2.3 Numerical Results and Discussion

The equations of motion for the clamped panel-cavity system, presented in section 2.2, are solved to determine its noise transmission characteristics. The model parameters, considered in the simulation, are presented in Table 2.1. Noise transmission analysis of the panel-cavity system is carried out for clamped boundary conditions using plate characteristic functions. The response characteristics are also evaluated for simply supported conditions, where the terms L_{ijmn} and p^e_{mn} are computed using the formulations presented in Appendix A. In the case of clamped plate, the terms L_{ijmn} and p^c_{mn} are evaluated using numerical integration technique.

The response characteristics are evaluated for harmonic sound pressure excitations, uniformly distributed over the plate area. The incident sound pressure is assumed to be normal to the surface of the flexible panel, while the excitation frequency range is selected to cover first few natural frequencies of the cavity and the structure. The damping was introduced as the modal damping in the plate and cav-

ity modes. The damping ratios, corresponding to the plate and cavity modes, are assumed to be identical in the 0.02 to 0.1 range.

Table 2.1: Material properties of the cavity-plate system

Parameter	Notation	Numerical Value
modulus of elasticity	E	71×10^{11} N/m^2
Poisson's ratio	ν	0.3
density of the plate	ρ_p	2700 kg/m^3
density of air	ρ_a	1.21 kg/m^3
speed of sound	c	344 m/s

The modal summation is performed to include 36 plate modes and large number of cavity modes ($i = j = 7$ and $k = 10$) to achieve adequate convergence. A relative convergence criteria of 10^{-4} was selected which was satisfied using 36 plate modes.

2.3.1 Natural Frequencies of the Plate and Cavity

Table 2.2 and Table 2.3 present the first 36 natural frequencies of the simply supported and clamped-plates respectively. These results are presented for a square plate ($a = b = d = 0.5m$). The natural frequencies of the simply supported plate are computed from Equation (2.21) and (2.22), while those of the clamped plate are obtained using the plate characteristic functions. An examination of the tabulated results clearly reveals that natural frequencies of the clamped plate are considerably larger than those of the simply supported plate. The natural frequencies of the cavity, bounded by rigid walls, are listed in Table 2.4. The table shows that the cavity

Table 2.2: Natural frequencies of the simply supported plate

$$[a = b = 0.5m, \quad \Omega_{mn} = \sqrt{\frac{\rho_p h a^4}{D}}\omega_{mn}]$$

N	m	n	Ω_{mn}	ω_{mn}, rad/s	$\beta = \frac{\omega_{mn}}{\omega_{11}}$
1	1	1	19.739	183.788	1.000
2	1	2	49.348	459.470	2.500
3	2	1	49.348	459.470	2.500
4	2	2	78.957	735.152	4.000
5	1	3	98.696	918.940	5.000
6	3	1	98.696	918.940	5.000
7	2	3	128.305	1194.621	6.500
8	3	2	128.305	1194.621	6.500
9	1	4	167.783	1562.197	8.500
10	4	1	167.783	1562.197	8.500
11	3	3	177.653	1654.091	9.000
12	2	4	197.392	1837.879	10.000
13	4	2	197.392	1837.879	10.000
14	3	4	246.740	2297.349	12.500
15	4	3	246.740	2297.349	12.500
16	1	5	256.610	2389.243	13.000
17	5	1	256.610	2389.243	13.000
18	2	5	286.219	2664.925	14.500
19	5	2	286.219	2664.925	14.500
20	4	4	315.827	2940.607	16.000
21	3	5	335.567	3124.395	17.000
22	5	3	335.567	3124.395	17.000
23	1	6	365.175	3400.077	18.500
24	6	1	365.175	3400.077	18.500
25	2	6	394.784	3675.758	20.000
26	6	2	394.784	3675.758	20.000
27	4	5	404.654	3767.652	20.500
28	5	4	404.654	3767.652	20.500
29	3	6	444.132	4135.228	22.500
30	6	3	444.132	4135.228	22.500
31	5	5	493.480	4594.698	25.000
32	4	6	513.219	4778.486	26.000
33	6	4	513.219	4778.486	26.000
34	5	6	602.046	5605.532	30.500
35	6	5	602.046	5605.532	30.500
36	6	6	710.612	6616.365	36.000

Table 2.3: Natural frequencies of the clamped plate

$$[a = b = 0.5m, \quad \Omega_{mn} = \sqrt{\frac{\rho h a^4}{D}}\omega_{mn}]$$

N	m	n	Ω_{mn}	ω_{mn}, rad/s	$\beta = \frac{\omega_{mn}}{\omega_{11}}$
1	1	1	35.999	335.179	1.000
2	1	2	73.405	683.463	2.039
3	2	1	73.405	683.463	2.039
4	2	2	108.236	1007.763	3.007
5	1	3	131.902	1228.115	3.664
6	3	1	131.902	1228.115	3.664
7	2	3	165.023	1536.497	4.584
8	3	2	165.023	1536.497	4.584
9	4	1	210.526	1960.170	5.848
10	1	4	210.526	1960.170	5.848
11	3	3	220.059	2048.923	6.113
12	2	4	242.667	2259.426	6.741
13	4	2	242.667	2259.426	6.741
14	4	3	296.366	2759.409	8.233
15	3	4	296.366	2759.409	8.233
16	1	5	309.038	2877.391	8.585
17	5	1	309.038	2877.391	8.585
18	2	5	340.590	3171.171	9.461
19	5	2	340.590	3171.171	9.461
20	4	4	371.376	3457.808	10.316
21	3	5	393.356	3662.459	10.927
22	5	3	393.356	3662.459	10.927
23	6	1	427.357	3979.038	11.871
24	1	6	427.357	3979.038	11.871
25	2	6	458.531	4269.294	12.737
26	6	2	458.531	4269.294	12.737
27	5	4	467.291	4350.855	12.981
28	4	5	467.291	4350.855	12.981
29	6	3	510.647	4754.536	14.185
30	3	6	510.647	4754.537	14.185
31	5	5	562.178	5234.331	15.617
32	6	4	583.749	5435.169	16.216
33	4	6	583.749	5435.176	16.216
34	6	5	677.745	6310.354	18.827
35	5	6	677.745	6310.355	18.827
36	6	6	792.461	7378.452	22.013

Table 2.4: Natural frequencies of the rigid cavity

$[a = b = d = 0.5m]$

N	i	j	k	ω_{ijk}, rad/s	$\beta = \frac{\omega_{ijk}}{\omega_{111}}$
1	0	0	0	0.000	0.000
2	0	1	0	2161.416	6.449
3	1	0	0	2161.416	6.449
4	0	0	1	2161.416	6.449
5	1	0	1	3056.703	9.120
6	1	1	0	3056.703	9.120
7	0	1	1	3056.703	9.120
8	1	1	1	3743.682	11.169
9	0	2	0	4322.831	12.897
10	2	0	0	4322.831	12.897
11	0	0	2	4322.831	12.897
12	0	2	1	4833.073	14.419
13	1	2	0	4833.073	14.419
14	1	0	2	4833.073	14.419
15	2	0	1	4833.073	14.419
16	2	1	0	4833.073	14.419
17	0	1	2	4833.073	14.419
18	1	1	2	5294.366	15.796
19	2	1	1	5294.366	15.796
20	1	2	1	5294.366	15.796
21	2	0	2	6113.407	18.239
22	2	2	0	6113.407	18.239
23	0	2	2	6113.407	18.239
24	0	3	0	6484.247	19.346
25	2	1	2	6484.247	19.346
26	1	2	2	6484.247	19.346
27	2	2	1	6484.247	19.346
28	3	0	0	6484.247	19.346
29	0	0	3	6484.247	19.346
30	1	0	3	6834.997	20.392
31	1	3	0	6834.997	20.392
32	0	3	1	6834.997	20.392
33	3	0	1	6834.997	20.392
34	3	1	0	6834.997	20.392
35	0	1	3	6834.997	20.392
36	1	1	3	7168.605	21.387

resonances occur only at higher frequencies. The corresponding plate and beam characteristic functions, derived for clamped plate is presented in Appendix B.

2.3.2 Comparison of Noise Reduction Obtained using PCF and BCF

The noise reduction (NR) through the flexible panel is computed using Equation (2.55). The results obtained using plate characteristic functions (PCF) are compared with those obtained using beam characteristic functions (BCF), for different damping ratios. From Equations (2.51), (2.54) and (2.55), it is evident that the noise reduction is dependent upon the generalized force, p^c_{mn}, acting on the panel. For uniform pressure loading considered in this analysis, the generalized force, p^c_{mn}, exists only corresponding to the odd numbered plate modes, as evident in Equations (A.7) and (A.9). The noise reduction analysis thus need to be performed only for plate modes with odd numbered half-waves. In obtaining the results using beam characteristic functions, the plate natural frequencies were computed by Rayleigh Ritz method, where the products of the beam functions were used as the assumed mode shapes [15].

The analyses are carried out to evaluate the noise reduction at x/a y/b $z/d = 0.5$. Figures 2.2 to 2.4 present a comparison of the noise reduction characteristics obtained using PCF and BCF, for different values of plate and cavity damping ratios (0.02, 0.05, 0.1). The noise reduction is presented as a function of the normalized frequencies, $\beta = \omega/\omega_{11}$, where the ω_{11} represents the fundamental natural frequency of the plate. The figures reveal a good agreement between the results obtained using plate functions and beam functions. Figure 2.2 illustrates sharp drop in noise reduction corresponding to the plate modes (1,1), (1,3) and (3,1), (3,3), (1,5) and (5,1), (3,5) and (5,3), and (5,5), and the cavity modes (0,0,1) and (0,0,2). A comparison of the results obtained using BCF and PCF reveals a maximum error of 2-3 dB at low value of plate and cavity damping ratios. The difference between the

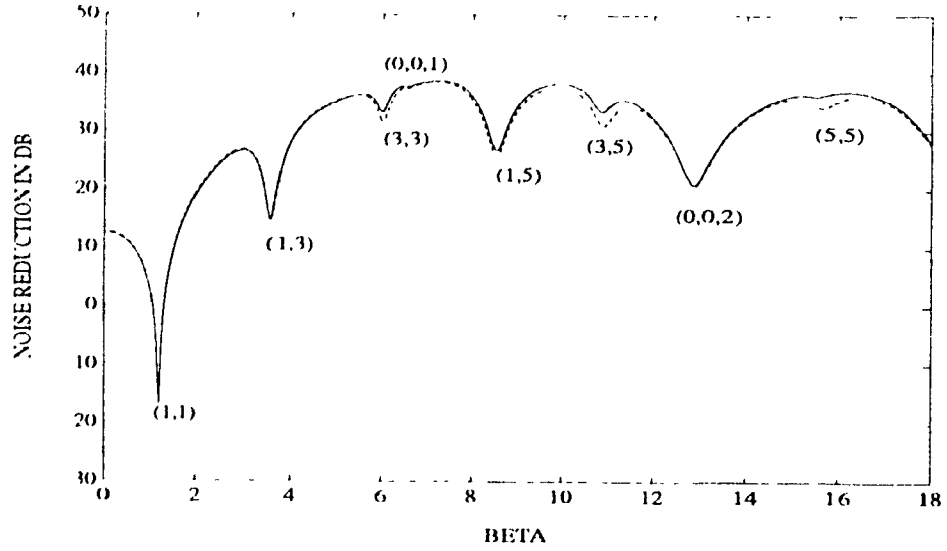

Figure 2.2: Comparison of NR obtained by PCF and BCF ($\zeta_{mn} = \gamma_{ijk} = 0.02$) ($x/a = y/b = z/d = 0.5$; $\zeta_{mn} = \gamma_{ijk} = 0.02$; — PCF - - - BCF)

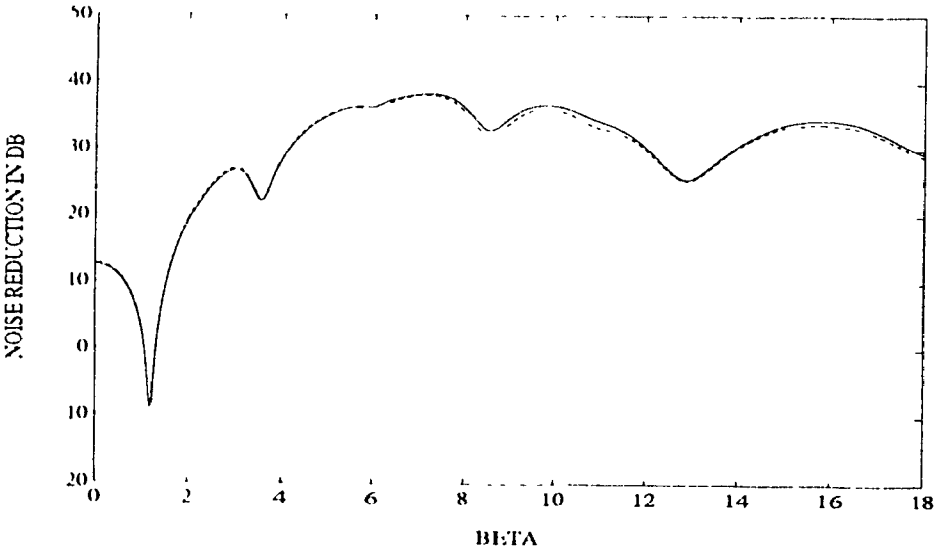

Figure 2.3: Comparison of NR obtained by PCF and BCF ($\zeta_{mn} = \gamma_{ijk} = 0.05$) ($x/a = y/b = z/d = 0.5$; $\zeta_{mn} = \gamma_{ijk} = 0.05$; — PCF - - - BCF)

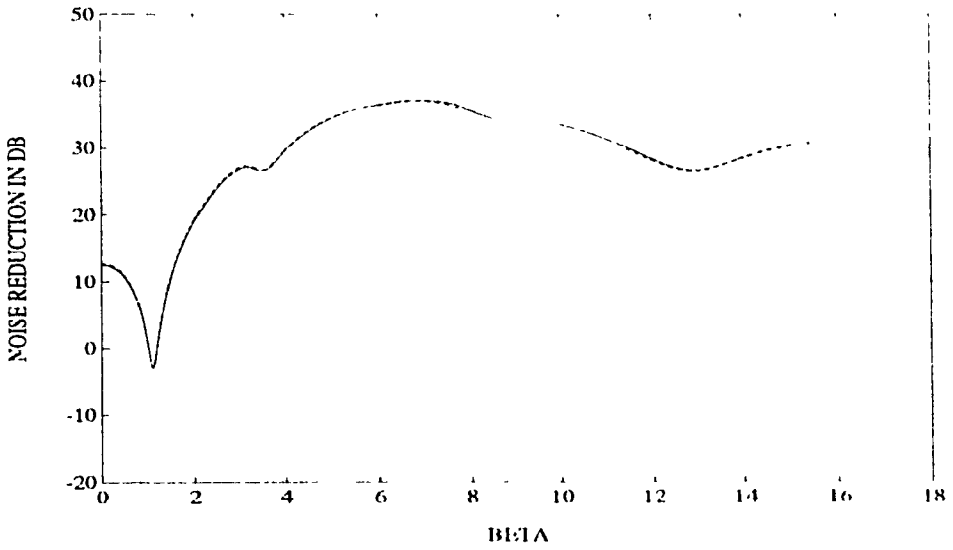

Figure 2.4: Comparison of NR obtained by PCF and BCF (ζ_{mn} γ_{ijk} 0.1) ($x/a = y/b = z/d = 0.5$; $\zeta_{mn} = \gamma_{ijk} = 0.1$; PCF - - - BCF)

results tend to decrease when damping ratios are increased, as seen in Figures 2.3 and 2.4. Since, it has been established that plate characteristic functions represent the plate modes more accurately [13,14], the noise reduction estimated using PCF can thus be considered more accurate. Further, the computational time required to estimate the NR using PCF is considerably smaller than that required with the use of BCF. The excessive computational time required by the BCF is attributed to their use in the Rayleigh-Ritz method to represent the plate modes. For example, if one uses 36 terms in the summation in Rayleigh-Ritz method, then the computational time using BCF is 36 times the computational time taken by the use of PCF.

2.3.3 Effect of Various Structural and Geometrical Parameters

The influence of various structural and fluid parameters on the noise reduction characteristics of the cavity-backed flexible panel is investigated using PCF to define the plate modes. The strong influence of structural and cavity damping on the

noise reduction is evident from Figures 2.2 to 2.4. The structural and cavity damping properties are introduced as "modal damping", with identical values of ζ_{mn} and γ_{ijk}. Figure 2.5 further illustrates the influence of damping on the noise reduction characteristics. At low excitation frequencies, an increase in damping tends to reduce the response only at the resonant frequencies of the coupled system. At higher excitation frequencies (above 500 Hz), however, an increase in damping deteriorates the NR characteristics, except near the system resonant frequencies associated with the cavity mode.

The cavity pressure and thus the NR are strongly related to the location of the point of interest inside the cavity. The noise reduction analysis are performed to compute the response at various locations inside the cavity. Figure 2.6 illustrates the variation in NR in the (x, y) plane located at $z/d = 0.5$. While the response at low frequencies does not vary with the location in the (x, y) plane, an increased NR closer to the walls can be observed at higher excitation frequencies. Figure 2.7 illustrates the variation in NR at different location along z axis. from the figure it is evident that NR is maximum at the mid-location of the cavity ($z/d = 0.5$), and minimum near the panel ($z/d = 0.0$). At an excitation frequency near the cavity mode, however, the changes in NR along z-axis are observed to be insignificant.

The influence of physical size of the cavity on NR are further investigated and presented in Figures 2.8 and 2.9. The effect of the depth of the cavity on noise reduction computed at $x/a = y/b = z/d = 0.5$ is shown in Figure 2.8. The cavity depth greatly influences the fundamental resonant frequency of the system, and an increase in the cavity depth yields improved NR at lower excitation frequencies. The fundamental natural frequency of the nominal plate-cavity system, considered in this study ($d/a = 1.0$), is approximately $1.12\omega_{11}$. The first natural frequency of the system is 1.25 times the fundamental plate natural frequency, ω_{11}, when the cavity depth is reduced by 50 percent. When the cavity depth was increased to $d = 2.0a$ the first natural frequency is found to be $1.03\omega_{11}$. A shallow cavity tends to increase the

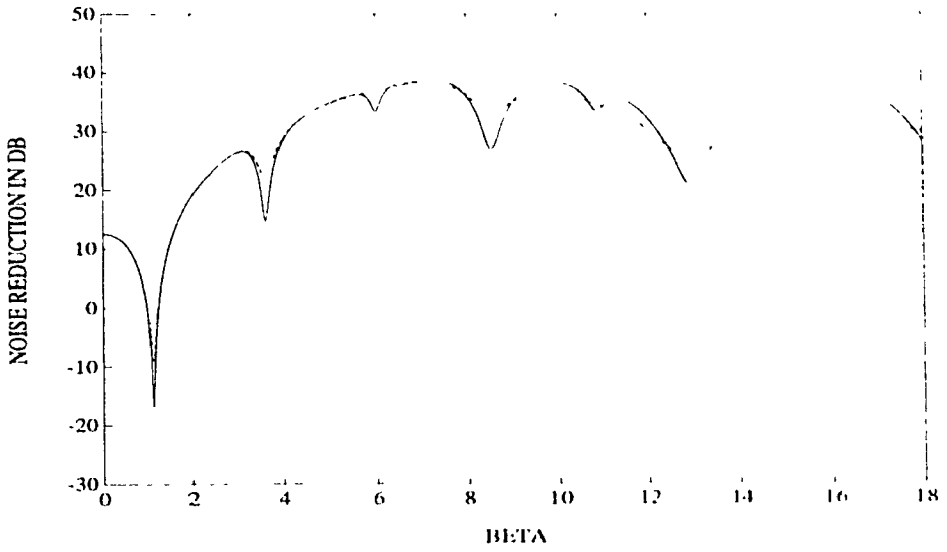

Figure 2.5: NR against frequency for different damping ratios ($x/a = y/b = z/d = 0.5$; $\zeta_{mn} = \gamma_{ijk} = 0.02$, - ζ_{mn} γ_{ijk} 0.05, ... $\zeta_{mn} = \gamma_{ijk} = 0.1$)

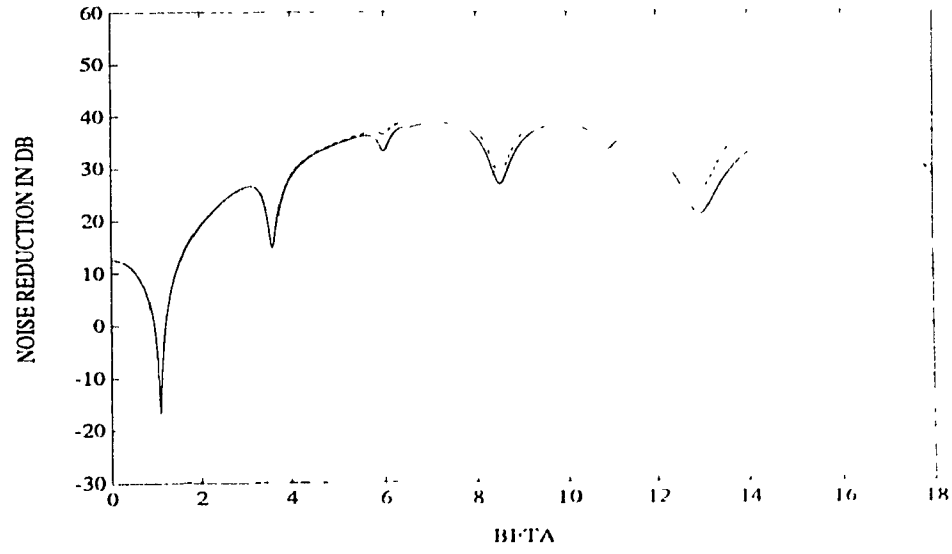

Figure 2.6: NR against frequency at different positions ($z/d = 0.5$, — $x/a = y/b = 0.5$, - - - $x/a = y/b = 0.33$, ... x/a y/b 0.25)

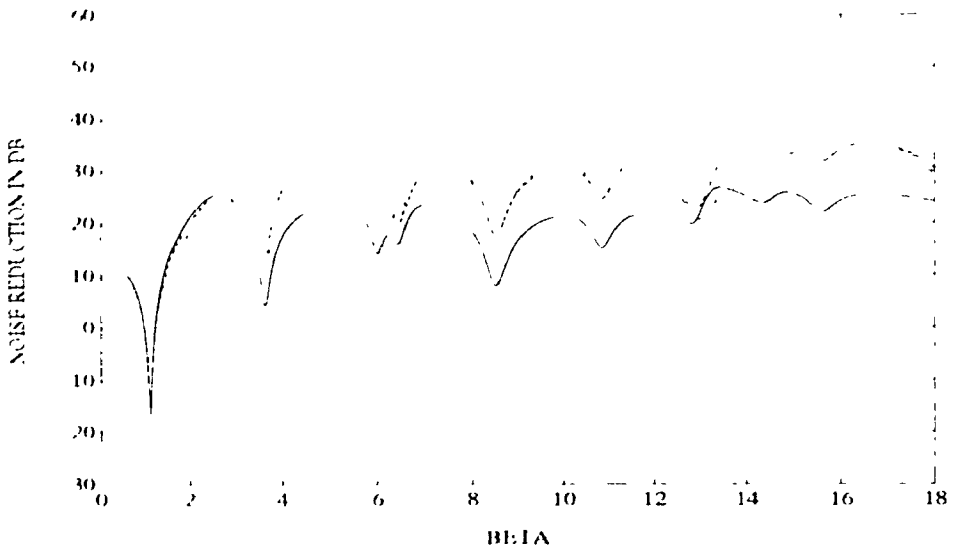

Figure 2.7: NR against frequency at different depths
(x/a y/b - 0.5; ζ = 0.02, z/d = 0.0, - - - z/d = 0.25, ... z/d = 0.5, -.-.- z/d 0.75)

system stiffness at lower frequencies and yields poor noise reduction (frequencies up to ω - $8.0\omega_{11}$). A deeper cavity increases the noise reduction at lower frequencies.

The noise reduction computed at the mid-point of the cavity (x/a = y/b = z/d = 0.5), for different sizes of the cavity, are presented in Figure 2.9. The NR of the cavity panel system are presented as a function of excitation frequency in Hz. The fundamental natural frequency of the plate and the plate-cavity system decreases as the plate size increases. The figure shows reduced vibration of the plate and hence better noise reduction when the cavity size is increased. For cavity size a b d = $2.0m$ the NR is found to be more or less constant at frequencies above 200 Hz. Even though the noise amplification in the case of large cavity is quite high at very low frequencies, in the audio range of frequencies it gives better noise reduction as compared to the noise reduction in smaller cavity.

Figure 2.10 illustrates the effect of plate thickness on the noise reduction computed at mid point of the cavity. The NR characteristics are computed for three

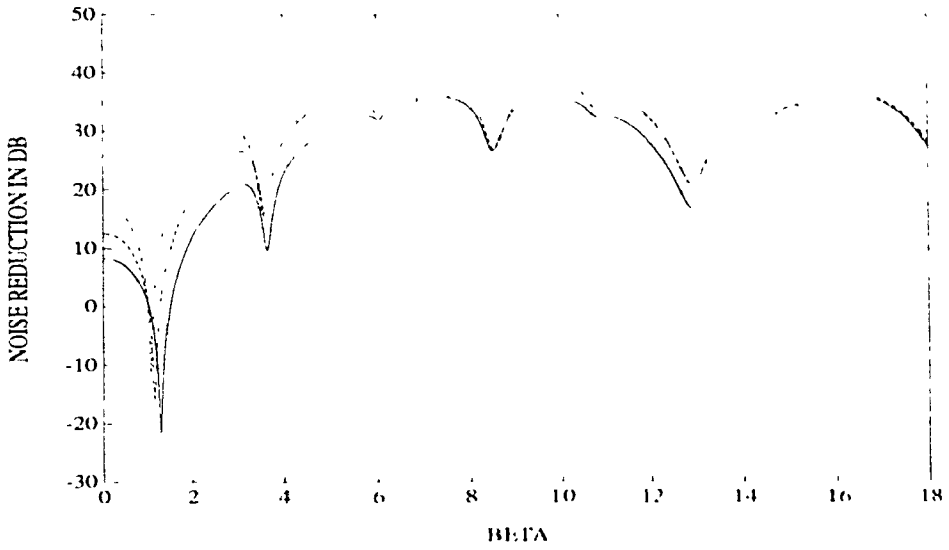

Figure 2.8: NR against frequency for cavities of different depth
($x/a = y/b = z/d = 0.5$; $d/a = 0.5$, - - $d/a = 1.0$, ... d/a 1.5, . . d/a 2.0)

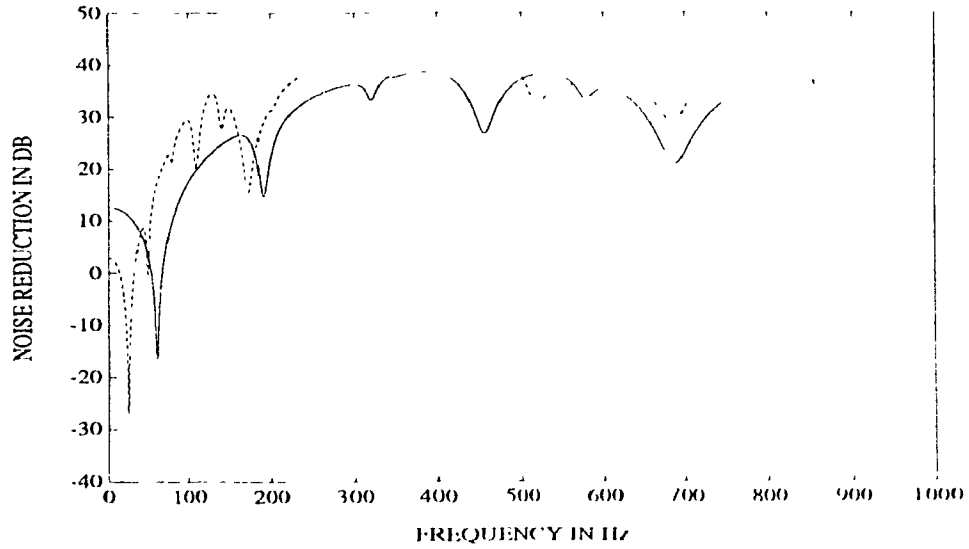

Figure 2.9: NR against frequency for different cavity sizes
($x/a = y/b = z/d = 0.5$; $a = b = d = 0.5m$, - a b d $1.0m$, . . .
$a = b = d = 2.0m$)

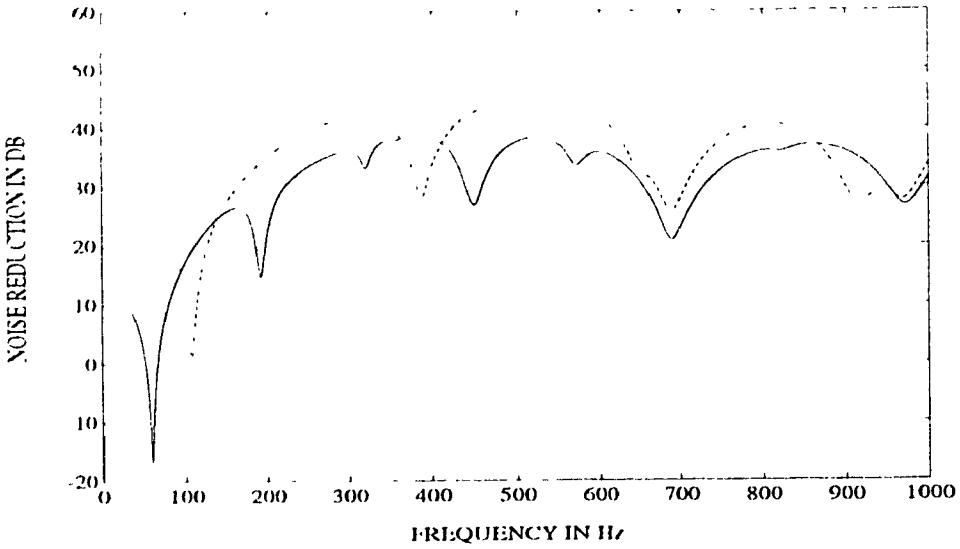

Figure 2.10: NR against frequency for different plate thickness
($x/a = y/b = z/d = 0.5$; — $h = 0.0015m$, - - - $h = 0.003m$, ... $h = 0.006m$)

values of plate thickness, $h = 0.0015m, 0.003m, 0.006m$. The plate natural frequency is directly proportional to the plate thickness and hence doubling of the plate thickness doubles the natural frequency. The figure also shows that as the plate thickness increases the ratio of first system natural frequency to the corresponding fundamental plate natural frequency decreases. The noise reduction is observed to be increased with the plate thickness throughout the frequency range.

The generalized cavity and external forces are related to the mass density of the plate, as described in Equation (2.25) and (2.26). The plate density thus influences the noise reduction, and the NR can be related to a proportional function of $20 \log \rho_p$. Doubling of the plate density is thus expected to yield a 6 dB increase in the NR. The corresponding reduction in the plate natural frequencies caused by an increase in the density, however, tends to increase the transmitted noise. The overall influence of the plate density on the NR response is illustrated in Figure 2.11. The increase in plate density increases the NR corresponding to higher plate modes and the cavity mode frequencies. The increase in NR at the cavity mode frequency, specifically, is quite significant. The NR can also be related to the air density in a similar manner. The

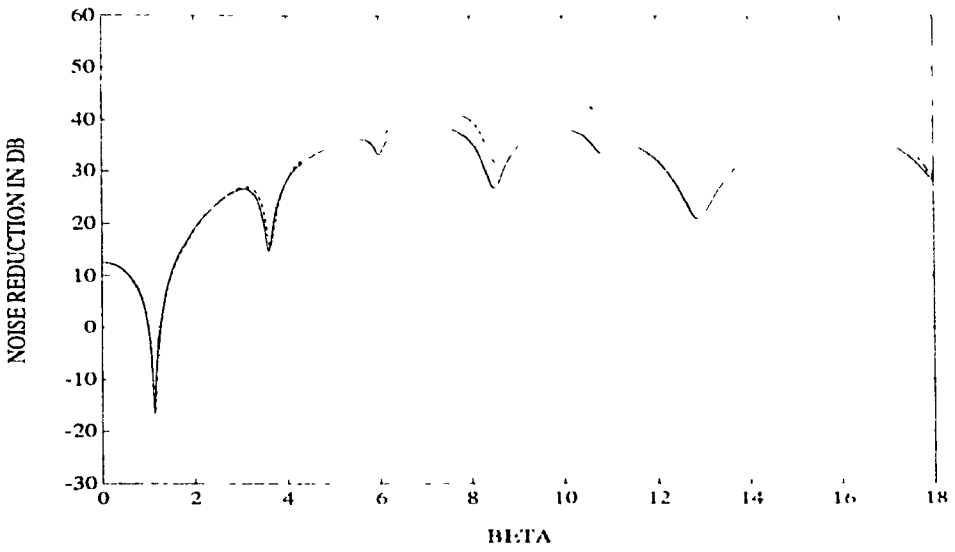

Figure 2.11: NR against frequency for different plate densities
($x/a = y/b = z/d = 0.5$; --- $\rho_p = 2700 kg/m^3$, - - - $\rho_p = 5400 kg/m^3$)

NR is proportional function of $-20 \log \rho_a$. Figure 2.12 illustrates the influence of fluid density of the NR response computed at mid-location of the cavity. The fundamental natural frequency of the coupled system approaches nearly $1.3\omega_{11}$, when the fluid density is increased to $2.42 kg/m^3$. The NR in the entire frequency range decreases with an increase in the fluid density, as shown in Figure 2.12.

The influence of plate boundary conditions on NR of the plate cavity system is further investigated. Figure 2.13 presents the NR response at the mid point of the cavity with simply supported and clamped plates plotted against excitation frequency in Hz. The figure shows that a clamped plate yields better noise reduction almost throughout the frequency range. The boundary condition affects the plate controlled system natural frequencies. The first system natural frequency with simply supported boundary condition is found to be 45 Hz, which is 1.5 times the fundamental plate natural frequency with simply supported condition. A similar analysis on the cavity with clamped plate shows that the first natural frequency of the system is 59 Hz which is 1.1 times the fundamental plate natural frequency. The system natural frequency controlled by cavity, however, does not change with the plate boundary condition.

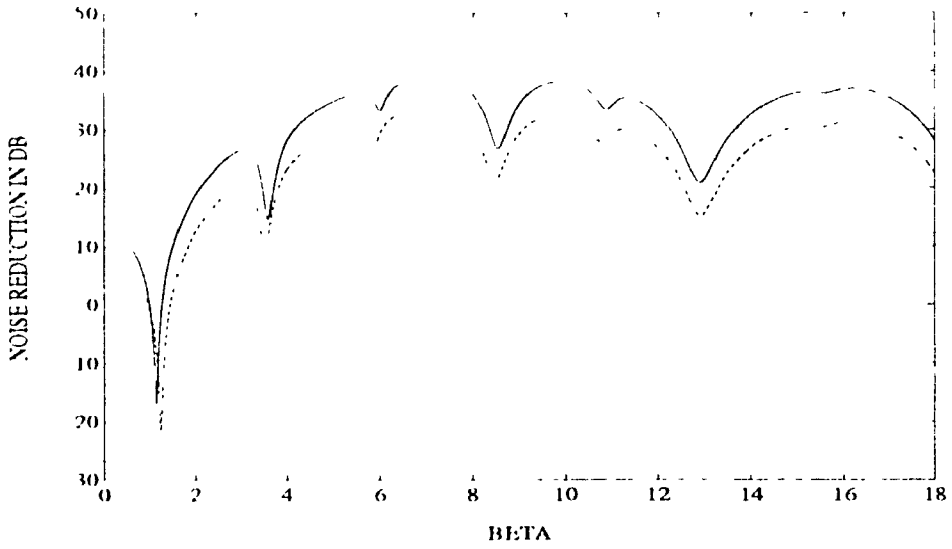

Figure 2.12: NR against frequency for different cavity fluid densities
($x/a = y/b = z/d = 0.5$; $\rho_a = 1.21 kg/m^3$, - - - $\rho_a = 2.42 kg/m^3$)

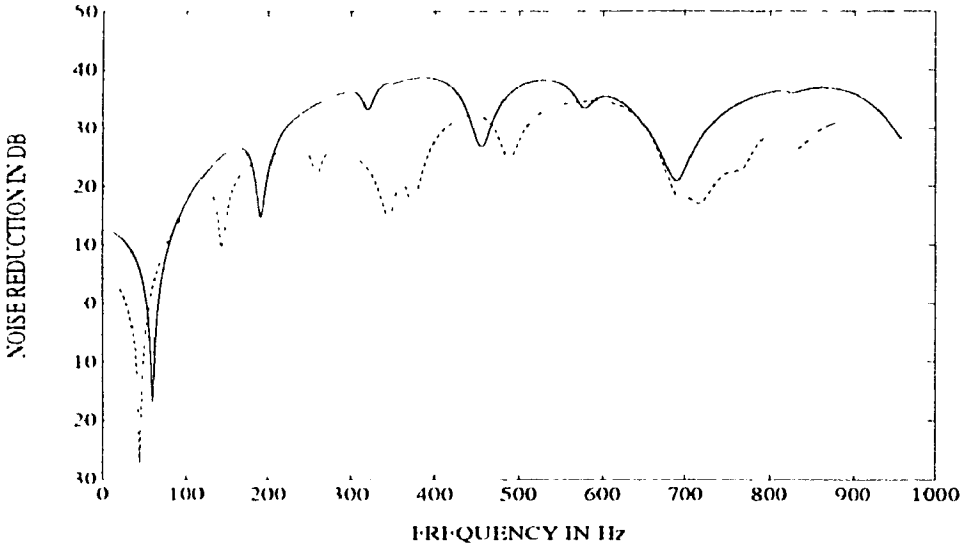

Figure 2.13: NR against frequency for different plate boundary conditions
($x/a = y/b = z/d = 0.5$; — Clamped, - - Simply Supported)

2.4 Summary

An analytical model of the cavity-panel system is developed using modal coupling analysis. Computer simulations are performed to evaluate the noise reduction through the cavity backed flexible plate. The response characteristics, computed using PCF, are compared to those evaluated through BCF in Rayliegh Ritz method. A parametric study is performed to establish the influence of various structural and fluid parameters on the NR characteristics. The analytical model developed in this section is validated through laboratory experimentation in the following chapter.

Chapter 3

An Experimental study of the Plate-Cavity System

3.1 Introduction

The sound transmission loss through a cavity backed flexible plate has been evaluated using the modal coupling analysis. The results of the study, presented in chapter 2, revealed that maximum transmission of sound occurs at the system natural frequencies, and that the modal response of the system can be classified into two modes: (i) cavity controlled modes; (ii) panel controlled modes. A cavity controlled mode is defined as one which has most of its energy stored in the cavity sound field, while a panel controlled mode is defined as one which has most of its energy stored due to panel-vibration The natural frequencies corresponding to cavity controlled modes are close to natural frequencies of the rigid cavity and the natural frequencies corresponding to the plate controlled modes are close to the natural frequencies of the plate. The first natural frequency of the coupled system considered in this study was observed to be associated with the panel controlled mode. This natural frequency, however, varied with changes in the cavity depth and the boundary conditions.

The above analytical findings and the model, however, need to be validated. the

model validation can be realized through measurements of sound transmission loss in a controlled acoustical chamber. The model refinements may then be performed upon comparison of measured response to the model response. A rectangular enclosure with a clamped flexible plate forming one of its walls was fabricated and measurements were performed to analyze the noise transmission loss. The experimental results are compared to the analytical results to demonstrate the validity of the model and the analytical techniques. In view of the lack of an acoustic chamber and ideal clamping condition, the emphasis, however, is placed on a limited validation. The limited validation involved the comparison of analytical and experimental results in a qualitative manner.

3.2 Measurement of Sound Transmission Loss

The sound transmission loss may be measured using either sound pressure or sound intensity levels. Sound intensity describes the magnitude and direction of net flow of acoustic energy at a given position. This is in contrast to the sound pressure which is a scalar quantity. It can be shown that in a medium without mean flow, the intensity vector equals the time averaged product of the instantaneous pressure and the corresponding instantaneous particle velocity at the same position[40]:

$$\vec{I} = \overline{p(t) \cdot \vec{u}(t)} \tag{3.1}$$

where $\vec{I}$ is the sound intensity vector, $p(t)$ is the instantaneous pressure, $\vec{u}(t)$ is the instantaneous particle velocity and the 'over bar' characterizes the time average of the product. The intensity vector in a direction r can be expressed as:

$$\vec{I}_r = \overline{p(t) \cdot \vec{u}_r(t)} \tag{3.2}$$

where $u(t)$ is the instantaneous particle velocity in direction r. The primary advantage of the sound intensity is that it distinguishes between the active and reactive components of a sound field, while the sound pressure measurement does not make this distinction. A sound intensity measurement system responds only to the active part of the sound field, while the reactive part of the sound field is rejected.

A plane wave propagating in a free field is an example of a purely active sound field. It can be shown that the magnitude of the intensity in such a free field is given by[40]:

$$|I| = p_{rms}^2/\rho c \tag{3.3}$$

where ρc is the impedance of the medium and p_{rms} is the root mean square (rms) pressure. From the definitions of sound pressure level (SPL) and sound intensity level (SIL), it is evident that the SPL is numerically equal to SIL in a pure free field.

In a purely reactive sound field the sound intensity is zero, which means that there is no net flow of sound energy. An ideal standing wave is an example of pure reactive field. In a standing wave, there exists a 90° phase difference between the particle velocity, u, and the pressure, p. The pressure has its maximum values at the walls where the particle velocity is zero. Another example of a purely reactive sound field is a diffused field, where, by definition, the energy flow at a given position is identical in all directions. The net flow of sound energy at any point and thus the sound intensity is zero.

In a general sound field, however, SIL is neither equal to SPL nor equal to zero. The SIL and SPL are related through the local sound pressure-intensity index, defined as:

$$\delta_{PI} = L_P - L_{|I|} \tag{3.1}$$

where δ_{PI} is referred to as the local sound-pressure intensity index, L_P is the sound pressure level and $L_{|I|}$ is the magnitude of the sound intensity level at the point.

3.3 Experimental Apparatus and Measurement Procedures

The panel-cavity system used in the experiment was a rectangular wooden box with five rigid walls and one flexible panel on one side. The box was fabricated by glueing together 5 pieces of $31.5mm$ thick wood fibre board panels. The thickness of $31.5mm$ was obtained by glueing panels of $19mm$ and $12.5mm$ together. The depth of the cavity could be changed from zero to $1.0m$ by sliding the backwall of the enclosure. Weather strips were used to prevent possible leakage of sound energy through the edges of the backwall. A $1.5mm$ thick aluminium sheet was used as the flexible plate on one side of the box. The plate was first clamped between two $19mm \times 25.4mm$ metallic strips using 10 screws on each side. The panel assembly was glued onto the box, around the edges, using a bonding cement to achieve the boundary conditions close to the clamped condition. The coordinates and the internal dimensions of the enclosure are illustrated in Figure 3.1.

An external sound field was generated using a speaker located in front of the horizontally placed test enclosure, with the flexible wall facing the speaker. Both speaker and test box were placed in the laboratory with a horizontal separation of 1m. The entire experimental apparatus was placed in a common laboratory environment where the background noise level was measured in the $56 - 58dB$ range. The speaker was driven by the signal generator built in to the B & K 2035 signal analyzer, which

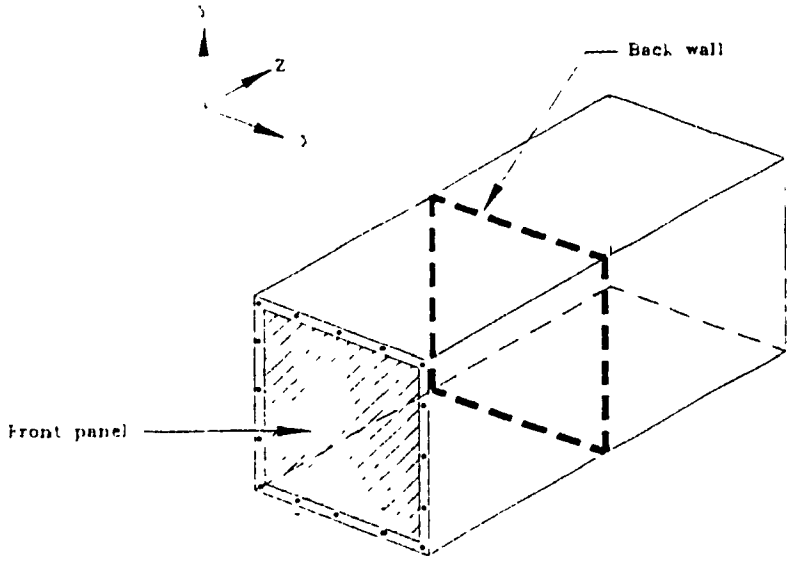

Figure 3.1: Geometry of the test enclosure

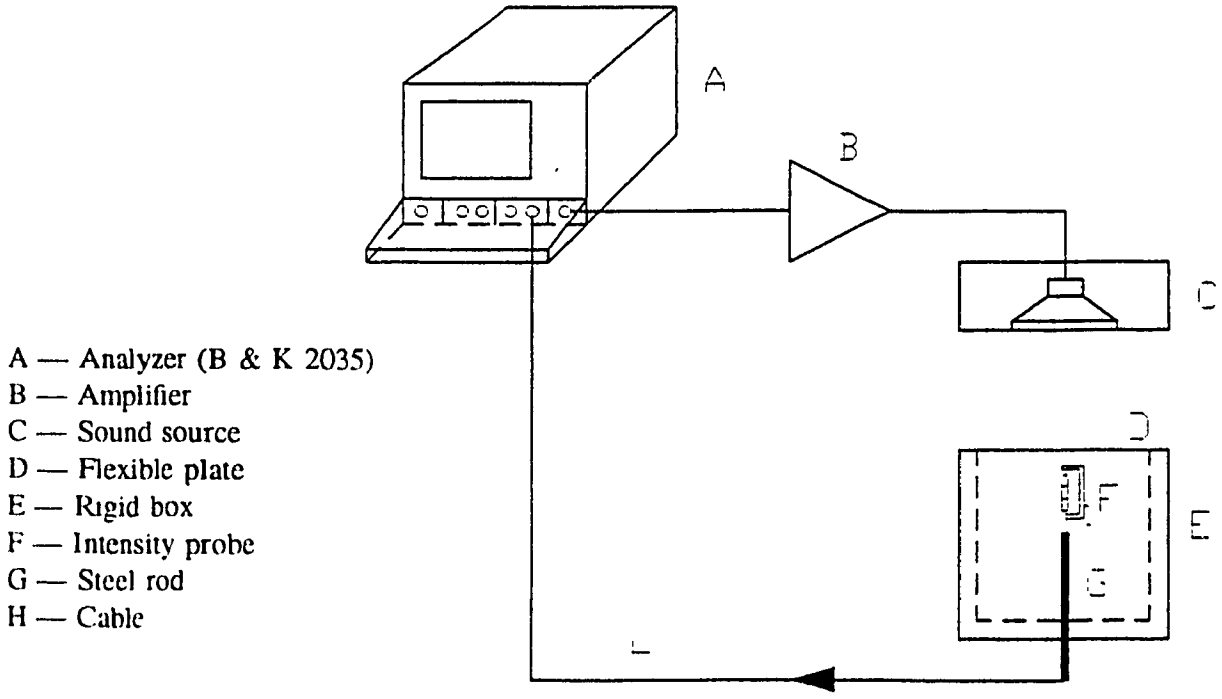

Figure 3.2: Schematic of the experimental apparatus

was amplified using an external amplifier. Tests were performed using 'white noise' excitation in the frequency range of 30-1000Hz and pure tones at different discrete frequencies ranging from 15Hz to 1000Hz. The amplifier gain was held constant during all measurements in order to maintain a constant level of incident sound pressure. Figure 3.2 illustrates the schematic of sound generation system.

The external sound and the transmitted sound levels were measured using a sound intensity probe comprising of two microphones (B & K type 1181 with 50mm spacer) placed $50mm$ apart. In order to measure the internal cavity sound pressure and intensity levels, intensity probe was attached to the end of a slender aluminium rod, which was inserted into the cavity through small holes drilled on the back wall. The movable backwall was designed with a total of 9 holes to acquire the measurements at different locations within the cavity. The holes, not in use, during a measurement, however, were blocked. Both intensity and pressure levels were measured at various points. The measurements were performed over a 3×3 grid at $z/d = 0.25, 0.5, 0.75$ inside the box.

3.4 Results and Discussion

3.4.1 Natural Frequency of the Plate

Vibration tests were performed to determine the fundamental natural frequency of the flexible plate and to verify the validity of the clamped boundary conditions. An accelerometer, weighing 0.00125kg, was attached to the plate, and the plate was excited with an impact force using a hammer. The input force and response acceleration signals were analyzed to yield the frequency response function of the vibrating plate using the B & K dual channel signal analyzer. The measured frequency response function (not shown), when the plate was clamped using 6 screws on each side, showed that the fundamental natural frequency of the plate was 30 Hz. This

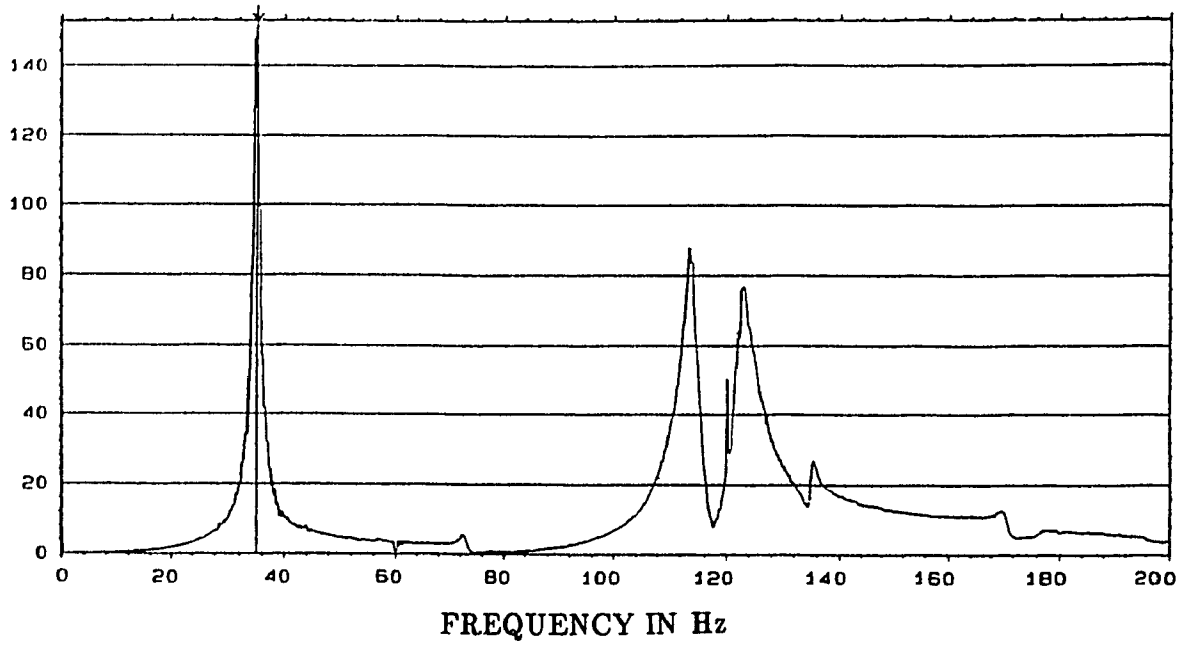

Figure 3.3: Measured frequency response function of the flexible plate

frequency is very close to the theoretical fundamental natural frequency of the plate with simply supported boundary condition (29.25 Hz) and very far from the theoretical natural frequency of a clamped plate (53.35 Hz). Figure 3.3 illustrates the frequency response function of the plate, when the number screws used for clamping the plate was increased to 10 on each side. From the frequency response function it is clear that the measured fundamental natural frequency of the plate is 35Hz. The measured natural frequency is still considerably lower than the theoretical one for the clamped boundary condition. This discrepancy in natural frequencies can be attributed to the inability to achieve the clamped boundary conditions. The boundary conditions of the experimental plate may be characterized by a flexible end condition with rotational motion. The analytical model of noise reduction thus needs to be modified by assuming a flexible boundary condition.

3.4.2 Measurement and Analysis of Noise Transmission Loss

The sound pressure sensors and the intensity probe need to be calibrated prior to the measurements. The calibration procedure is described in Appendix C.

The horizontal distance between the sound source and the plate was selected to achieve nearly uniform external sound pressure at the plate surface. The speaker was driven to generate white noise sound pressure. It should be noted that all the measured data are average of 5 measurements. The sound levels and intensity levels were measured at the surface of the flexible wall of the enclosure and compared with those measured at the same location with the enclosure removed. The data was analyzed to verify assumption of spatially uniform pressure distribution. Figures 3.4 and 3.5 illustrate the SPL, measured at different locations near the wall with and without the flexible plate, respectively. The figures clearly demonstrate near uniform incident pressure distribution. The contour plots of corresponding SIL measured at the wall surface with and without the plate are illustrated in Figures 3.6 and 3.7, respectively. A comparison of Figures 3.4 and 3.5 reveals that the existence of plate in the way of sound wave does not affect the incident sound pressure level distribution. The sound intensity level, however, reduces when plate is present in the path of sound, as shown in Figures 3.6 and 3.7. This difference is attributed to the directional property of the sound intensity, where the reflected sound waves act against the incident waves leading to lower intensity.

The sound pressure and intensity spectra of the incident white noise, measured at the center of the plate with and without the plate cavity system are depicted in Figures 3.8 to 3.9, respectively. The spectra of the measured pressure and intensity levels, measured without the plate are observed to be reasonably close to 'white noise'. The presence of the plate, however, changes the spectrum as seen in Figure 3.8 and 3.9. The spectrum obtained without the plate is considered as the true incident pressure for evaluating the noise reduction characteristics.

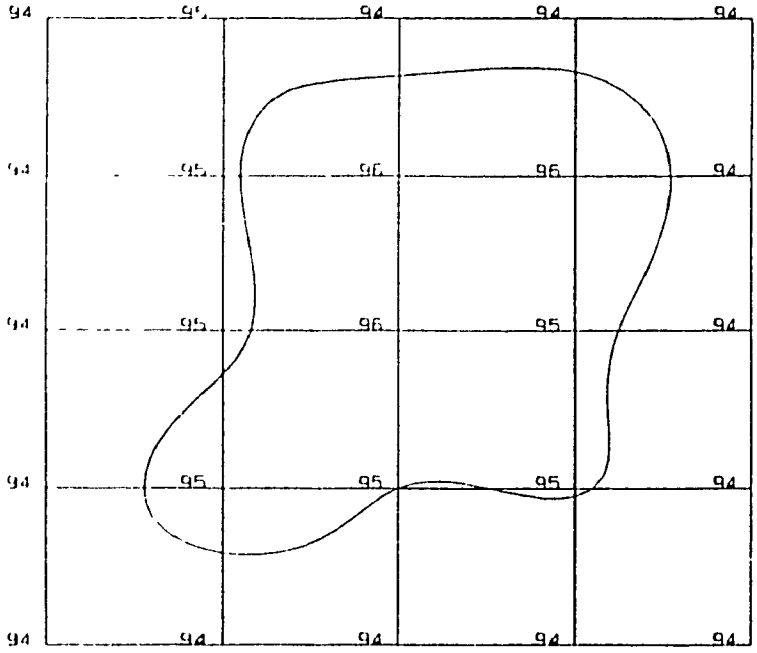

Figure 3.4 Contour map of the external sound pressure measured near the plate surface
(weighing: linear, frequency range: 30-1000Hz)

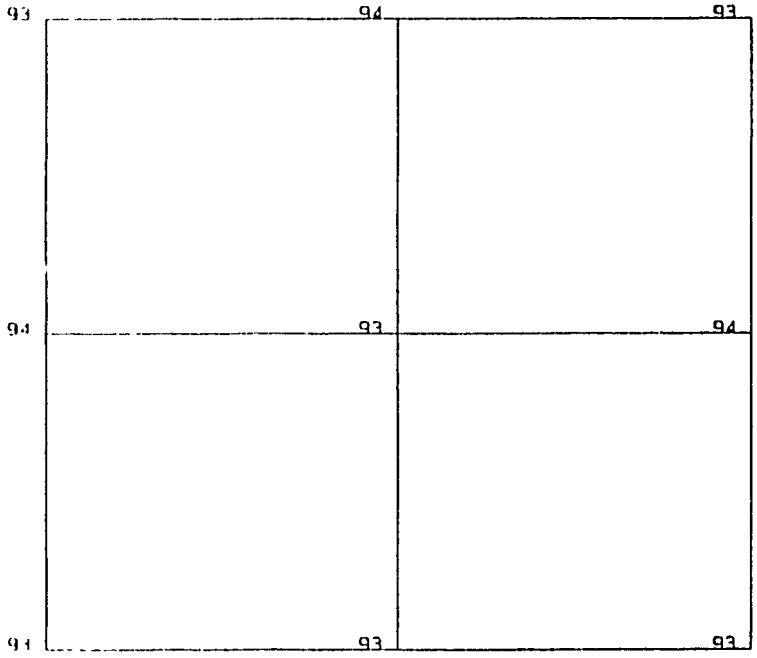

Figure 3.5: Contour map of the external sound pressure at the location, when plate-cavity system is removed
(weighing: linear, frequency range. 30-1000Hz)

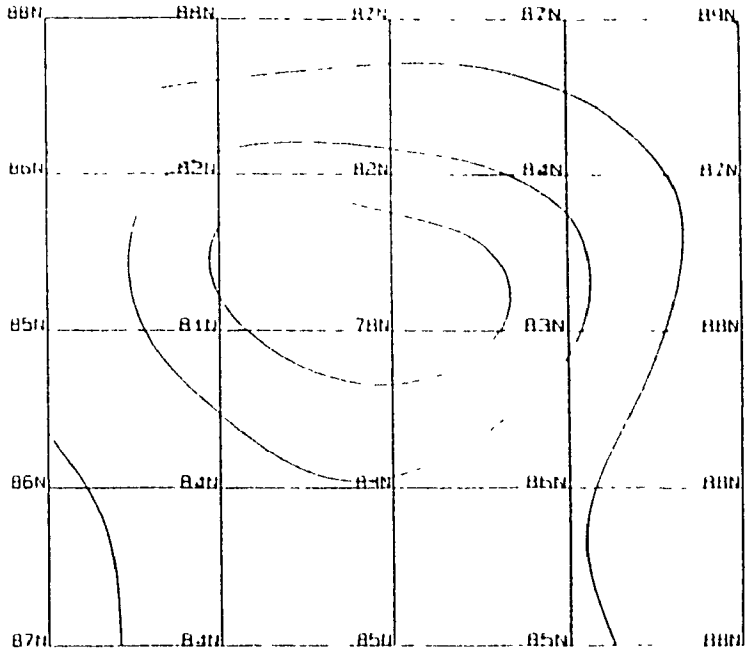

Figure 3.6: Contour map of sound intensity I_z near the plate surface (weighing: linear, frequency range: 30 1000Hz, mic spacer: 50 mm)

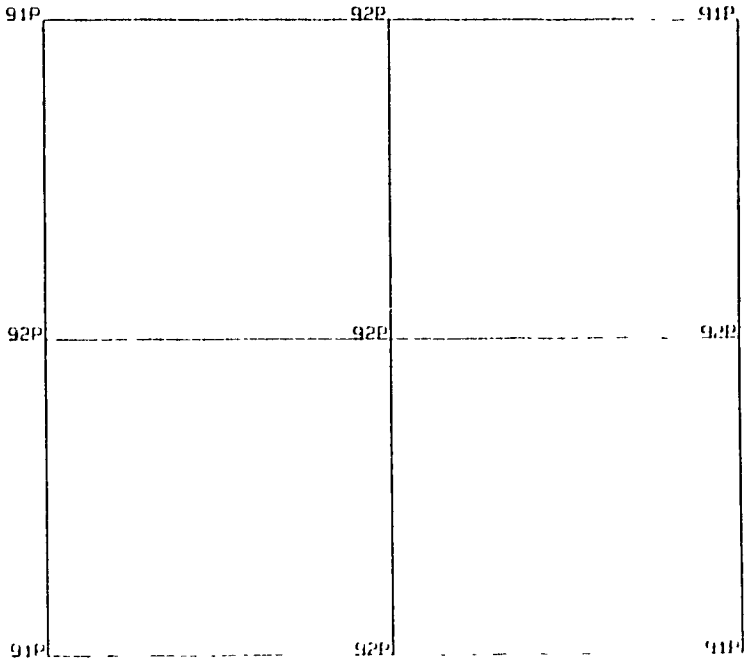

Figure 3.7: Contour map of the external sound intensity at the location, when plate cavity system is removed
(weighing: linear, frequency range: 30-1000Hz, mic spacer: 50 mm)

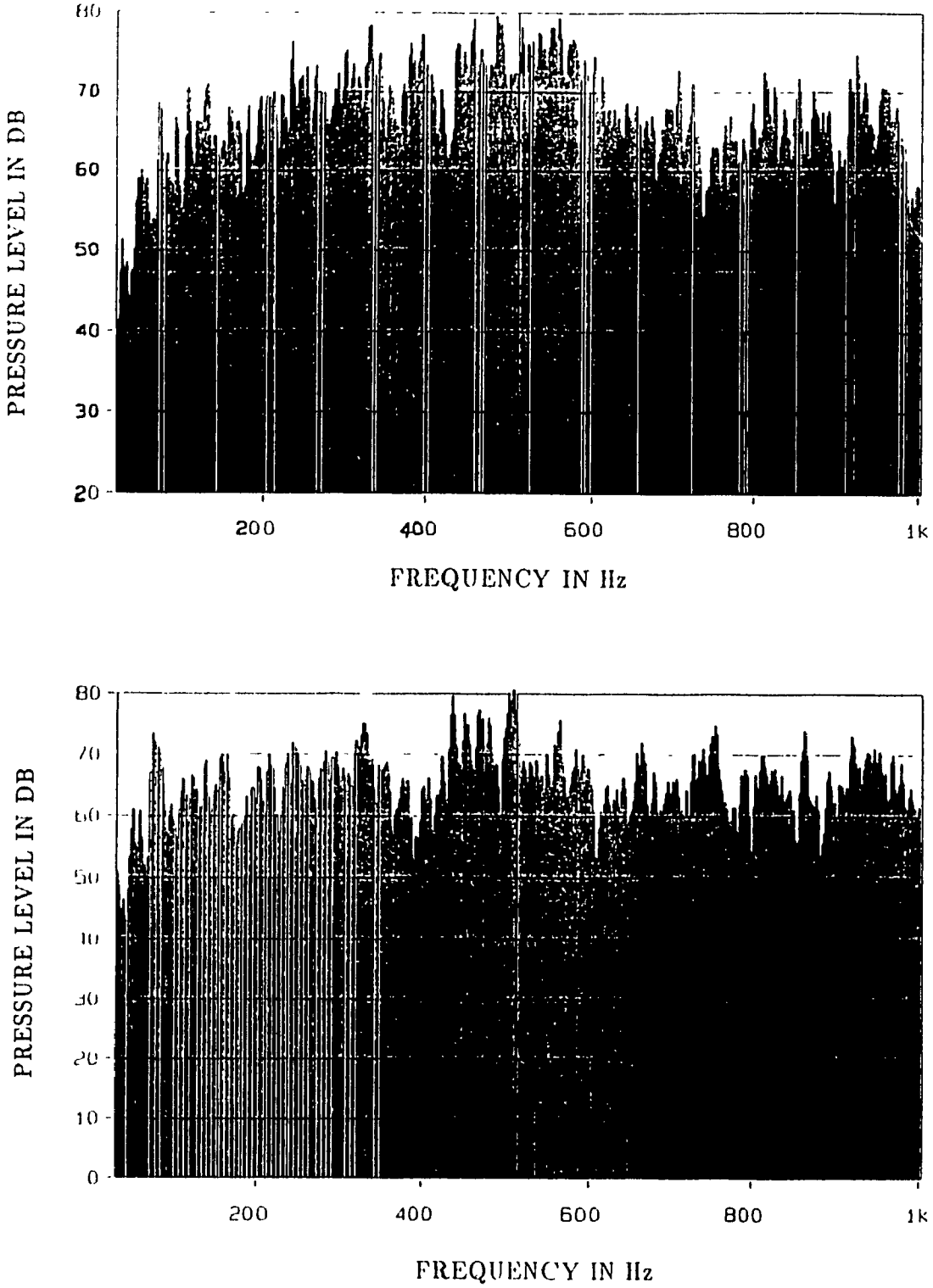

Figure 3.8: Sound pressure spectrum measured at the plate surface ($x/a = y/b = 0.5$) with and without the test enclosure
(weighing: linear, frequency range: 30-1000Hz)

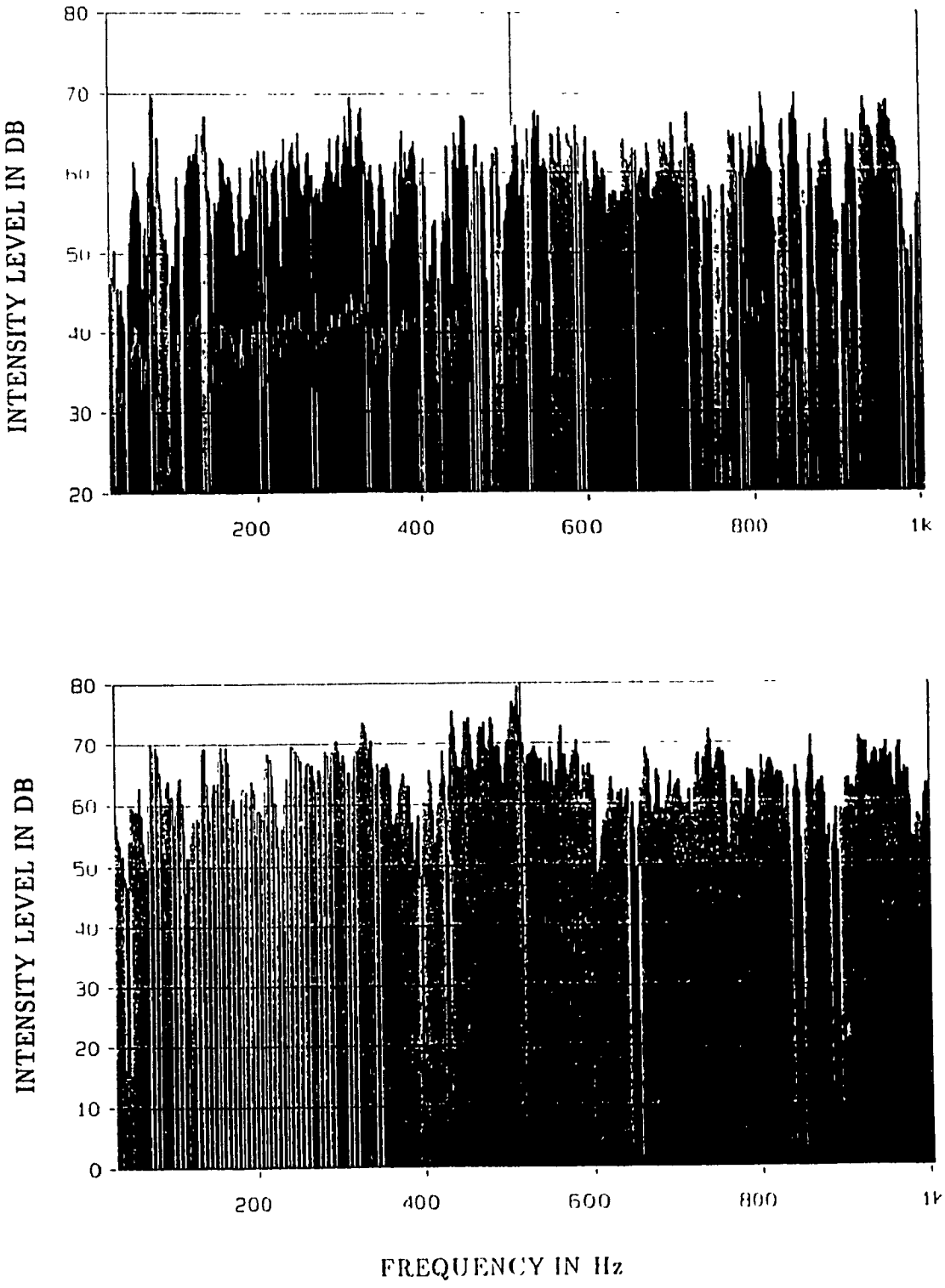

Figure 3.9: Sound intensity spectrum measured at the plate surface ($x/a \quad y/b \quad 0.5$) with and without the test enclosure
(weighing: linear, frequency range: 30-1000Hz, mic spacer: 50 mm)

A comparison of Figures 3.5 and 3.6 illustrates a 2dB difference between the pressure and intensity levels at each location of the flexible plate, when the plate with the box has been removed from that place. This difference may be explained by considering the theory of sound intensity, as described earlier in section 3.2. The local pressure-intensity index, δ_{PI}, the difference between the sound pressure level and the magnitude of the intensity level, is zero in a free field ($L_P = L_{|I|}$) and equal to L_P ($L_{|I|} = 0$) in a reactive field. In a reflected sound field, however, δ_{PI} can assume any value and be even negative ($L_{|I|} > L_P$). The negative δ_{PI} value could be caused by either system errors or the presence of standing waves in the sound field. The standing wave pattern formed indoors or between parallel surfaces, may lead to local pressure-intensity index of any value between plus or minus half of the standing wave ratio expressed in decibels and system errors may or may mot be associated with the measurements[40]. Guy and Li[41] have discussed the possible causes of negative values of δ_{PI} in a standing wave pattern. The pressure and intensity levels measured at different points within the laboratory room along the z direction revealed the existence of a standing wave pattern in the room where the experiments were conducted. A difference between the measured pressure and intensity levels is thus expected, depending upon the coordinates where measurement is performed.

The sound pressure and intensity levels at different points just outside the back-wall of the enclosure are depicted in Figure 3.10 and 3.11, respectively. The pressure level contour plot shows that the pressure levels at this location are nearly 3-4 dB less than the incident pressure levels, indicating the possibility of leakage of sound through the edges of the backwall. The negative values of the sound intensity levels shown in Figure 3.11 indicate that sound field near backwall is caused by the reflections from the room walls. Sound pressure and intensity levels were also measured outside the side walls to ensure the rigidity of the wooden walls. The measured intensity levels in different directions showed that the sound transmission through the wooden walls was very small, hence ensuring the rigidity of the walls.

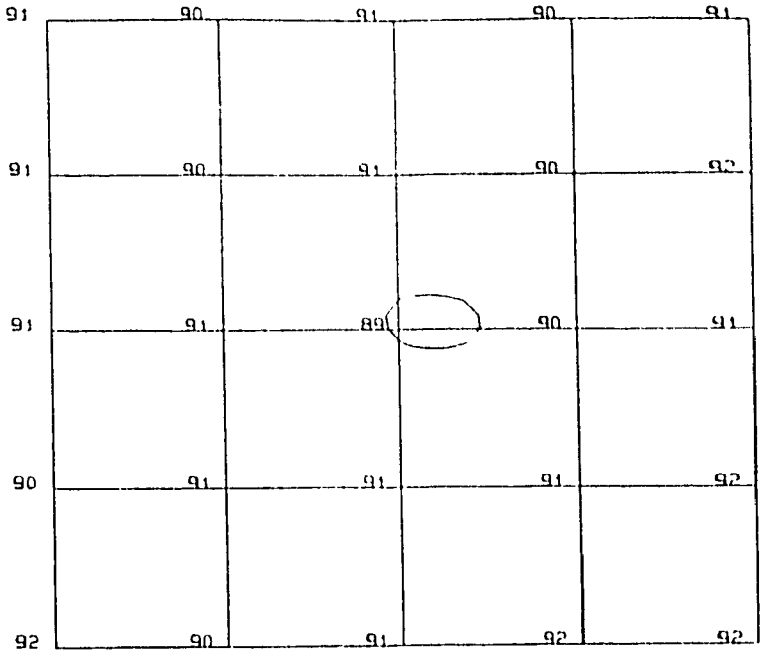

Figure 3.10: Contour map of the sound pressure measured outside the backwall (weighing: linear, frequency range: 30-1000Hz)

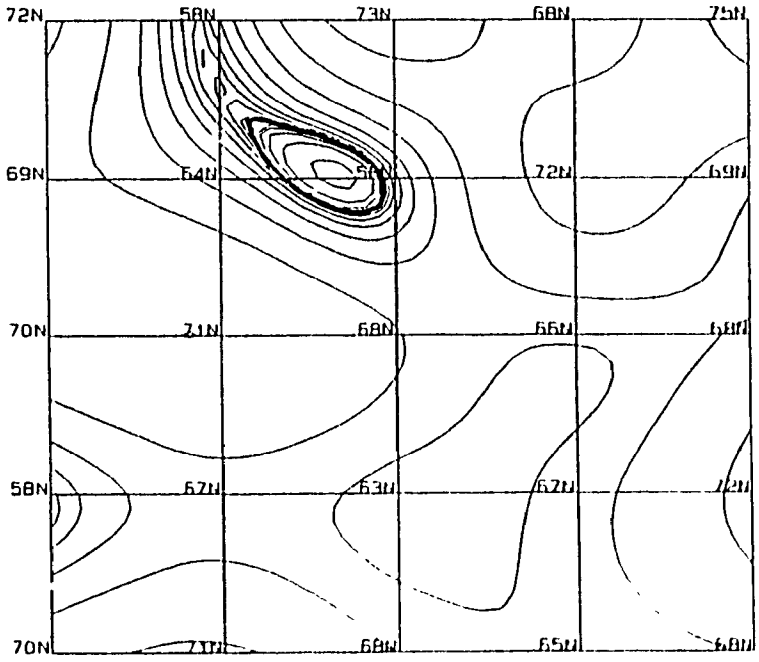

Figure 3.11: Contour map of the sound intensity at the measured outside the backwall (weighing: linear, frequency range: 30-1000Hz, mic spacer: 50 mm; N designates negative values)

The sound pressure and intensity levels were measured within the cavity at different locations along the z-axis ($x/a = y/b = 0.5$) using the intensity probe attached to a slender rod. The measured data was analyzed and presented in Figures 3.12 to 3.17. Figures 3.12, to 3.14 present the spectra of measured SPL at $x/a = y/b = 0.5; z/d = 0.25, 0.5, 0.75$ and Figures 3.15 to 3.17 illustrate the SIL at $x/a = y/b = 0.5; z/d = 0.25, 0.5, 0.75$. The peaks in the frequency spectra correspond to the system resonances. Small variations (dips and peaks) in the spectra of the pressure and intensity levels inside the cavity are not considered as the resonances, Since these variations may be caused by the fluctuations in the incident pressure itself.

The noise reduction through the plate is obtained either by subtracting the internal pressure from the external pressure or by subtracting internal intensity from the external intensity. Noise reduction computed from measurement of pressure and intensity levels at different locations inside the cavity are presented in Figures 3.18 and 3.19. The response characteristics in these figures are plotted against non-dimensionalyzed frequency, $\beta = \omega/\omega_{11}$, where ω_{11} is the measured fundamental plate natural frequency. The noise reduction were computed for measurements performed at $z/d = 0.5$ and 0.75, $x/a = y/b = 0.5$. In obtaining the noise reduction the pressure and intensity levels at the exterior mid point of the panel was taken as the external pressures and intensity levels. It is observed that the NR measured using both methods exhibit the same trend throughout the frequency range. The NR measured using the intensity method is found to be slightly larger than that obtained using pressure method. These differences may be attributed to the different pressure and intensity levels measured by the probe, as illustrated in Figures 3.4, 3.6, 3.14 and 3.15.

Since it was not possible to attain the clamped boundary condition for the plate, a direct correlation between the theoretical and experimental results can not expected. The experimental values of NR, however, are compared to the analytical values in an attempt to verify the general pattern and limited validation in a qualitative manner.

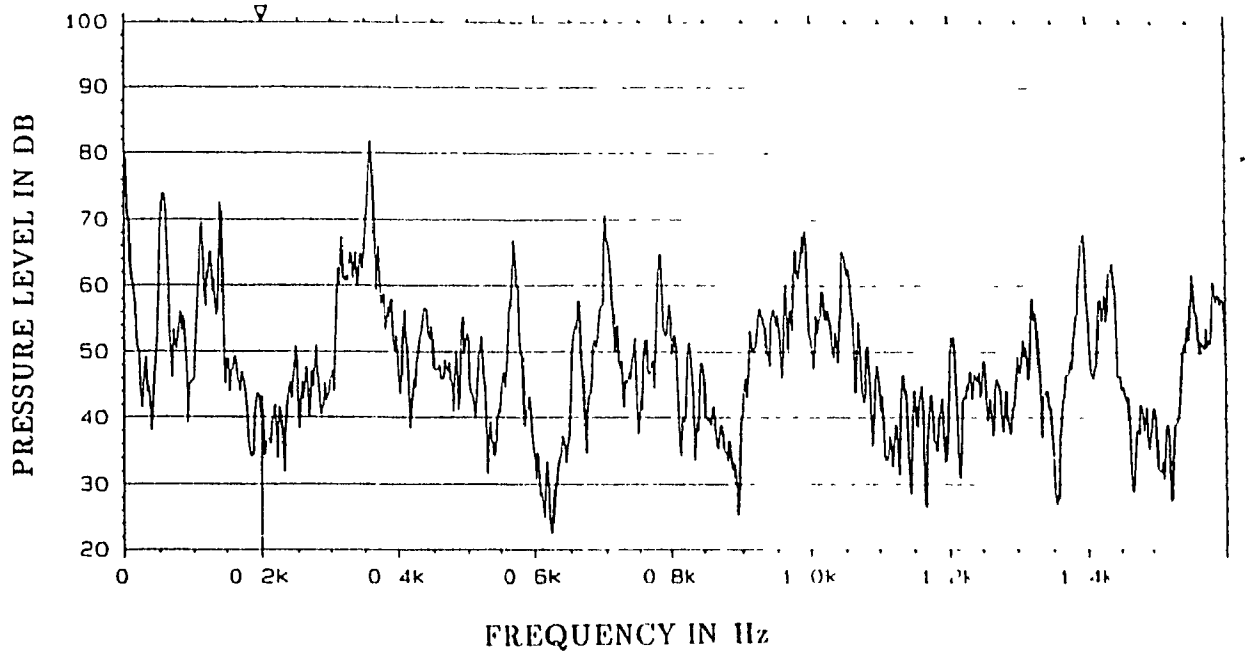

Figure 3.12: Cavity sound pressure spectrum measured at x/a y/b 0.5, z/d 0.25
(weighing: linear, frequency range: 30-1000Hz)

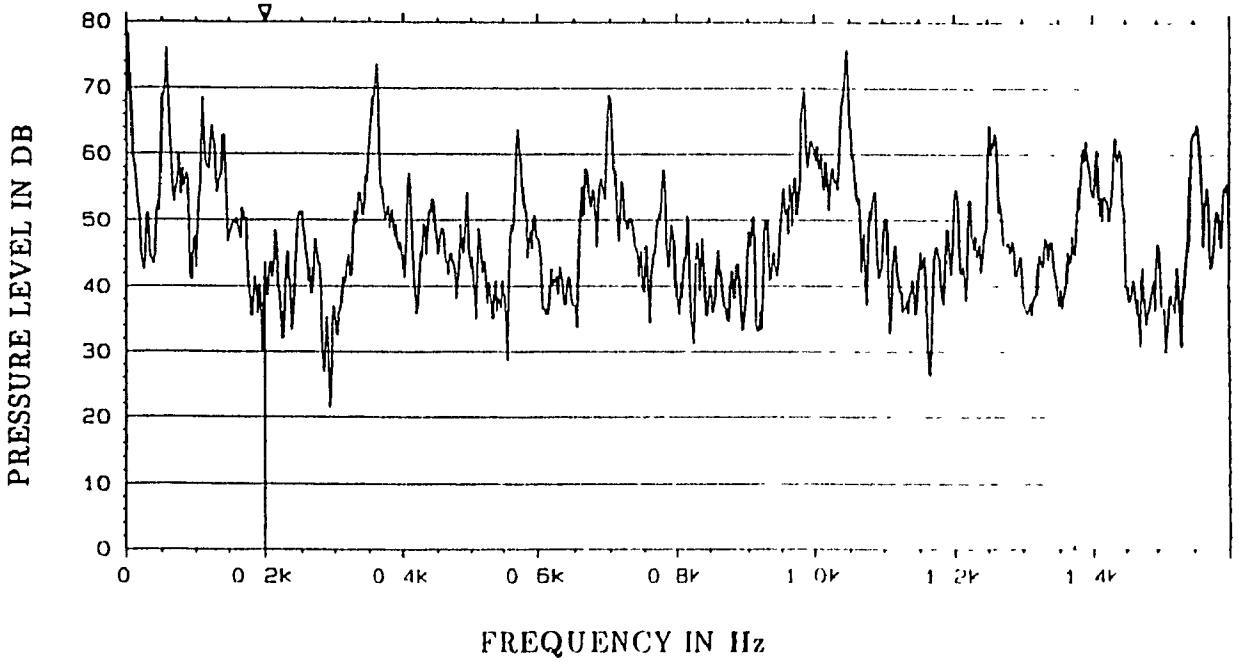

Figure 3.13: Cavity sound pressure spectrum measured at x/a y/b 0.5, z/d 0.5
(weighing: linear, frequency range: 30-1000Hz)

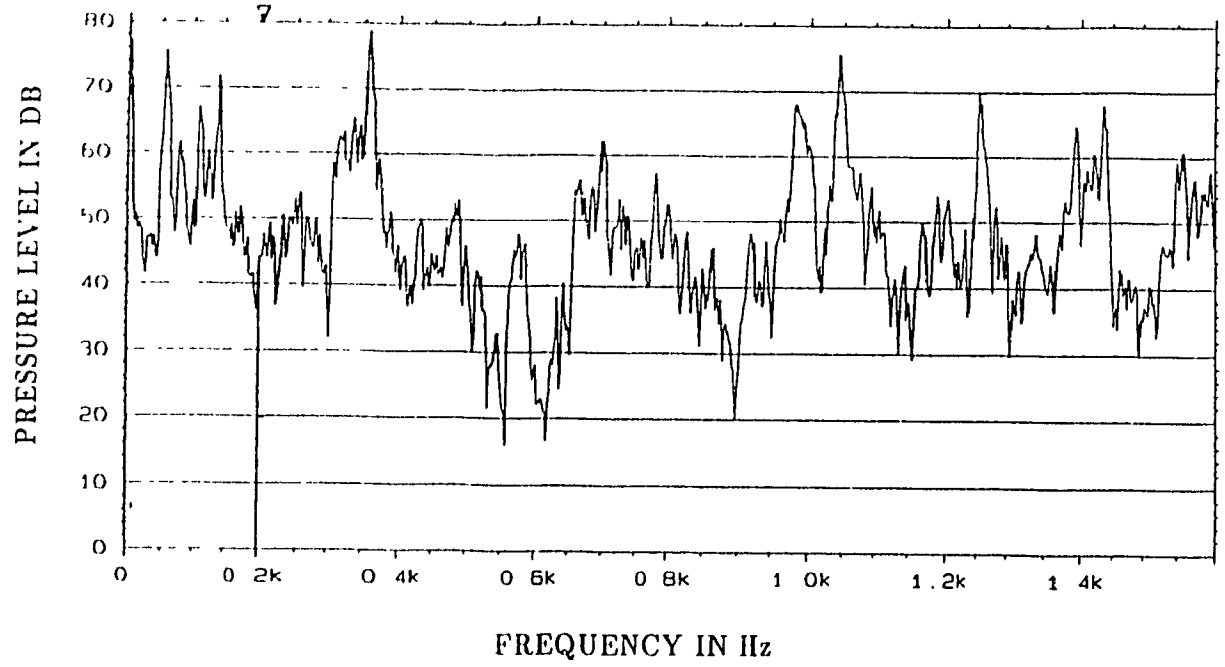

Figure 3.14: Cavity sound pressure spectrum measured at $x/a = y/b = 0.5$, $z/d = 0.75$
(weighing: linear, frequency range: 30-1000Hz)

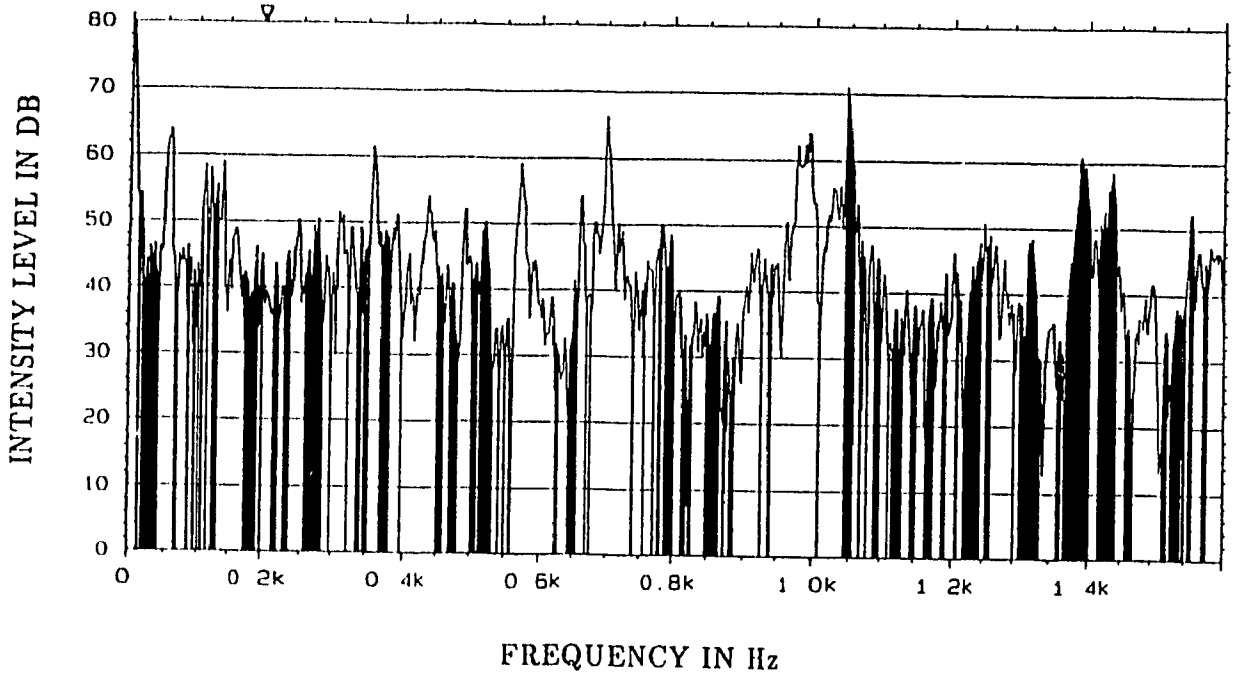

Figure 3.15: Cavity sound intensity spectrum measured at $x/a = y/b = 0.5$, $z/d = 0.25$
(weighing: linear, frequency range: 30-1000Hz, mic spacer: 50 mm)

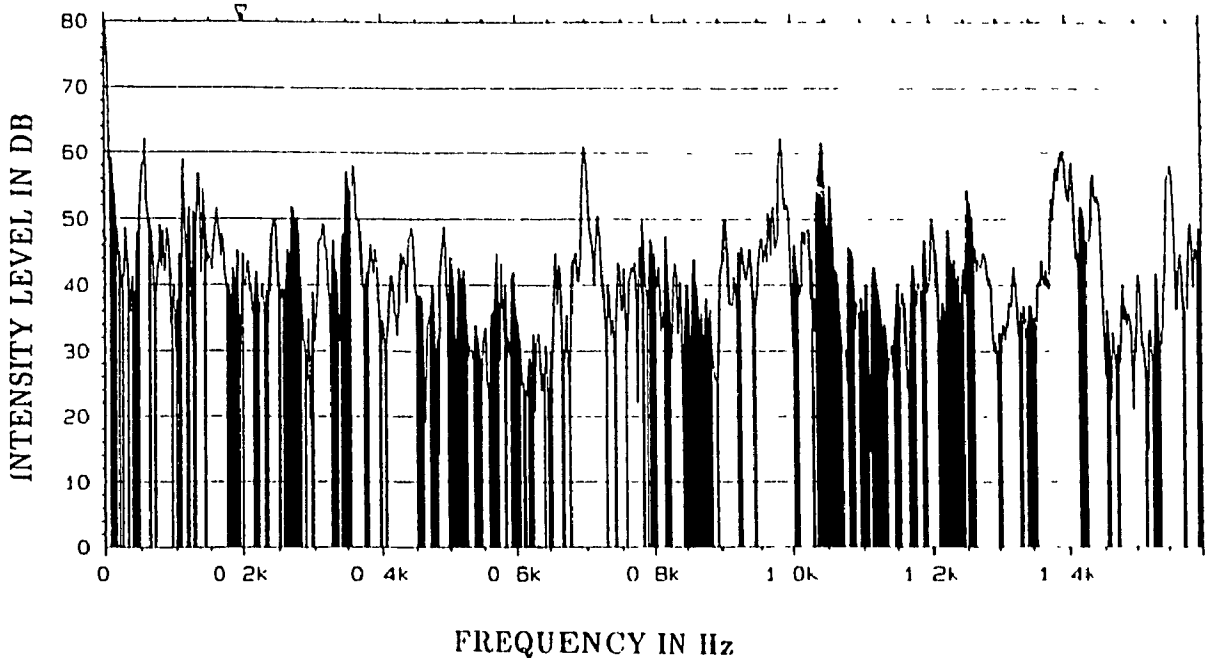

Figure 3.16: Cavity sound intensity spectrum measured at $x/a = y/b = 0.5$, $z/d = 0.5$
(weighing: linear, frequency range: 30-1000Hz, mic spacer: 50 mm)

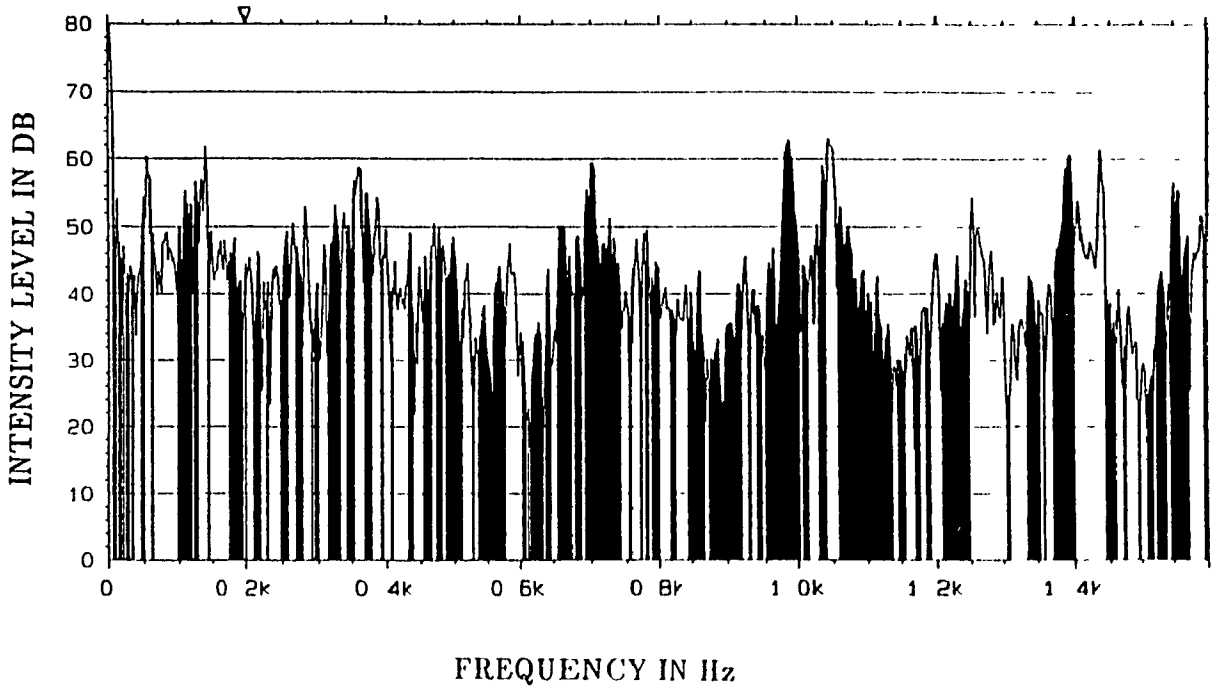

Figure 3.17: Cavity sound intensity spectrum measured at $x/a = y/b = 0.5$, $z/d = 0.75$
(weighing: linear, frequency range: 30-1000Hz, mic spacer: 50 mm)

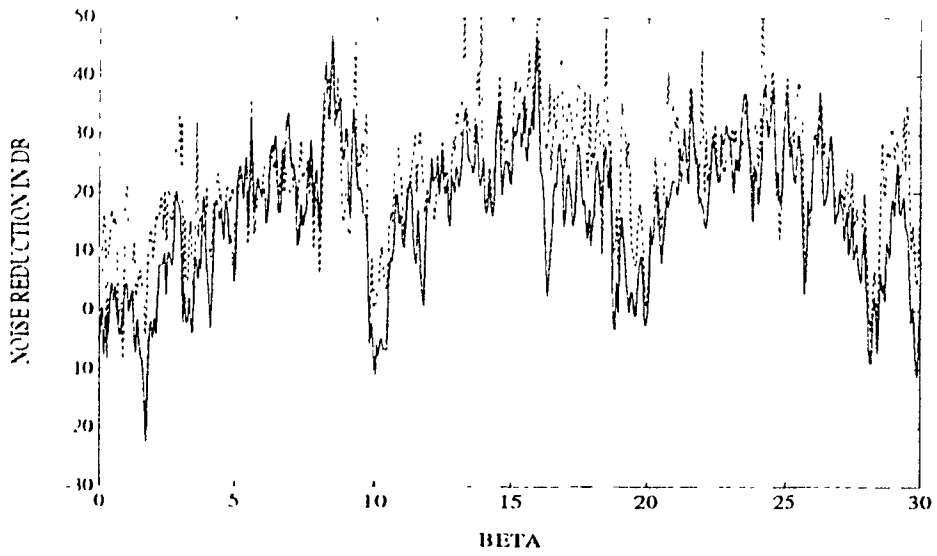

Figure 3.18: Measured NR at $x/a = y/b = 0.5$, $z/d = 0.5$
(pressure method, - - - intensity method)

The measured NR characteristics are compared to those computed for simply supported and clamped boundary conditions as shown Figure 3.20 and 3.21. Figure 3.20 shows the computed and measured response characteristics, at the mid-point plotted against excitation frequency, where the frequency is in Hz. The NR characteristics of the plate with simply supported and clamped boundary conditions, in general, do not correlate well the measured data. The poor correlation between the analytical and experimental results may be attributed to many factors. The primary factor that effects the NR values is the inability to realize exact boundary conditions as discussed earlier. While analytical and experimental results show similar general trend, the experimental noise reduction characteristics reveal large number of peaks. This may be attributed to excitation of higher plate modes due to spatial non-uniformity of the incident pressure. It should be noted that the theoretical values were obtained for uniform harmonic pressure excitations, which excites only odd numbered plate modes. Further the assumed numerical values of damping of the plate and cavity may also contribute to the poor correlation between analytical and experimental results.

The noise reduction characteristics were also measured at the centre of the

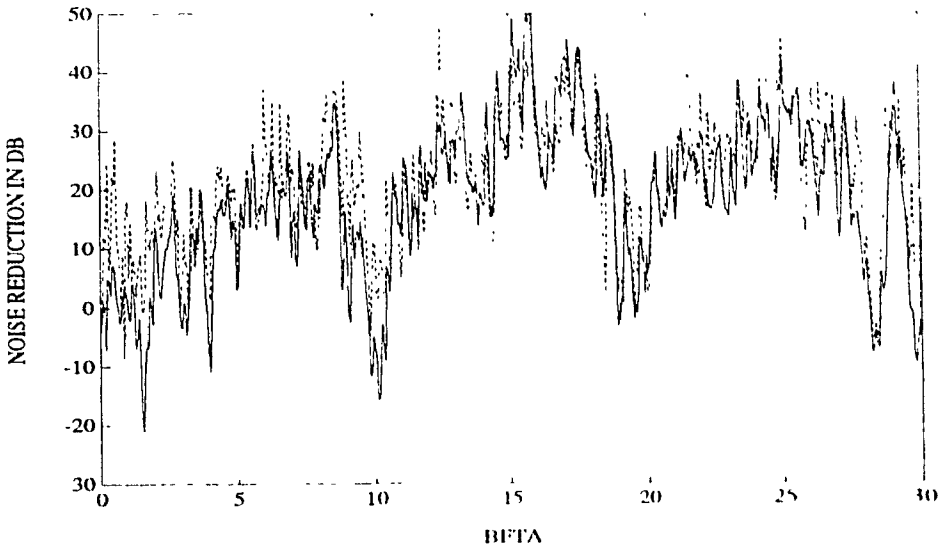

Figure 3.19: Measured NR at $x/a = y/b$ 0.5, z/d 0.75
(— pressure method, - - - intensity method)

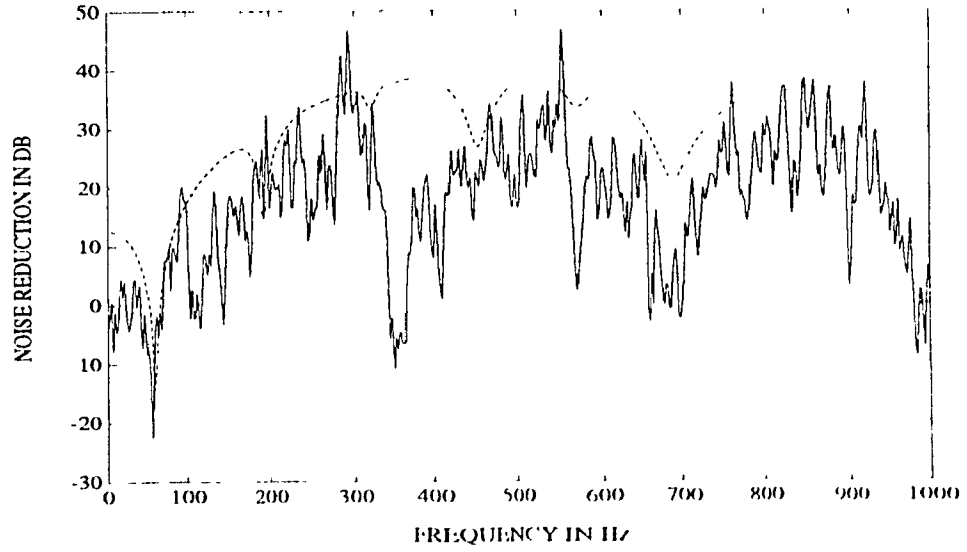

Figure 3.20: Comparison of experimental and analytical NR at x/a y/b z/d 0.25 under white noise excitation
(— experimental, - - - analytical-clamped plate, ... analytical simply supported plate)

cavity under sinusoidal excitations at various discrete frequencies in the 45-400 Hz range. The NR values computed from the experimental data are compared to those obtained from the analytical model as shown in Figure 3.21. The comparison reveals a reasonable correlation between the measured and computed values for clamped boundary condition near the fundamental resonant frequency, and similar general trends. The magnitude of the measured NR, specifically at high frequencies, however, are considerably lower than the computed values for both boundary conditions.

Figures 3.20 and 3.21, reveal that the first resonance of the coupled system is comparable to the theoretically estimated value. The measured value of first resonant frequency of the coupled system is 55 Hz, which is very close to 59 Hz, computed for clamped boundary condition. The magnitude of measured noise reduction near this frequency is also quite close to the theoretical value of -14 dB. The negative sign shows that there is an amplification of sound at the mid point of the box at the fundamental resonance. The comparison of analytical and experimental values of NR also exhibits a reasonable correlation near the cavity mode. The measured data exhibits the cavity controlled mode near 675 Hz, which compares to the computed value for clamped as well as simply supported boundary conditions. The magnitudes of noise reduction, however, do not correlate with the theoretical values at these modes.

The NR characteristics are also measured for different depths of the cavity. The NR values, measured at $z/d = 0.5$ are presented for two different cavity depths in Figure 3.22. A comparison of Figure 3.22 to the corresponding analytical result, presented in Figure 2.8 reveals similar general trends. The first natural frequency of the system is found to have decreased as observed from the leftward shift of the 'dip'. The NR is more for a deeper cavity almost at all frequencies as seen from both Figures 2.8 and 3.22. Both analytical and experimental results, however, showed poor noise reduction for deeper cavity in the 400-500 Hz frequency range. Figures 3.23 and 3.24 illustrate the variation in NR values when the measurements are performed at various locations along the z-axis for white noise and sinusoidal excitations, respectively. A

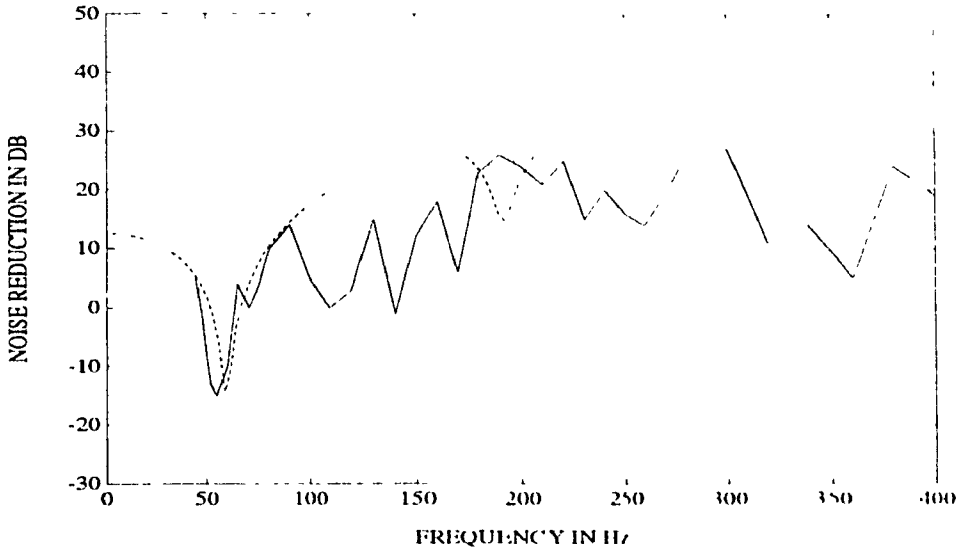

Figure 3.21: Comparison of experimental and analytical NR at x/a - y/b z/d 0.25 under sinusoidal excitation
(— experimental, - - - analytical-clamped plate, ... analytical simply supported plate)

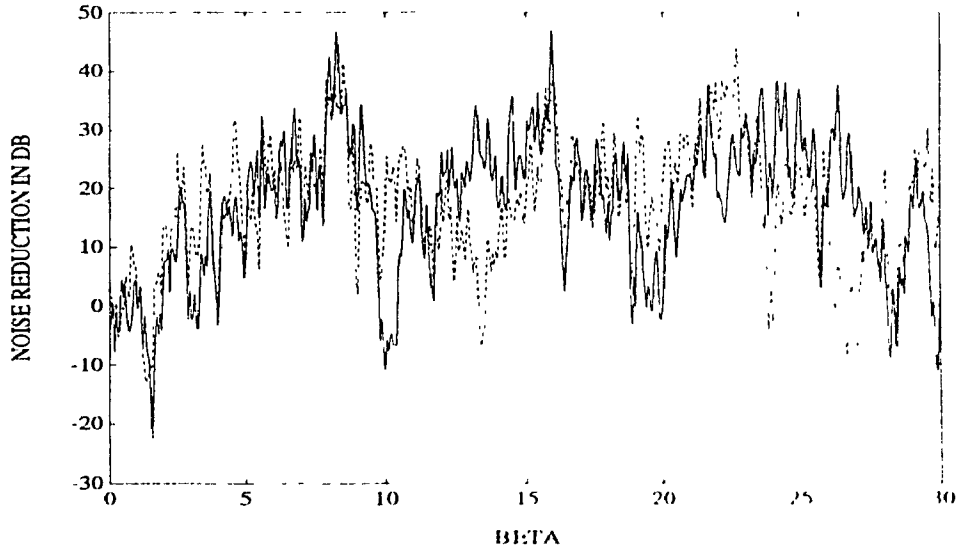

Figure 3.22: Comparison of measured NR for cavities of different depth
($x/a = y/b = z/d = 0.5$, – $d/a = 1.0$,- - $d/a = 1.5$)

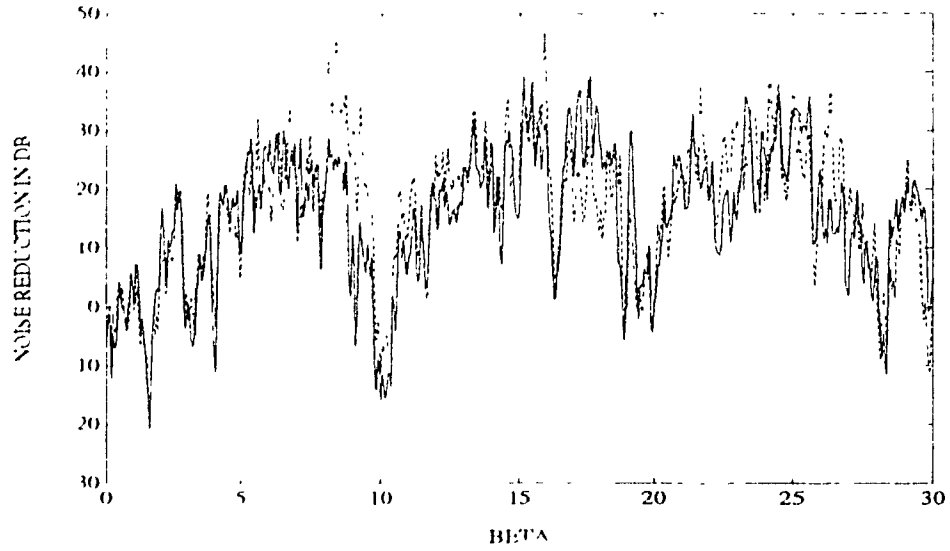

Figure 3.23: Comparison of NR measured at different location along z-axis under white noise excitation
($x/a = y/b = 0.5$, $z/d = 0.25$,- - $z/d = 0.5$, ... $z/d = 0.75$)

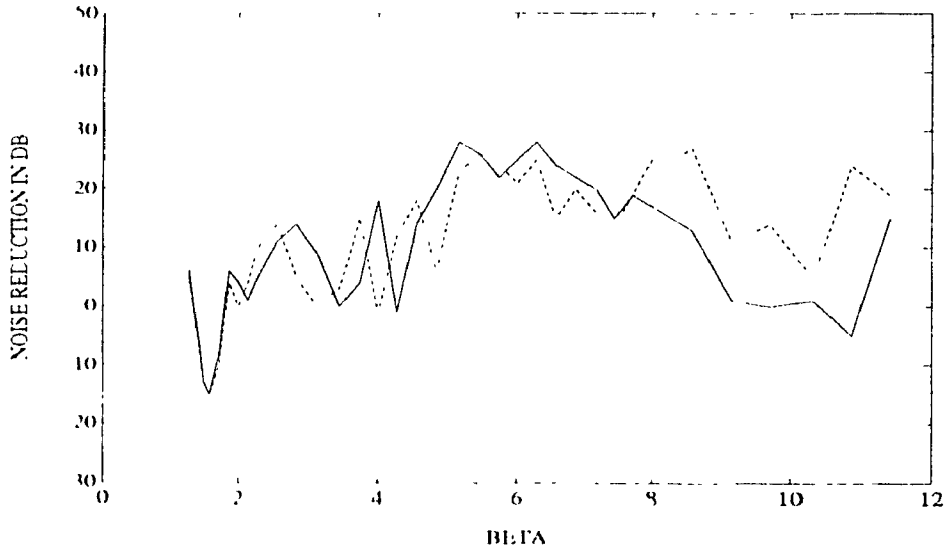

Figure 3.24: Comparison of NR measured at different location along z-axis under sinusoidal excitation
(x/a $y/b = 0.5$, $z/d = 0.25$,- - - $z/d = 0.5$, ... $z/d = 0.75$)

similar general trend is observed between the experimental result in Figures 3.23 and 3.24 and the corresponding analytical result, presented in Figures 2.7. There is a significant change in the noise reduction with variations in measurement location along the z-axis, as seen in Figures 2.7 and 3.24. The changes in NR can be observed near the cavity modes (eg. at $\beta = 1.2$ in Figure 3.24).

3.5 Summary

The sound transmission loss through a cavity backed plate was evaluated using modal coupling analysis in chapter 2. In order to validate the theoretical results obtained experiments were conducted on a rectangular box with a flexible plate forming one of the walls. The experimental NR data was compared to the analytical results obtained for clamped and simply supported boundary conditions to validate the analytical models, and to experimental investigate the influence of cavity dimension on the NR. The comparison revealed a reasonable agreement near the fundamental system frequency. Although the analytical and experimental data revealed a similar general trend in the entire frequency, a quantitative validation could not be realized due to poor boundary condition and lack of controlled acoustic chamber.

Chapter 4

Active Control of Noise Transmission through a Cavity Backed Plate

4.1 Introduction

Inherent limitations of passive methods of noise reduction, the desire to achieve improved control of noise, and developments in sensor and control technologies, have all culminated in studies on active control of transmitted noise. While active vibration control systems have been extensively investigated and implemented, the active noise control has been the subject of relatively limited studies. The mechanism of active control of noise transmission has been studied in the recent years due to an intense interest to reduce the internal noise levels in aircrafts and moving vehicles. Although active noise control in ducts has met with considerable success, its application to three-dimensional sound fields have been limited due to associated computational and design difficulties.

The effectiveness of active noise and vibration control system, in majority of the studies, have been investigated using simplified lumped-parameter models. The mo-

tion of flexible (and hence distributed) structures is described by variables depending not only upon time but also upon space. The motion is thus governed by the partial differential equations to be satisfied inside a given domain that defines structures and the boundary conditions. Majority of the active noise and vibration control concepts, developed for lumped parameter models, thus cannot be applied to such distributed parameter systems. Alternatively, modal control techniques that control the response characteristics of a structure by controlling its modes, may be applied. The active control concepts developed for lumped parameter systems can then be applied to the distributed-parameter systems, since both types of systems can be easily described in terms of their modal response and coordinates.

While the location and number of active control forces to be applied to lumped parameter system are not of great concern, the location and number of control forces applied to a distributed -parameter system affect the performance considerably. Further, the number of active force generators in a distributed parameter system must be limited in order to reduce the cost and weight of the active control system. Modal control by point control forces can control only limited number of modes. It has been showed by Meirovitch et al.[35] that the number of modes controlled is equal to the number of point forces used.

In the present chapter, actively controlled point forces are generated to reduce the noise transmission through a cavity-backed plate. The active control forces are generated using the state feedback and a proportional control law with certain phase angle. The noise reduction characteristics are evaluated using the modal control concept in conjunction with the modal coupling analysis technique. The noise reduction characteristics are compared to those of the passive cavity plate system, and the results are discussed to enhance an understanding of the modal control concept in noise transmission.

4.2 Mathematical Model

The active noise reduction of panel-cavity system is investigated using point forces that are applied directly to the flexible plate. The point forces are generated actively using proportional control laws. An analytical model of the panel-cavity system with active point forces is formulated by incorporating the proportional force generators to the model presented in chapter 2.

Consider the cavity backed flexible plate model described previously in section 2.2.2. The plate is subjected to actively controlled point forces at selected locations, f_{pq} acting at (x_p,y_q), $p = 1,2,\ldots,n$; and $q = 1,2,\ldots,n$. The governing differential equation of motion of the plate can be expressed in the frequency domain as:

$$D\Delta^2 w + i\omega C w - \rho_p h\omega^2 w = p^c(x,y,\omega) - p^c(x,y,0,\omega) + f_{pq}\delta(x-x_p)\delta(y-y_q) \tag{4.1}$$

The point nature of the active f_{pq} is characterized by Dirac delta functions, $\delta(x-x_p)$ and $\delta(y-y_p)$. The control force is generated using state feedback in conjunction with proportional control laws. A phase angle between the control force and the state variable is introduced to account for delays due to signal processing and generator dynamics[45]

$$f_{pq} = F_d e^{i\phi_d} + F_v e^{i\phi_v} + F_a e^{i\phi_a} \tag{4.2}$$

where F_d, F_v and F_a are the components of the control force generated corresponding to displacement, velocity and acceleration feedback, respectively, such that

$$F_d = K_d w(x_p, y_q)$$

$$F_v = K_v \omega \bar{w}(x_p, y_q)$$
$$F_a = K_a \omega^2 \bar{w}(x_p, y_q) \tag{4.3}$$

where $\bar{w}(x_p, y_q)$ is the Fourier transform of plate deflection at (x_p, y_q). ϕ_d, ϕ_v, and ϕ_a are the phase difference between the components of control force and the corresponding state variable. The plate deflection w can be expressed in terms of normalized plate modes as in Equation (2.21):

$$w = \sum_{m=1}^{\infty} \sum_{n=1}^{\infty} q_{mn}(\omega) \psi_{mn}(x, y) \tag{4.4}$$

Using Equations (4.3) and (4.4) the control force f_{pq} can be written as:

$$f_{pq} = (K_d e^{\iota\phi_d} + \omega K_v e^{\iota\phi_v} + \omega^2 K_a e^{\iota\phi_a}) \sum_{m=1}^{\infty} \sum_{n=1}^{\infty} q_{mn}(\omega) \psi_{mn}(x_p, y_q) \tag{4.5}$$

The internal cavity and external pressure can be expressed in terms of the plate normal modes in the following manner:

$$p^c_{mn}(\omega) = \frac{1}{\rho_p h} \int_0^a \int_0^b p^c(x, y, \omega) \psi_{mn}(x, y) dx dy \tag{4.6}$$

$$\bar{p}^e_{mn}(\omega) = \frac{1}{\rho_p h} \int_0^a \int_0^b p^e(x, y, 0, \omega) \psi_{mn}(x, y) dx dy \tag{4.7}$$

Substitution of the pressures from Equations (4.6) and (4.7) and plate deflection, w, in Equation (4.1) and the use of properties of normal modes yields.

$$\left[\frac{q_{mn}}{H_{mn}}\right] - \frac{f_{pq}}{\rho_p h} \int_0^a \int_0^b \psi_{uv} \delta(x - x_p) \delta(y - y_q) dx dy \quad [p'_{mn} \quad p'_{mn}(q_{rs})] \tag{4.8}$$

where H_{mn}, p^c_{mn}, and p'_{mn} are defined in Equations (2.24), (2.25) and (2.26) respectively. Using the properties of Dirac delta functions, Equation (4.8) can be written as:

$$\left[\frac{q_{mn}}{H_{mn}}\right] - \frac{f_{pq}}{\rho_p h}\psi_{rs}(x_p, y_q) = [\bar{p}^c_{mn} - p^c_{mn}(\bar{q}_{rs})] \tag{4.9}$$

Equation (4.9) can be written in a matrix form, by substituting for f_{pq} from Equation (4.5) as:

$$\left[\left[\frac{1}{H_{mn}}\right] - [F]\right]\{q_{mn}\} = \{\bar{p}^c_{mn} - \bar{p}^c_{mn}(q_{rs})\} \tag{4.10}$$

where,

$$[F] = \left[\frac{(K_d e^{\iota\phi_d} + \omega K_v e^{\iota\phi_v} + \omega^2 K_a e^{\iota\phi_a})}{\rho_p h}\right]\psi_{mn}(x_p, y_q)\psi_{rs}(x_p, y_q)$$

and p^c_{mn} is given by Equation (2.47) as:

$$p^c_{mn} = \frac{\rho_a \omega^2}{\rho_p h}\sum_{\iota=0}^{\infty}\sum_{\jmath=0}^{\infty}\sum_{k=0}^{\infty} H_{\iota\jmath k}\sum_{m=1}^{\infty}\sum_{n=1}^{\infty}\bar{q}_{rs}L_{\iota\jmath mn}L_{\iota\jmath rs} \tag{4.11}$$

The plate motion and the acoustic field inside the cavity with the control forces can be determined by solving the above coupled system of equations for $\bar{q}_{mn}$. Equation (4.10) is a coupled system of equations and the solution for q_{mn} is hard to obtain. The simplifying assumptions made in chapter 2, however, will help in solving for q_{mn}. It was assumed that for a very shallow cavity the cross acoustic terms ($r \neq m$, $s \neq n$) are negligible when compared to the direct terms ($r = m$, $s = n$). Using this deduction, Equation (4.10) may be represented by the following uncoupled set of equations:

$$\{q_{mn}\} = [J_{mn}]\{p^c_{mn}\} \tag{4.12}$$

where J_{mn} is frequency response function of the system along with the control forces and is given by:

$$[J_{mn}] = \left[\left[\left[\frac{1}{H_{mn}}\right] - [F]\right]^{-1} + \frac{\rho_a\omega^2}{\rho_p h}\sum_{i=0}^{\infty}\sum_{j=0}^{\infty}\sum_{k=0}^{\infty} H_{ijk}L^2_{ijmn}\right]^{-1} \tag{4.13}$$

The cavity pressure can be evaluated using Equation (2.53) given by:

$$p^c(x,y,z,\omega) = \rho_a\omega^2\sum_{i=0}^{\infty}\sum_{j=0}^{\infty}\left[f(z) + \sum_{k=0}^{\infty}\sqrt{abd}H_{ijk}(\omega)X_{00k}(z)\right]$$

$$\sum_{m=1}^{\infty}\sum_{n=1}^{\infty} q_{mn}L_{ijmn}\sqrt{d}X_{ij0}(x,y) \tag{4.14}$$

The application of control force changes the frequency response function of the coupled plate-cavity system. The new frequency response function is given by Equation (4.13. The effect of control forces is an addition term $[F]$ in the expression for frequency response function. It can be noted that $[J_{mn}]$ is a $m.n$ x $m.n$ matrix and is invertible. Equation (4.14) is used to evaluate the cavity inside pressure. NR with the control forces can be found using Equation (2.54).

4.3 Results and Discussion

The control scheme and control forces, described by Equation (4.3), are formulated based on the rationale that the low frequency noise can be reduced by reducing the structural modes of vibration. In this section, the theory presented in the previous section has been illustrated using some numerical examples. The panel cavity

system, described in chapter 2, incorporating control forces, is analyzed to evaluate the noise reduction characteristics. Numerical results are presented for both simply supported and clamped boundary conditions. Once again, for a clamped plate, plate characteristic functions have been used to represent the plate modes, the external sound pressure loading is assumed to be uniform all over the plate.

For convenience, the numerical evaluation have been performed in terms of non dimensional quantities. The non-dimensional position, velocity and acceleration feedback gains are expressed as:

$$K_d^* = \frac{K_d}{\rho_p h \omega_{11}^2 ab}$$
$$K_v^* = \frac{K_v \omega}{\rho_p h \omega_{11}^2 ab}$$
$$K_a^* = \frac{K_a \omega^2}{\rho_p h \omega_{11}^2 ab} \tag{4.15}$$

Figures 4.1 to 4.6 show the effect of active control force on the noise reduction as a function of the driving frequency ($\beta = \frac{\omega}{\omega_{11}}$), with one control force located at the centre of the plate. In all these cases the control force is applied at a phase difference of π with respect to the external disturbance force. The effects of position feedback on the noise reduction of cavity-plate system with clamped and simply-supported plate boundary conditions are illustrated in Figures 4.1 and 4.2, respectively. Control force with position feedback mostly affects the stiffness properties of the plate and thus tends to increase the resonant frequencies associated with the plate controlled modes. The control force developed using position feedback tends to increase the noise reduction only at extremely low frequencies and only slightly near the system natural frequencies. With clamped plate boundary condition, the stiffness of the plate increases approximately 3 times the stiffness without the control forces, when the position control gain is 0.8 The increase in the noise reduction due to control force with position feedback, however, is not significant.

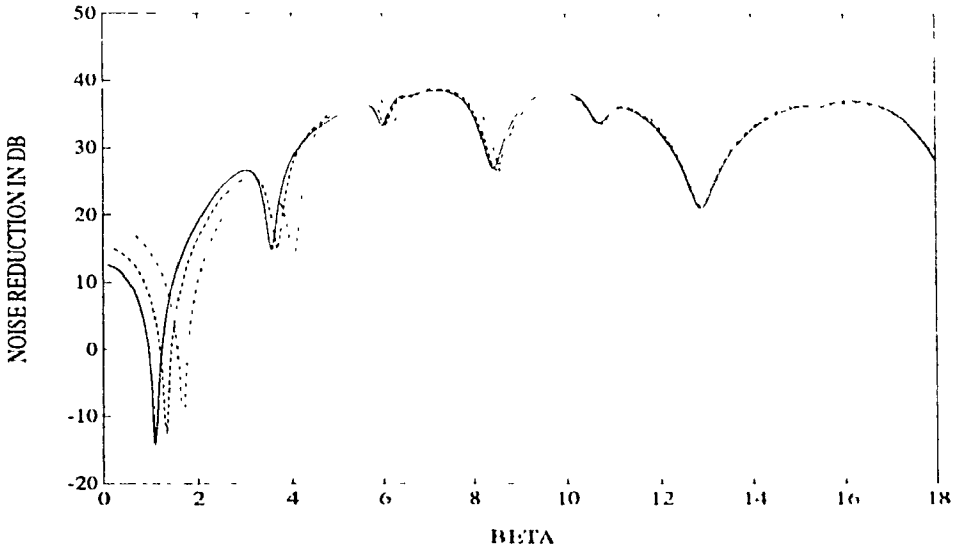

Figure 4.1: Effect of position feedback control on NR clamped plate ($\phi_d = \pi$, — control gain=0.0, - - - $K_d^* = 0.1$, ... $K_d^* = 0.1$, . . $K_d^* = 0.4$)

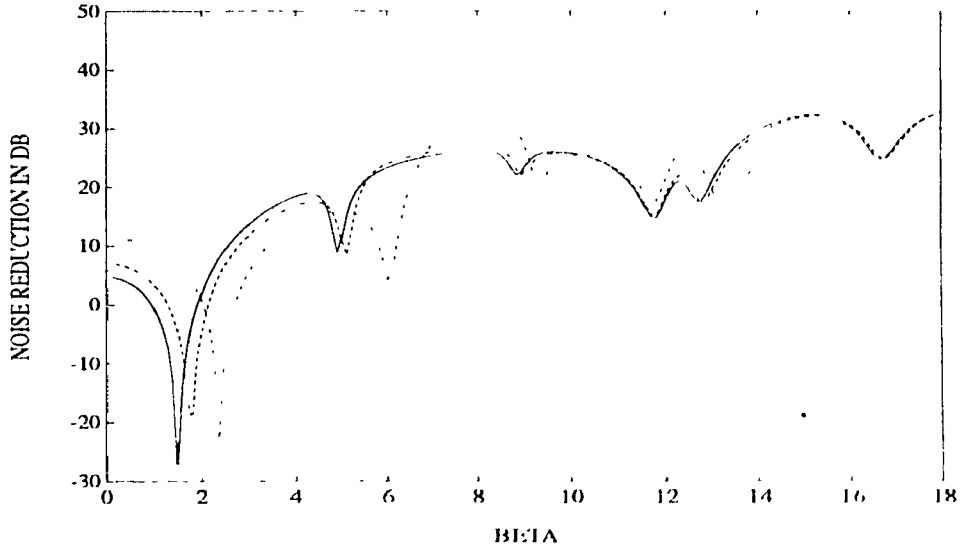

Figure 4.2: Effect of position feedback control on NR simply supported plate ($\phi_d = \pi$, — control gain=0.0, - - - $K_d^* = 0.25$, ... $K_d^* = 0.5$, . . $K_d^* = 2.0$)

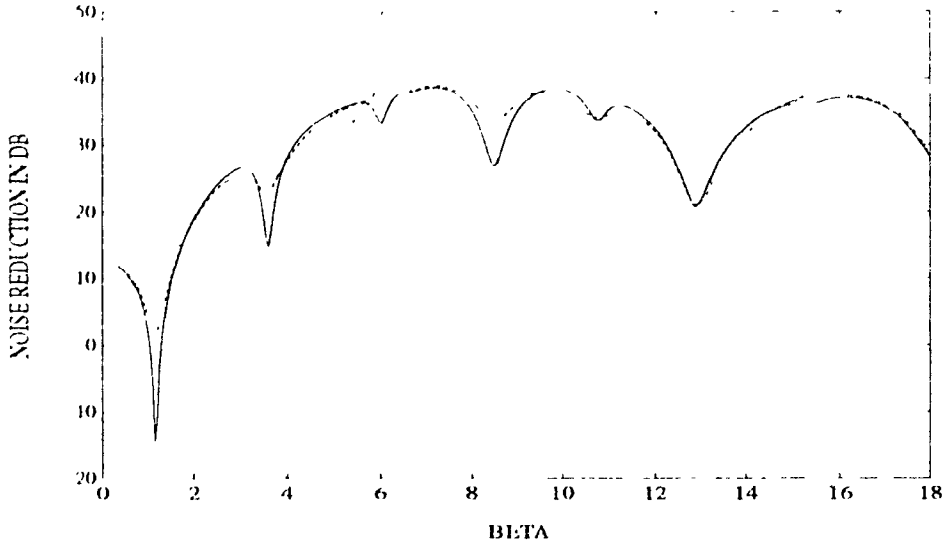

Figure 4.3: Effect of velocity feedback control on NR-clamped plate ($\phi_o = \pi$, control gain=0.0, - - - $K_v^* = 0.05$, ... $K_v^* = 0.1$, -.-.- $K_v^* = 0.2$)

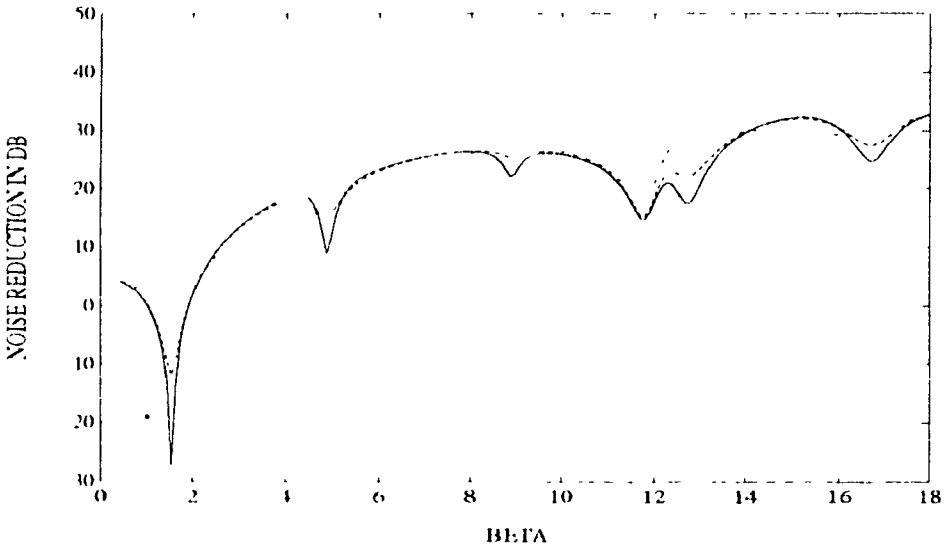

Figure 4.4: Effect of velocity feedback control on NR-simply supported plate ($\phi_o = \pi$, control gain=0.0, - - - $K_v^* = 0.05$, ... $K_v^* = 0.1$, -.-.- $K_v^* = 0.2$)

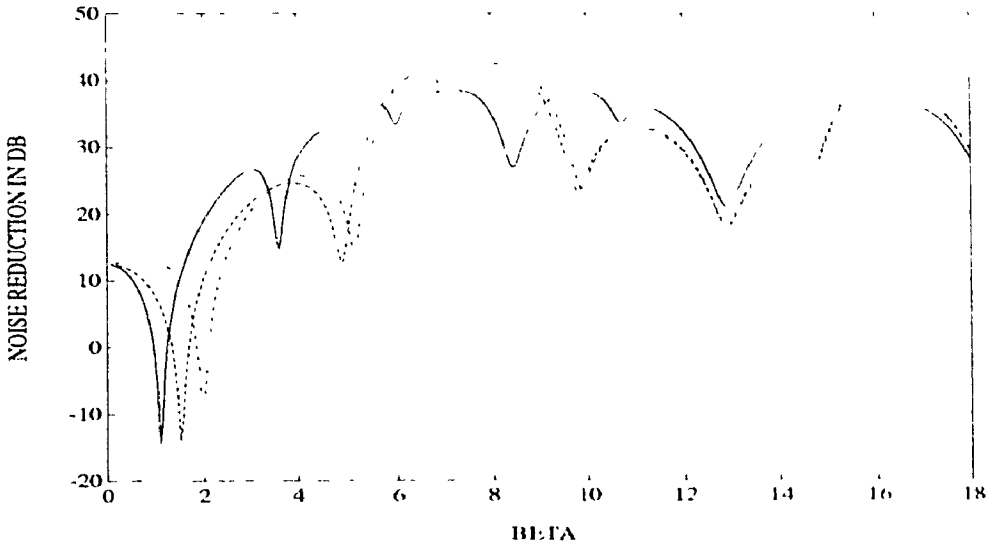

Figure 4.5: Effect of acceleration feedback control on NR clamped plate ($\phi_a = \pi$, -- control gain=0.0, - - - $K_a^* = 0.1$, ... $K_a^* = 0.2$, . . $K_a^* = 0.3$)

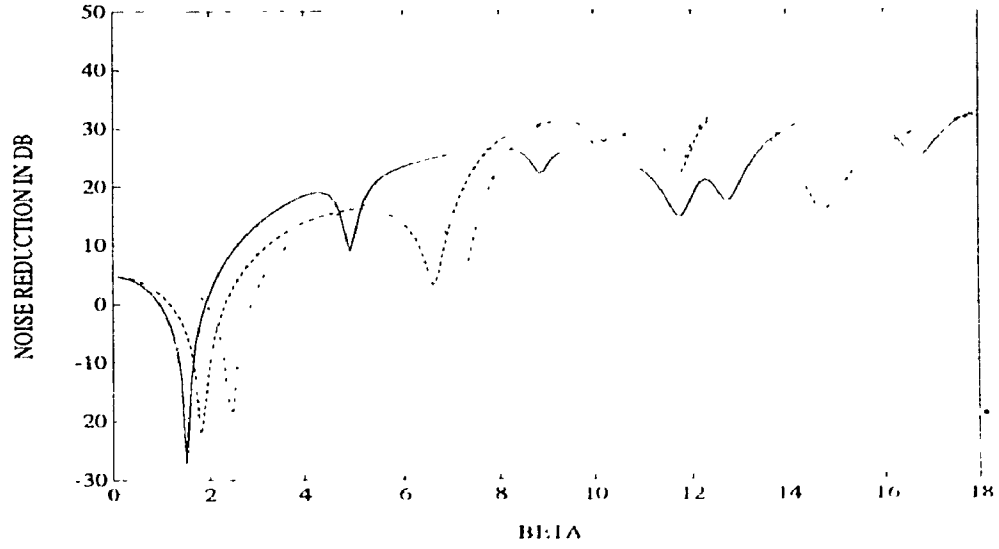

Figure 4.6: Effect of acceleration feedback control on NR-simply supported plate ($\phi_a = \pi$, - control gain=0.0, - - $K_a^* = 0.5$, ... $K_a^* = 1.0$, . . $K_a^* = 2.0$)

The effect of one control force applied at the centre of the plate using velocity feedback and a phase difference of π is illustrated in Figures 4.3 and 4.4. The NR values are computed for clamped as well as simply supported boundary condition. The control force proportional to the velocity response of the plate mostly affects the plate damping, ζ_{mn}. The total damping ratio of the plate can be computed by adding the passive and active components:

$$\zeta_{mn} = \zeta_{mn} + \frac{\omega_{11}}{2\omega_{mn}}[K_v^* \psi_{mn}(x_p, y_q)\psi_{rs}(x_p, y_q)] \tag{4.16}$$

Figures 4.3 and 4.4 show that the control force developed with velocity feedback suppresses the plate controlled modes due to increased damping and thus yields increased noise reduction at the system resonant frequencies. A comparison of Figures 4.1 to 4.4 shows that the application of a control force developed using the velocity feedback yields significant increase in noise reduction than the force developed using the position feedback.

The effect of acceleration feedback is more or less same as that of position feedback, as shown in Figures 4.5 and 4.6. The acceleration feedback force changes the inertia force of the system. The control force thus developed opposes the inertia force due to the phase difference of π incorporated in the control law. The system natural frequencies corresponding to the plate controlled modes thus increase with an increase in the acceleration gain. The noise reduction tends to increase only near the (3,3) plate-controlled mode frequencies, irrespective of the gain and the boundary conditions.

In order to find out the effect of control force phase on the performance, simulations have been carried out for different phase angle between the control force and the external pressure loading. While the Figure 4.7 shows the effect of position feedback at different phase angles, Figure 4.8 shows the effect of velocity feedback at different phase angles. In Figure 4.7, control forces applied with phase angles other than π is

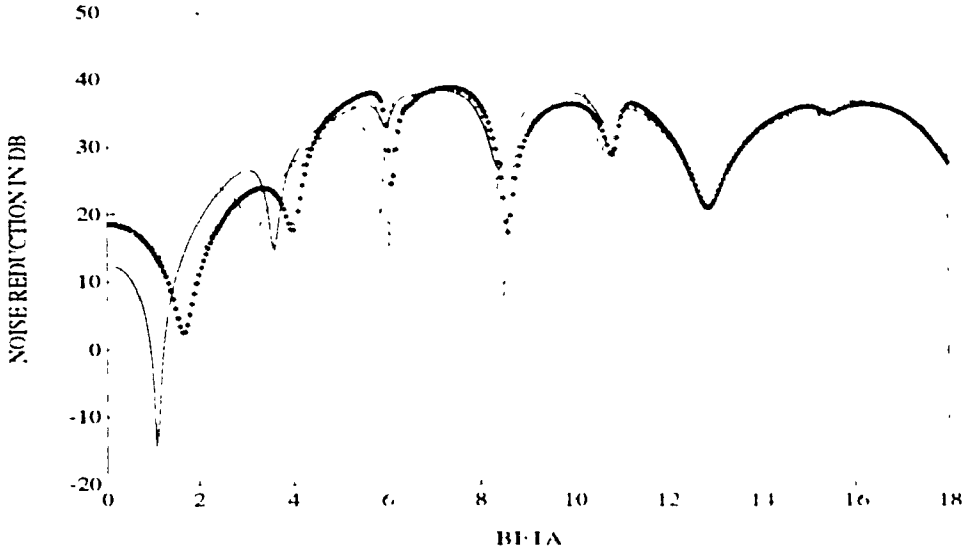

Figure 4.7: Effect of position feedback control force at different phase angles on NR ($K_d^* = 0.4$, control gain=0.0, - - - $\phi_d = \pi/1$, ... $\phi_d = \pi/2$, . . . $\phi_d = 2\pi/3$, *** $\phi_d = 5\pi/6$)

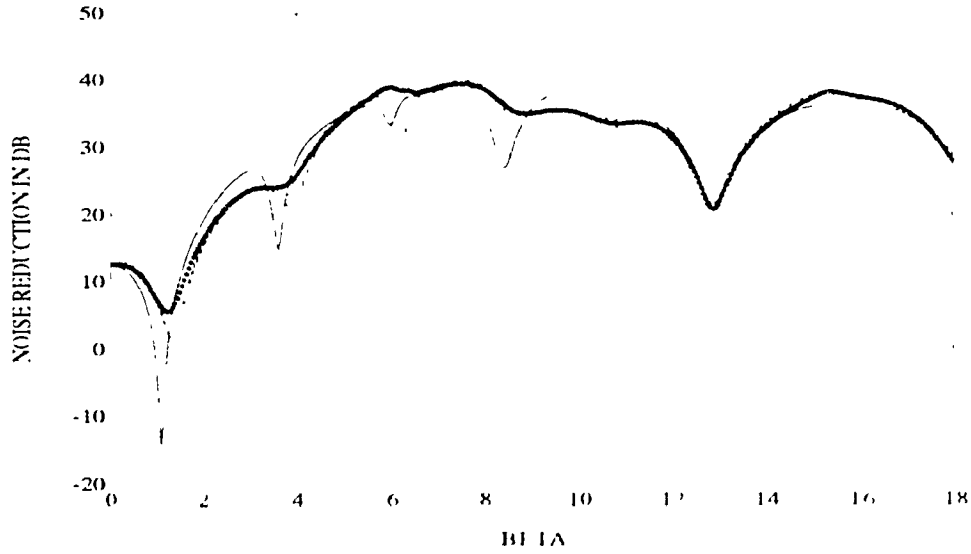

Figure 4.8: Effect of velocity feedback control force at different phase angles on NR ($K_v^* = 0.1$, control gain=0.0, - - - $\phi_v = \pi/1$, ... $\phi_v = \pi/2$, . . . $\phi_v = 2\pi/3$, *** $\phi_v = 5\pi/6$)

observed to have affected the noise reduction significantly. At very low frequencies (near the first mode) there is significant improvement in noise reduction. At frequencies near the system modes corresponding to the (3,3), (1,5), and (3,5) plate modes, however, the noise reduction is observed to have deteriorated. When the control force with position feedback is applied at a phase other than π, the damping of the system also changes and hence the noise transmitted is lesser. This is equivalent to applying the control force with velocity feedback along with position feedback. Control force applied at a phase of $\pi/4$ is observed to have the most significant effect in improving the noise reduction.

The effect of velocity feedback control force at different phase angles is more or less same, in the sense that, the phase angle changes the damping properties of the system. When the control force is applied at $\pi/2$ phase, the effect is same as that of position feedback force of the same magnitude, as seen from Figure 4.8. The noise reduction is found to have deteriorated through out the frequency range. The best result is obtained with the control force applied at a phase angle of $5\pi/6$.

When two or more control gains are used together, there is significant improvement in the noise reduction as seen in Figures 4.9 to 4.10. Noise reduction with the position and velocity feedback together applied to the actuator is shown in Figure 4.9 for different values of control gains. The effect is same as using position feedback and applying it at different phase angles which was discussed earlier. There is significant improvement in noise reduction at frequencies near the first mode and reasonable improvements at other modes. At frequencies away from any modes, however, the noise reduction is found to have slightly deteriorated. Control force generated using acceleration feedback along with position and velocity feedbacks (Figure 4.10) improves the noise reduction at frequencies near the system natural frequencies and deteriorates at frequencies away from the natural frequencies. At frequencies in the range 500 - 850 Hz, however, the noise reduction is found to have decreased. Both negative acceleration and positive acceleration feedback have the same effect, accept

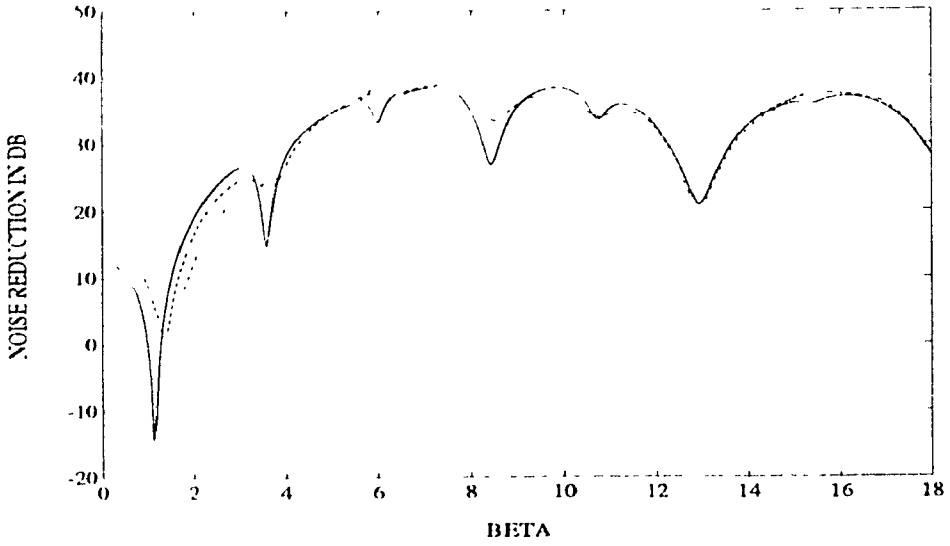

Figure 4.9: Effect of control force with position and velocity feedback on NR
(control gain=0.0, - - - $K_d^* = 0.1; K_v^* = 0.05$, ... $K_d^* = 0.3; K_v^* = 0.05$, -.-. $K_d^* = 0.3; K_v^* = 0.15$)

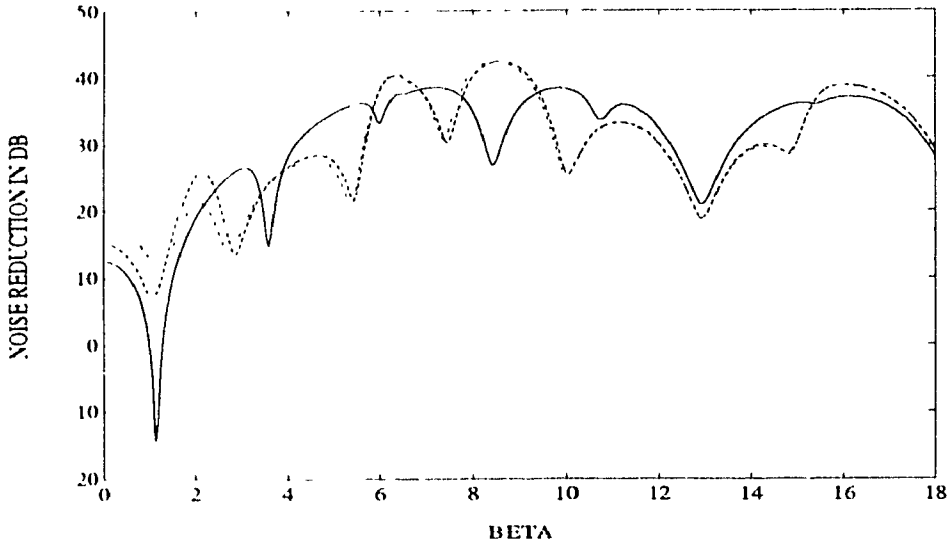

Figure 4.10: Effect of control force with position, velocity and acceleration feedback on NR
(control gain=0.0, - - - $K_d^* = 0.1; K_v^* = 0.1; K_a^* = 0.1$, ... $K_d^* = 0.3; K_v^* = 0.1; K_a^* = 0.1$, -.-. $K_d^* = 0.3; K_v^* = 0.2; K_a^* = 0.15$)

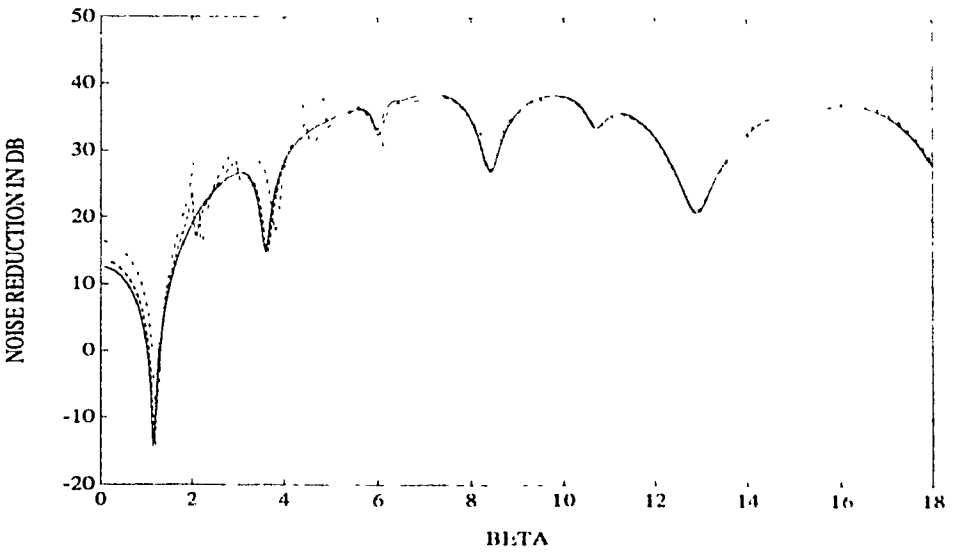

Figure 4.11: Effect of position feedback control force on NR, located at x/a y/b 0.25
($\phi_a = \pi$, --- control gain=0.0, - - $K_d^* = 0.1$, ... $K_d^* = 0.4$, . . K_d^* 0.7)

that the shifting of the peak near the first natural frequency is opposite in direction

Theoretical analysis has been performed to find out the effect of control force location and number of control forces. First plate mode is the most dominant in transmitting the sound through the plate. In order to eliminate the first plate mode, the actuator should be located at the center of the plate. Meirovitch et al.[35, 39] have shown that for independent modal space control, the number of control forces is equal to the number of modes to be controlled. It is quite obvious that the control forces will be most efficient in reducing the noise transmitted when they are located at the antinodes.

Noise reduction evaluated with the actuator placed at $\frac{x}{a}$ 0.25; $\frac{y}{b}$ 0.25 is shown in Figures 4.11 to 4.13. These respectively show the noise reduction with, position, velocity, and acceleration feedback control forces. These are less efficient in reducing the first mode, but suppress higher modes. The control force generated using position feedback does not really improve the the noise reduction, when placed

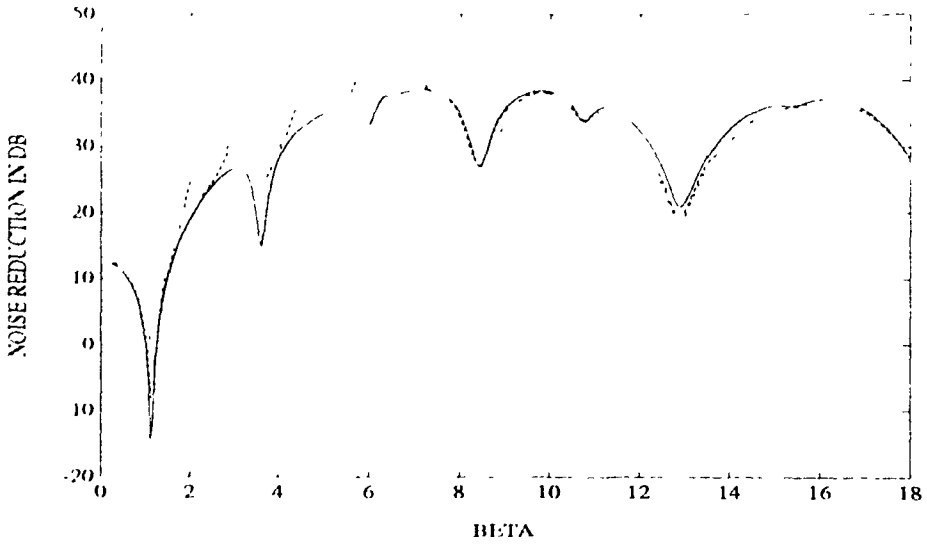

Figure 4.12: Effect of velocity feedback control force on NR, located at $x/a = y/b = 0.25$
($\phi_a = \pi$, control gain=0.0, - - - $K_v^* = 0.1$, ... $K_v^* = 0.2$, -.-.- $K_v^* = 0.4$)

at $\frac{x}{a} = 0.25$; $\frac{y}{b} = 0.25$, as seen from Figure 4.11. When the actuator is placed at points other than the center of the plate, it is found have excited some even numbered modes of the plate, which is clear from the sudden rise in the noise reduction plots.

Figure 4.12 shows the effect of control force with velocity feedback, when the actuator is placed at $\frac{x}{a} = 0.25$; $\frac{y}{b} = 0.25$. The figure shows some improvement in the noise reduction in frequency range 100-400 Hz. A number of peaks in the noise reduction plot can be seen in Figure 4.12 in this frequency range, which are attributed to the excitation of more plate modes than the plate without control force. The inability of the off-centered control force to suppress the first mode can also be observed in Figure 4.12. Control force generated using acceleration feedback, when the actuator is placed at $\frac{x}{a} = 0.25$; $\frac{y}{b} = 0.25$ is illustrated in Figure 4.13. Acceleration feedback also, is found to have improved the noise reduction in the frequency range 100 - 400 Hz, as seen from the figure. At frequencies higher than 400 Hz, however, the noise reduction is found to have deteriorated.

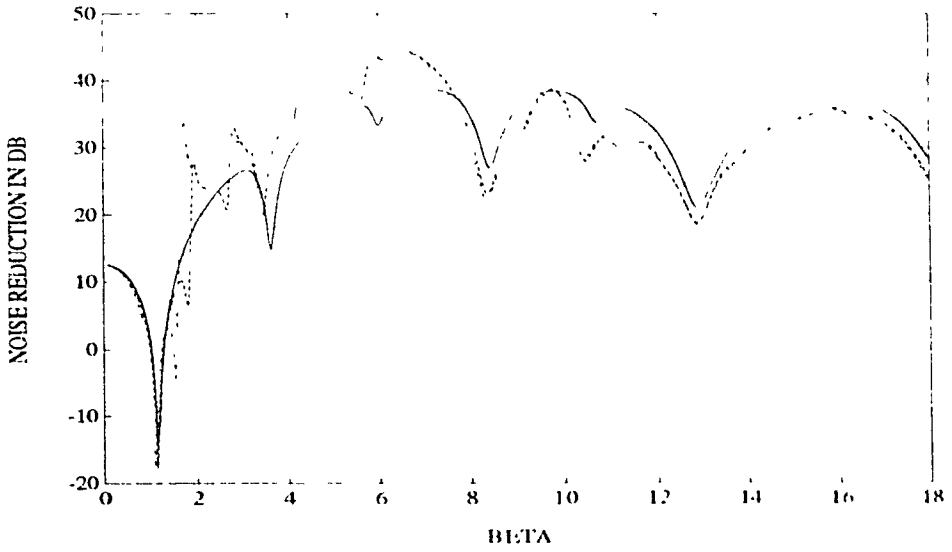

Figure 4.13: Effect of acceleration feedback control force on NR, located at x/a $y/b = 0.25$
($\phi_a = \pi$, -- control gain=0.0, - - - $K_a^* = 0.1$, ... $K_a^* = 0.2$, -.-.- $K_a^* = 0.4$)

The effect of multiple control forces on noise reduction is investigated. Two control forces located at the antinodes of the plate should be able to control at least two plate modes. Figures 4.14 to 4.16 illustrate the noise reduction evaluated for the same plate cavity system with two control forces located at $\frac{x}{a} = 0.5$; $\frac{y}{b} = 0.5$ and $\frac{x}{a} = 0.25$; $\frac{y}{b} = 0.25$. The control forces are generated using position and velocity feedback with different control gains. The second control force excites more plate modes which can observed in all the three figures. The control force applied at the center of the plate suppresses the first system mode and the second control force improves the noise reduction at higher frequencies. Once again, control force generated using velocity feedback (Figure 4.15) gives better result as compared to the noise reduction obtained using position feedback (Figure 4.14). Figure 4.16 shows the noise reduction evaluated with two control forces generated using both velocity and position feedback. The noise reduction is observed to have improved further by the use of control force with position and velocity feedback.

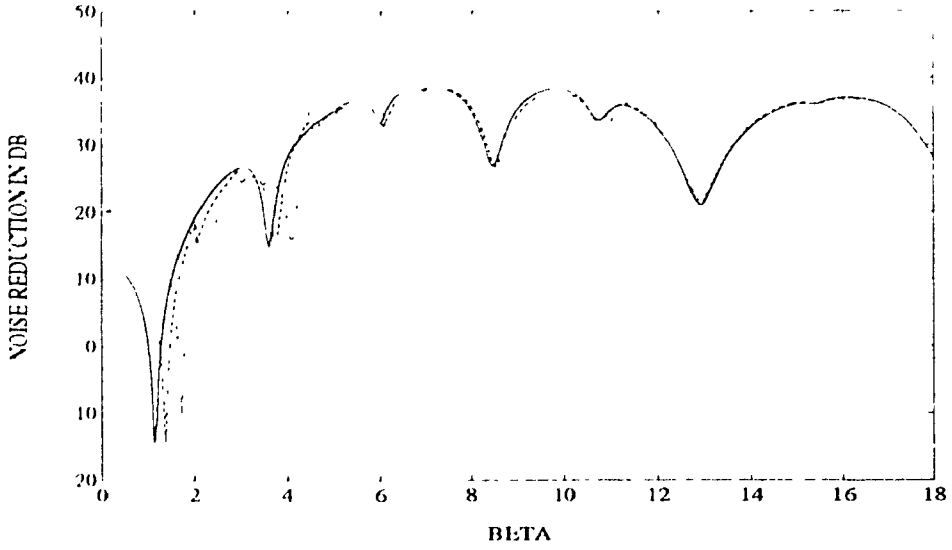

Figure 4.14: Effect of two control forces on NR- position feedback
(control gain=0.0, - - - $K^*_{d1} = 0.1$; $K^*_{d2} = 0.05$, ... $K^*_{d1} = 0.2$; $K^*_{d2} = 0.1$, -.-.- $K^*_{d1} = 0.4$; $K^*_{d2} = 0.2$)

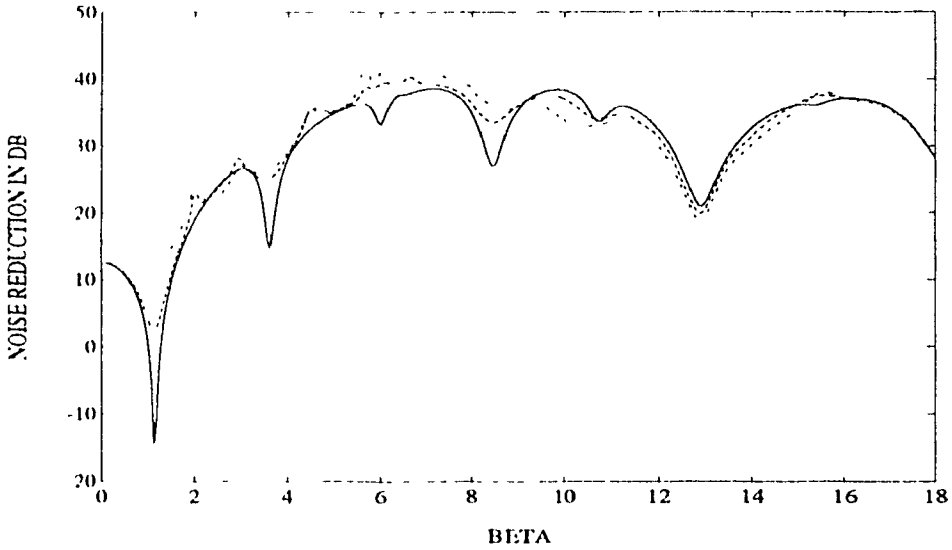

Figure 4.15: Effect of two control forces on NR- velocity feedback
(control gain=0.0, - - - $K^*_{v1} = 0.05$; $K^*_{v2} = 0.05$, ... $K^*_{v1} = 0.1$; $K^*_{v2} = 0.1$, -.-.- $K^*_{v1} = 0.15$; $K^*_{v2} = 0.15$)

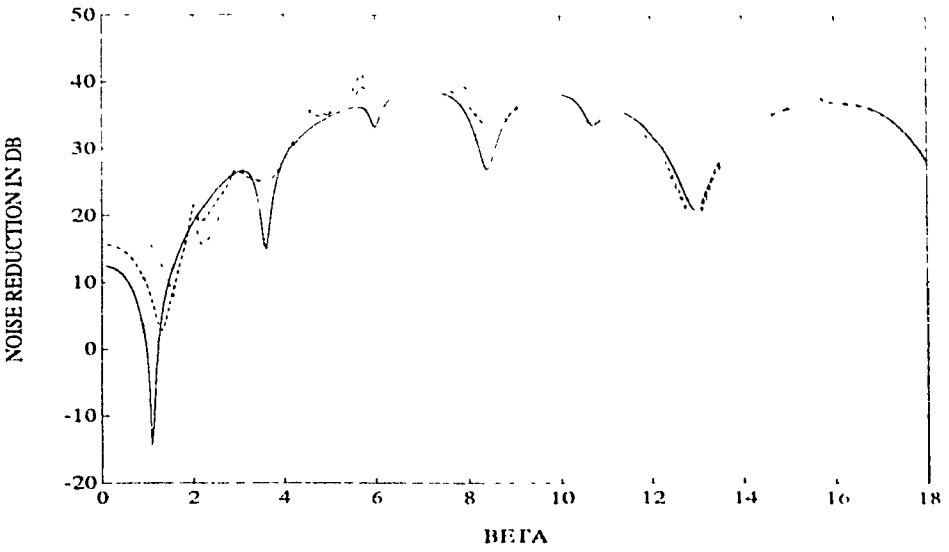

Figure 4.16: Effect of two control forces on NR- position and velocity feedback (— control gain=0.0, - - - $K^*_{d1} = 0.1$; $K^*_{d2} = 0.05$; $K^*_{v1} = 0.05$; K^*_{v2} 0.05, ... $K^*_{d1} = 0.2$; $K^*_{d2} = 0.1$; $K^*_{v1} = 0.1$; $K^*_{v2} = 0.1$, -.-.- $K^*_{v1} = 0.4$; $K^*_{d2} = 0.1$; K^*_{v1} 0.1; $K^*_{v2} = 0.1$)

4.4 Summary

Active control of sound transmission through a flexible panel into a rectangular cavity, based upon point control forces applied to the panel, is analytically studied. The response characteristics of the coupled panel-cavity system with multiple point control forces applied to the panel are analyzed using the modal coupling analysis technique. The active control forces are generated using the state feedback and a proportional control with certain phase angle. The noise transmission characteristics of the panel-cavity system with active control forces generated using position, velocity and acceleration feedback are evaluated for uniform sound pressure distribution. The result obtained showed that, control force generated using velocity feedback is most significant in reducing the noise transmission. The combination of velocity and position feedback further improves the noise reduction.

Chapter 5

Conclusion and Future Work

5.1 Conclusions

Modal coupling analysis has been used for the estimation of sound transmission loss through a cavity backed flexible plate. Use of Plate characteristic functions in place of beam characteristic functions has been studied and the effects of various structural and geometrical parameters on the noise reduction has been investigated. Studies have been also been conducted on the control of noise transmission using feedback controlled point forces. The following conclusions are drawn from the analytical and experimental studies performed on the plate-cavity system:

- Noise reduction results obtained using plate characteristic functions and beam characteristic functions are very close, and exhibit the same trend. However, computational time is significantly lower when plate characteristic functions are used.
- Damping in the plate-cavity system influences the noise reduction significantly, near the system natural frequencies.

- The coupled system modes are identified as two distinct modes:(i) those controlled by the plate modes; and (ii) those controlled by the rigid cavity modes The cavity depth has a major role in determining the first natural frequency of the system, which is close to the first plate natural frequency.

- Cavity depth, size of the cavity, plate thickness, and mass densities of the plate and cavity fluid affect the noise reduction. an appropriate selection of these parameters can thus help in reducing the noise transmission to the cavity.

- In controlling the noise transmission using feedback controlled point forces, the velocity feedback is observed to be most effective. The combination of velocity and position feedbacks also yields considerable improvement in the noise reduction.

- A direct verification of the theoretical results using experimental means was not possible due to inability to realize the clamped boundary condition of the plate, and lack of a controlled acoustic chamber. Further, the spatial uniformity of the external pressure was not achieved. However, comparison of theoretical and experimental results revealed reasonable correlation in a qualitative manner, specifically at low excitation frequencies.

5.2 Recommendation for Future Work

The theoretical analysis has been conducted for a uniformly distributed pressure excitation, which does not represent the realistic sound fields. A real time adaptive control scheme should be developed to control of time dependent random fluctuations in the external sound field.

The study has presented noise reduction analysis for clamped and simply supported flexible plates. The experimental results reveal that the actual boundary condition lies in between the two boundary conditions. In order to achieve a direct

correlation between experimental and the analytical results, the analytical model needs to be refined by incorporating realistic boundary condition.

In order to effectively control the transmission of sound, the active control means are necessary. Although, the analytical study an point control forces generated using proportional control laws resulted in improved noise control characteristics, alternative control laws should be explored to further improve the noise reduction. The hardware including force generators, controller and feedback sensors should be realized to experimentally evaluate the noise attenuation potentials. The dynamics of the force generator should be considered and incorporated in the analytical model.

Other possible work involves the study of noise transmission phenomenon with more than one flexible wall and noise control using point forces.

Bibliography

[1] Lyon, R. H., "Noise Reduction of Rectangular Enclosures With One Flexible Wall," Journal of Acoustical Society of America, volume 35, No. 11, 1963.

[2] Dowell, E. H. and Voss, H. M., "The Effect of Cavity on Panel Vibrations," AIAA Journal, volume 1, 1963.

[3] Pretlove, A. J., "Free Vibration of a Rectangular Panel Backed by a Closed Rectangular Cavity," Journal of Sound and Vibration, volume 2, No. 3, 1965.

[4] Pretlove, A. J., "Forced Vibration of a Rectangular Panel Backed by a Closed Rectangular Cavity," Journal of Sound and Vibration, volume 3, No. 3, 1966.

[5] Kihlman, T., "Sound radiation into a rectangular room. Application to airborne sound transmission in buildings". Acustica, volume 18, No. 11. 1967.

[6] Bhattacharya, M. C. and Crocker, M. J., "Forced Vibration of Panel and Radiation of Sound Into a room," Acustica, volume 22, No. 5, 1970.

[7] Guy, R.W. and Bhattacharya, M. C., "The Transmission of Sound Through a Cavity Backed Finite Plate," Journal of Sound and Vibration, volume 27, No. 2, 1973.

[8] Narayanan, S. and Shanbhag, R. L., "Sound Transmission Through Elastically Supported Sandwich Panels Into a Rectangular Enclosure," Journal of Sound and Vibration, volume 77, No. 2, 1981.

[9] Narayanan, S. and Shanbhag, R. L., "Acoustoelasticity of a Damped Sandwiched panel Backed by a Cavity," Journal of Sound and Vibration, volume, 1981

[10] Guy, R.W., "The steady state Transmission of sound at normal and oblique incidence through a thin panel backed by a rectangular room - a multi-modal analysis," Acustica, volume 43, 1979.

[11] Dowell, E. H., "acoustoelasticity," NASA CR-145110, 1977

[12] Wayne B. Mcdonald, Vaicaitis, R., and Myers, M. K., "Noise Transmission Through Plates into An Enclosure," NASA TP-1173, 1978.

[13] Bhat R. B., Mundkur G. and Singh J., "Plate Characteristic Functions and Natural Frequencies of Vibration of Plates by Iterative Reduction of Partial Differential Equation," Journal of Vibration and Acoustics, volume 115, 1993.

[14] Bhat R. B., and Mundkur G., "Vibration of Plates Using Plate Characteristic Functions Obtained by Reduction of Partial Differential Equation," Journal of Sound and Vibration, No. 1, volume 161, 1993.

[15] Bhat R. B., and Mundkur G., "Plate Characteristic Functions to Study Sound Transmission loss Through Panels," Second International Congress on Recent Developments in Air and Structure-Borne Sound and Vibration, 1992.

[16] Ross, Donald, Kervin, Edward M., and Dyer I.,"Flexural Vibration Damping of Multiple layer plates," Rep. No. 564, Bolt Beranek and newman Inc., 1958.

[17] Dym, Clive L., and Lang, Mark A., "Transmission of sound through Sandwich Panels," Journal of Acoustical Society of America, volume 56, No. 5, 1974.

[18] Rimas Vaicaitis, "Noise transmission by Viscoelastic Sandwich Panels," NASA TN D-8516.

[19] Nelson, P.A., Curtis, A.R.D., Elliot, S.J., and Bullmore, A.J., "The active minimization of harmonic enclosed sound fields, Part 1. Theory," Journal of Sound Vin., volume 117, No. 1, 1987.

[20] Nelson, P.A., Hammond J.K., Joseph, P., and Elliot, S.J., "Active Control of Stationary Random Fields," Journal of Acoustical Society of America, volume 87, 1990.

[21] Baz, A. Poh, S., "Performance of an active control system with piezoactuators," Journal of Sound and Vibration, volume 126, No. 2, 1988.

[22] Burdess, J. S. and Metcalfe, A. V., "Active Control of forced harmonic vibration in finite degree of freedom system with negligible damping," Journal of Sound and Vibration, volume 91, No. 3, 1983.

[23] Balas, M., "Active Control of flexible systems," J. Optimization Theor. Appl volume 25, 1978.

[24] Fuller, C. R., Silcox, R. J., Metcalfe, V. L., and Brown, D. E., "Experiments on Structural control of sound transmitted through an elastic plate," Proceedings of American Control Conference, Pittsburg, 1989.

[25] Fuller, C. R.,"Active control of sound transmission/radiation from elastic plates by vibration inputs," Journal of Sound and Vibration, volume 136, No. 1, 1990.

[26] Meirovitch, L. and Thangjitham, S., "Active Control of Sound Radiation Pressure," ASME Journal of Vibration Acoustics 112, 1990.

[27] Snyder, S.D., and Hansen, C.H.; "Active Noise Control in Ducts: Some Physical insights," Journal of Acoustical Society of America, volume 86, 1989.

[28] Fuller, C. R., and Jones, J. D., "Experiments on reduction of propeller induced interior noise by active control of cylinder vibration," Journal of Sound and Vibration, volume 112, No. 2, 1987.

[29] Fuller, C. R., Silcox, R. J., and Lester, H. C., "Mechanisms of active in cylindrical fuselage structures," AIAA Conference paper, AIAA-87, 1987.

[30] Jones, J. D., and Fuller, C. R., "Active control of sound fields in elastic cylinders by multicontrol forces," AIAA Conference paper, AIAA-87, 1987.

[31] Warner, J. V., and Bernhard, R. J., "Digital control of sound in three dimensional structures," AIAA Conference paper, AIAA-87, 1987.

[32] Pan, J., Hansen, C. H. and Bies, D. A., "Active control of noise transmission through a panel into a cavity: 1. Analytical study," Journal of Acoustical Society of America, volume 87, No. 5, 1990.

[33] Pan, J., and Hansen, C. H., "Active control of noise transmission through a panel into a cavity: 2. Experimental study," Journal of Acoustical Society of America, volume 90, No. 3, 1991.

[34] Pan, J., and Hansen, C. H., "Active control of noise transmission through a panel into a cavity: 3. Effect of actuator location," Journal of Acoustical Society of America, volume 90, No. 3, 1991.

[35] Meirovitch, L., and Norris, M., "Vibration control," Proceedings of Inter-Noise 84, 1984.

[36] Bullmore, A. J., Nelson, P. A., and Elliot, S. J., "Active minimization of acoustic potential energy in harmonically excited cylindrical enclosed sound field," AIAA Conference paper, AIAA-86, 1986.

[37] Morse, P., M., "Vibration and Sound," Mc-Graw Hill Book Company, 1948.

[38] Kantorovich, L. V. and Krylov, V. I., "Approximate methods of Higher Analysis (translated by Benster, C. D.)," New York: John Wiley.

[39] Meirovitch, L., Baruh, H., and Oz, H., "A comparison of control techniques for large flexible systems," Journal of Guided Control of Dynamics 6, 1983.

[40] Gade, S., "Validity of the sound intensity measurements," Bruel & Kjear Technical Review No. 1, 1985.

[41] Guy, R. W., and Li, J., "Journal of Acoustical Society of America" volume 92, No. 5, 1992.

[42] Krishnappa, G., "IEC 1043 Draft standard," Bruel & Kjear, 1991.

[43] "Intensity Measurements", B & K review, BA 7196-14, 1988.

[44] Fahy, F. J., "Sound Intensity"

[45] Hong, S., Rakheja, S., and Sankar, T. S., "Vibration-isolation Characteristics of an Active Electromagnetic Force Generator and the Inluence of Generator Dynamics", ASME transactions, 1990.

Appendix A

Evaluation of L_{ijmn} and $\bar{p}^e_{mn}$

A.1 Evaluation of L_{ijmn}

The quantity L_{ijmn}, known as 'acousto-stiffness coupling coefficiet' is evaluated in this section for a simply supported plate. Although similar derivation may be carried out for a plate with clamped boundary conditions, resulting analytical expressions are quite tedious. For clamped plates the terms L_{ijmn} were thus calculated using numerical integration.

The modes used for simply supported plate are:

$$\psi_{mn} = \frac{2}{\sqrt{ab}} sin(\frac{m\pi x}{a}) sin(\frac{n\pi y}{b}) \tag{A.1}$$

and the quantities L_{ijmn} are given by:

$$L_{ijmn} = \int_0^a \int_0^b \sqrt{d} X_{ij0}(x,y) \psi_{mn}(x,y) dx dy \tag{A.2}$$

Substituting ψ_{mn} and X_{ij0} from (A.1) and (A.2) yields:

$$L_{ijmn} = \frac{4}{ab}\left[\int_0^a \cos\left(\frac{i\pi x}{a}\right)\sin\left(\frac{m\pi x}{a}\right)dx \int_0^b \cos\left(\frac{j\pi y}{b}\right)\sin\left(\frac{n\pi y}{b}\right)dy\right] \qquad (A.3)$$

Solution of equation (A.3) leads to following expression for acousto-stiffness coupling coefficients.

$$L_{ijmn} = \begin{cases} 0 & \text{if } m+i \text{ and } n+j \text{ are even} \\ \frac{16mn}{\pi^2(m^2-i^2)(n^2-j^2)} & \text{if } m+i \text{ and } n+j \text{ are odd} \end{cases} \qquad (A.4)$$

A.2 Evaluation of $\bar{p}^e_{mn}$

The generalized external force $\bar{p}^e_{mn}$ is given by:

$$\bar{p}^e_{mn}(\omega) = \frac{1}{\rho_s h}\int_0^a \int_0^b p^e(x,y,\omega)\psi_{mn}(x,y)dxdy \qquad (A.5)$$

In the present analysis the external pressure has been assumed to be uniform all over the plate. Assuming $p^e(x,y,t) = P^e\cos(\omega t)$, and performing the Fourier transform yields:

$$p^e(x,y,\omega) = P^e \qquad (A.6)$$

where 'bar' ($\bar{}$) represent the Fourier transform. Upon substituting for $p^e(x,y,\omega)$, in (A.5), the generalized external force may be expressed as:

$$\bar{p}^e_{mn}(\omega) = \frac{P^e}{\rho_s h}\int_0^a \int_0^b \psi_{mn}(x,y)dxdy \qquad (A.7)$$

Once again, the above integration is performed for only simply supported plate. Numerical integration was performed to evaluate the generalised external force for a clamped plate. For simply supported plate, equation (A.7) can be reduced to:

$$p^e_{mn}(\omega) = \frac{P^e}{\rho_s h} \int_0^a \int_0^b \sin\left(\frac{m\pi x}{a}\right) \sin\left(\frac{n\pi y}{b}\right) dxdy \tag{A.8}$$

integration of (A.8) yields the following:

$$p^e_{mn} = \begin{cases} 0 & \text{if } m \text{ and } n \text{ are even} \\ \frac{8P^e\sqrt{ab}}{\rho_p hmn} & \text{if } m \text{ and } n \text{ are odd} \end{cases} \tag{A.9}$$

Appendix B

Beam and Plate Characteristic Functions

Table B.1: CC Beam characteristic function parameters
$X(x) = A\cos p1x + B\sin p1x + C\cosh p2x + D\sinh p2x$

n	$p1$	$p2$	A	B	C	D
1	4.7300	4.7300	1.0000	-1.0178	-1.0000	1.0178
2	7.8532	7.8532	1.0000	-0.9992	-1.0000	0.9992
3	10.9956	10.9956	1.0000	-1.0000	-1.0000	1.0000
4	14.1372	14.1372	1.0000	-0.9999	-1.0000	0.9999
5	17.2788	17.2788	1.0000	-1.0000	-1.0000	1.0000
6	20.4203	20.4203	1.0000	-1.0000	-1.0000	1.0000

Table B.2: CCCC Plate characteristic function parameters

$$X(x) = \cosh p2x - \cos p1x - \sigma\,[p1/p2 \sinh p2x - \sin p1x]$$
$$Y(y) = \cosh q2x - \cos q1x - \tau\,[q1/q2 \sinh q2x - \sin q1x]$$

m	n	$p1$	$p2$	σ	$q1$	$q2$	τ
1	1	4.3121	6.5261	1.5090	4.3121	6.5261	1.5090
1	2	3.8583	10.3026	2.6701	7.6902	9.0630	1.1788
1	3	3.6321	14.5121	3.9955	10.9100	11.8858	1.0894
1	4	3.5098	18.8478	5.3700	14.0852	14.8367	1.0534
1	5	3.4352	23.2300	6.7623	17.2440	17.8534	1.0353
1	6	3.3854	27.6341	8.1628	20.3956	20.9073	1.0251
2	1	7.6902	9.0630	1.1788	3.8583	10.3026	2.6701
2	2	7.3866	12.0012	1.6247	7.3866	12.0012	1.6247
2	3	7.1356	15.7158	2.2024	10.7156	14.2397	1.3280
2	4	6.9606	19.7593	2.8387	13.9549	16.7627	1.2012
2	5	6.8394	23.9572	3.5028	17.1520	19.4766	1.1355
2	6	6.7527	28.2366	4.1815	20.3277	22.3051	1.0973
3	1	10.9100	11.8859	1.0894	3.6321	14.5121	3.9955
3	2	10.7156	14.2308	1.3280	7.1356	15.7158	2.2024
3	3	10.5088	17.4516	1.6607	10.5088	17.4516	1.6607
3	4	10.3340	21.1445	2.0461	13.7951	19.5560	1.4176
3	5	10.1966	25.0959	2.4612	17.0291	21.9170	1.2870
3	6	10.0903	29.1972	2.8936	20.2318	24.4583	1.2089
4	1	14.0852	14.8367	1.0534	3.5098	18.8478	5.3700
4	2	13.9549	16.7628	1.2012	6.9606	19.7593	2.8387
4	3	13.7951	19.5560	1.4176	10.3340	21.1445	2.0461
4	4	13.6409	22.8978	1.6786	13.6409	22.8978	1.6786
4	5	13.5067	26.5779	1.9678	16.8992	24.9343	1.4755
4	6	13.3947	30.4709	2.2748	20.1239	27.1875	1.3510
5	1	17.2440	17.8534	1.0353	3.4352	23.2300	6.7623
5	2	17.1520	19.4766	1.1355	6.8394	23.9571	3.5028
5	3	17.0291	21.9170	1.2870	10.1966	25.0959	2.4612
5	4	16.8992	24.9343	1.4755	13.5067	26.5779	1.9677
5	5	16.7769	28.3421	1.6894	16.7769	28.3421	1.6894
5	6	16.6680	32.0137	1.9207	20.0160	30.3358	1.5156
6	1	20.3956	20.9073	1.0251	3.3854	27.6341	8.1628
6	2	20.3277	22.3051	1.0973	6.7527	28.2366	4.1815
6	3	20.2318	24.4583	1.2089	10.0903	29.1972	2.8936
6	4	20.1239	27.1875	1.3510	13.3947	30.4709	2.2748
6	5	20.0160	30.3361	1.5156	16.6680	32.0138	1.9207
6	6	19.9147	33.7883	1.6967	19.9148	33.7848	1.6965

Appendix C

Calibration of the Intensity Probe

The sound intensity probe can be calibrated either by using a sound intensity calibrater or through calibration of microphones for magnitude and phase error. The sound intensity calibrater permits simultaneous sensitivity adjustment of both channels of the analyzer (in pressure, particle velocity or intensity mode) and allows determination of the Pressure-Residual intensity index of the microphones, preamplifier analyzer combinations which employ microphone pairs with phase corrector units Calibration of sound intensity probe through calibration of the microphones is performed in two stages. First, the microphones are calibrated to read correct sound pressure levels. The phase calibration is then performed in a pressure coupler. This method of calibration was used for the calibration.

The B & K draft standard for intensity measurement (IEC 1043) [42] suggests the use of pink or white noise for calibration of the sound intensity meter. A pink noise in the frequency range 0-50k Hz was applied to a standing wave tube with a pressure coupler placed at the end of the tube. The intensity probe is placed in the coupler such that the diaphragms and static pressure equalization vents of both microphones are exposed to the same pressure variations. The spectra of sound pressure measured by the two microphones are thus expected to be identical.

The phase error is then computed from intensity and pressure measured in the coupler using the relationship:

$$\phi_{er} = \frac{\Delta r.f.\rho I_{re}}{p_{re}^2} \times 360 \qquad \text{(C.1)}$$

where Δr is the microphone spacing, f is the frequency of the signal, I_{re} is the residual sound intensity, p_{re} is the residual sound pressure, and ϕ_{er} is the phase error between the two channels of the analyzer in degrees. The measurements and computation revealed a phase error, ϕ_{er}, well below 0.02 degrees in the frequency range of interest. The pressure and intensity levels, in the coupler as measured by the intensity probe are presented in Figures C.1 to C.2. These figures show that the sound inside the coupler was more or less pink, at low frequencies (below 500 Hz). Figure C.1 illustrates the sound intensity measured in 'direction 1' and 'direction 2'. A comparison of the measured intensity in two direction reveals almost similar intensity level, except in the 125 Hz frequency band. The error in this band may be attributed to the directional error of the probe. Figure C.2 illustrates the sound pressure spectra measured in the two direction. Sound pressure levels are obsreved to be same in the two directions showing the uniformity of the sound pressure distribution in the pressure coupler. It can be observed that the input noise was pink in the range 0-500 Hz. In the figures showing the intensity levels, the dark strips and white strips differentiate between the positive and negative intensities. In the pressure level figures, however, the dark strip represent the cursor location at the time of printing the analyzer screen display.

The B & K draft standard for intensity measurement (IEC 1043) [42] gives the minimum P-I index requirements for the instruments of 'class 1' and 'class 2'. The draft assures a maximum measurement error of 0.5 dB in the range of 50-5000 Hz for a 'class 1' probe. The maximum measurement error for a 'class 2' probe is 1.0 dB in the range of 50-5000 Hz. Table C.1 shows the minimum recommended requirement by the IEC 1043 and measured P-I indices. To confirm the possible change in the

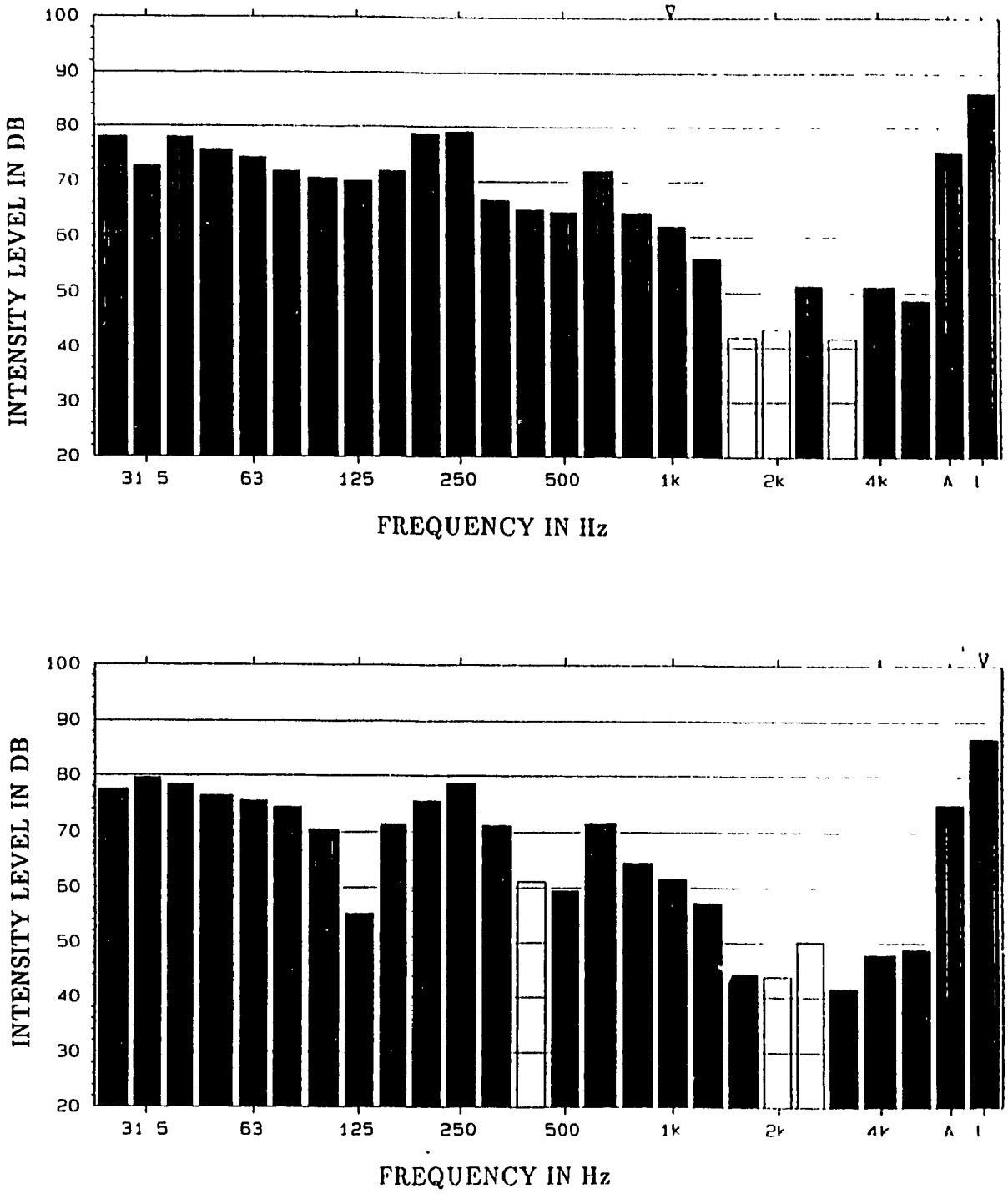

Figure C.1: Sound intensity levels measured in the coupler along two direction

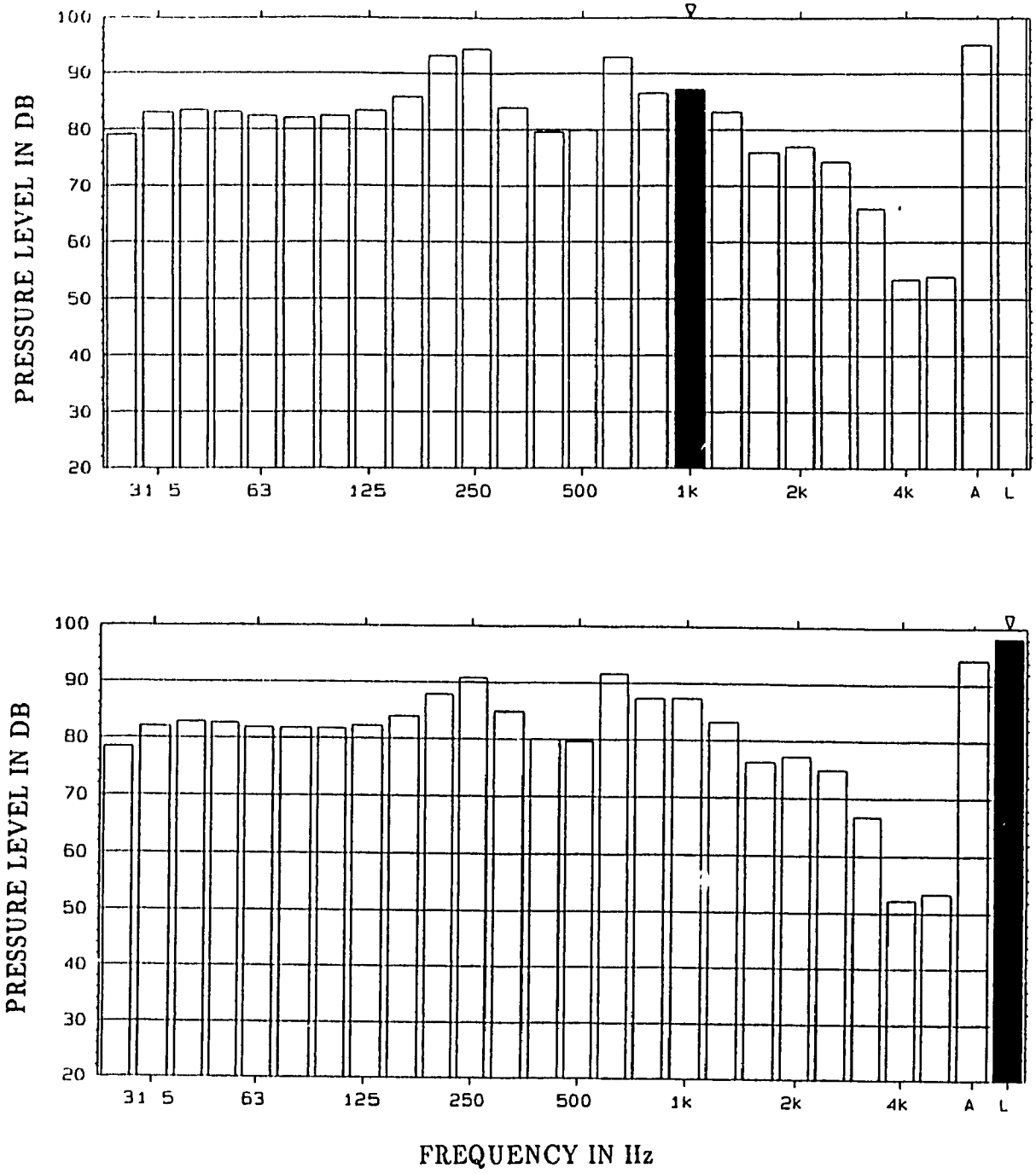

Figure C.2: Sound pressure levels measured in the coupler along two direction

directivity of the probe two measurements were performed, keeping the probe in the opposite direction for the second measurement. In the table the two measurements were designated by 'direction 1' and 'direction 2' respectively. From the table it is clear that the instrument meets the requirements for 'class 1' intensity probe at frequencies above 100 Hz. However, the table shows that only the requirement of a 'class 2' instrument is met at low frequencies.

Table C.1: Comparison of measured P-I index with the minimum requirement

1/3 octave band central frequency (Hz)	P-I index values (dB)			
	Required (IEC 1043)		Measured	
	class 1	class 2	Direction 1	Direction 2
50	12	6	10.5	9.2
63	13	7	11.5	9.4
80	14	8	13.5	10.6
100	15	9	14.8	15.1
125	16	10	16.4	20.9
160	17	11	17.0	15.5
200	18	12	17.3	15.3
250	19	13	18.7	15.2
315	19	14	19.9	18.5
400	19	14.5	18.0	29.3
500	19	15	19.0	31.5
630	19	16	25.1	22.8
800	10	16	25.2	26.9
1000	19	16	31.1	28.8
1250	19	16	30.4	30.6
1600	19	16	39.3	42.4
2000	19	16	36.2	41.0
2500	19	16	29.5	27.8